THESIS REPORT

Master's Degree

A Systems Engineering Approach to Design a Smart Tool Post Structure

by W.F. Ko
Advisor: G.M. Zhang

M.S. 95 -9

Sponsored by
the National Science Foundation
Engineering Research Center Program,
the University of Maryland,
Harvard University,
and Industry

Report Documentation Page

Form Approved
OMB No. 0704-0188

1. REPORT DATE	2. REPORT TYPE	3. DATES COVERED
1995		**00-00-1995 to 00-00-1995**

4. TITLE AND SUBTITLE	5a. CONTRACT NUMBER
A Systems Engineering Approach to Design a Smart Tool Post Structure	5b. GRANT NUMBER
	5c. PROGRAM ELEMENT NUMBER
6. AUTHOR(S)	5d. PROJECT NUMBER
	5e. TASK NUMBER
	5f. WORK UNIT NUMBER
7. PERFORMING ORGANIZATION NAME(S) AND ADDRESS(ES) **University of Maryland,The Graduate School,2123 Lee Building,College Park,MD,20742**	8. PERFORMING ORGANIZATION REPORT NUMBER
9. SPONSORING/MONITORING AGENCY NAME(S) AND ADDRESS(ES)	10. SPONSOR/MONITOR'S ACRONYM(S)
	11. SPONSOR/MONITOR'S REPORT NUMBER(S)

12. DISTRIBUTION/AVAILABILITY STATEMENT
Approved for public release; distribution unlimited

13. SUPPLEMENTARY NOTES

14. ABSTRACT
see report

15. SUBJECT TERMS

16. SECURITY CLASSIFICATION OF:			17. LIMITATION OF ABSTRACT	18. NUMBER OF PAGES	19a. NAME OF RESPONSIBLE PERSON
a. REPORT **unclassified**	b. ABSTRACT **unclassified**	c. THIS PAGE **unclassified**		**145**	

ABSTRACT

Title of Thesis: A SYSTEMS ENGINEERING APPROACH TO DESIGN A SMART TOOL POST STRUCTURE

Name of degree candidate: Wing Fu Ko

Degree and Year: Master of Science, 1995

Thesis directed by: Associate Professor Guangming Zhang,
Institute for Systems Research/ Mechanical Engineering

Precision machining has received more and more industry-wide attention as dimensional accuracy becomes a significant measure of quality in a product. The key in achieving today's quality requirement is, therefore, precision of a machine tool. Since the invention of the first CNC machine tool in the 1960's, machine tool research has entered an almost stagnant stage. There are numerous reasons for the slow progress, and the lack of system-wide studies of the machine tool performance is one of them.

The research presented in this thesis focuses on improving machining accuracy using a systems engineering approach. A conventional lathe during machining is taken under consideration as a machining system. The tool post is identified as a critical component in the machining system to achieve the defined machining accuracy. Smart material made actuators are used to design a new tool post structure that is capable of carrying out an active vibration control during machining.

In this thesis research, the fabrication of the designed tool post is completed. Results obtained from the initial tests strongly demonstrate its capability to attenuate tool vibration during machining in an active and intelligent way. Thus, the smart tool post

system fulfills the design objective of achieving microscopic level machining precision on a low cost conventional machine tool platform. Suggestion on the actuator specifications are made for further improvement on vibration compensation.

A Systems Engineering Approach to Design a Smart Tool Post Structure

by

Wing Fu Ko

Thesis submitted to the Faculty of the Graduate School
of The University of Maryland in partial fulfillment
of the requirements for the degree of
Master of Science
1995

Advisory Committee:

Associate Professor Guangming Zhang, Chairman/ Advisor
Associate Professor Thomas E. Fuja
Professor Andre Tits

ACKNOWLEDGMENTS

I would like to express my sincere appreciation to Professor Guangming Zhang for his encouragement and guidance throughout this work. Besides Professor Zhang, I also want to thank Professors Thomas Fuja, and Andre Tits for serving on my committee.

I particularly want to thank the support staff at the Institute for Systems Research, especially, Ms. Diane Ihasz, Ms. Mattie Riley, and Ms. Tina Y. Wong for all their help.

I am also indebted to many faculty members and my friends at the Institute for Systems Research and the Advanced Design and Manufacturing Laboratory for providing valuable assistance.

Acknowledgements are also in order for the financial support from the Advanced Research Projects Agency (ARPA) and the State of Maryland. Without their supports, this research work will not be able to accomplish what it has accomplished today.

Last but not the least, I want to thank all my friends for their supports and inputs to my work, especially, Mr. Wo-Pong Tsui, Mr. Alex Chu, Mr. Patrick Ko, Mr. Michael Paul Woo and Miss Siu-Ling Tan.

DEDICATION

To my family, especially my dad Siu and my mom Shin

TABLE OF CONTENTS

LIST OF FIGURES

LIST OF TABLES

1. Introduction

The research work presented in this thesis represents a pioneering effort to carry out an ambitious project. The main objective of the project is to develop a vibration control system for machine tools during operation. The machine tool selected as the test bed for this project is a conventional lathe. The research is focused on providing a practical solution to vibration control, a problem which has existed in the machining industry since it was born. Certainly, many fellow researchers have studied the problem and have made numerous attempts to search for such a practical solution. However, the results to date are not satisfactory. Therefore, this work is a revisit to a problem not being solved for centuries with a hope that the availability of newly developed active materials may provide a solution through an innovative approach.

As witnessed, the urgency of searching for a solution to reduce the vibration in machine tools during machining is growing as machining tolerances get tighter. Conventional machine tools are being pushed to their machining capability limits. If there is no effective method to improve the machining capability of these machine tools, most of these machines will be forced to be scrapped. The health of the manufacturing industry will be at great risk considering the fact that conventional machine tools and their variants are still dominating the industry. Since vibration is the main barrier to achieve high machining tolerance and has an adverse effect on machine tool life, building a vibration cancellation system for machine tools will provide a solution to these two problems.

The uniqueness of the current attempt is applying a systems engineering approach. The approach adopts the latest development in smart materials and their application techniques to the century-old problem. The strategy used in this work is to investigate the problem, build a virtual lathe model for system development and testing, and finally establish critical performance specifications for the design and fabrication of a smart tool post.

The thesis is organized based on the development of the study. It begins with a review of the related subjects. Following the review, a virtual machining system through mathematical modeling is built for understanding the mechanisms of a machining system as well as facilitating later tests and evaluation tasks. Alternative system design concepts are evaluated and the most promising design concept is selected. A series of experimentation is carried out to calibrate the system parameters associated with the key mechanical components. Special attention is given to the characterization of smart material made actuators. Based on the obtained results, the smart tool post structure is fabricated and tested. Results obtained from the experimental work are presented. They testify the confirmation between the design specifications and the tool post performance. The future work of this investigation is presented in the conclusion part of this thesis.

2. Literature Survey

2.1 History of Machine Tool Industry

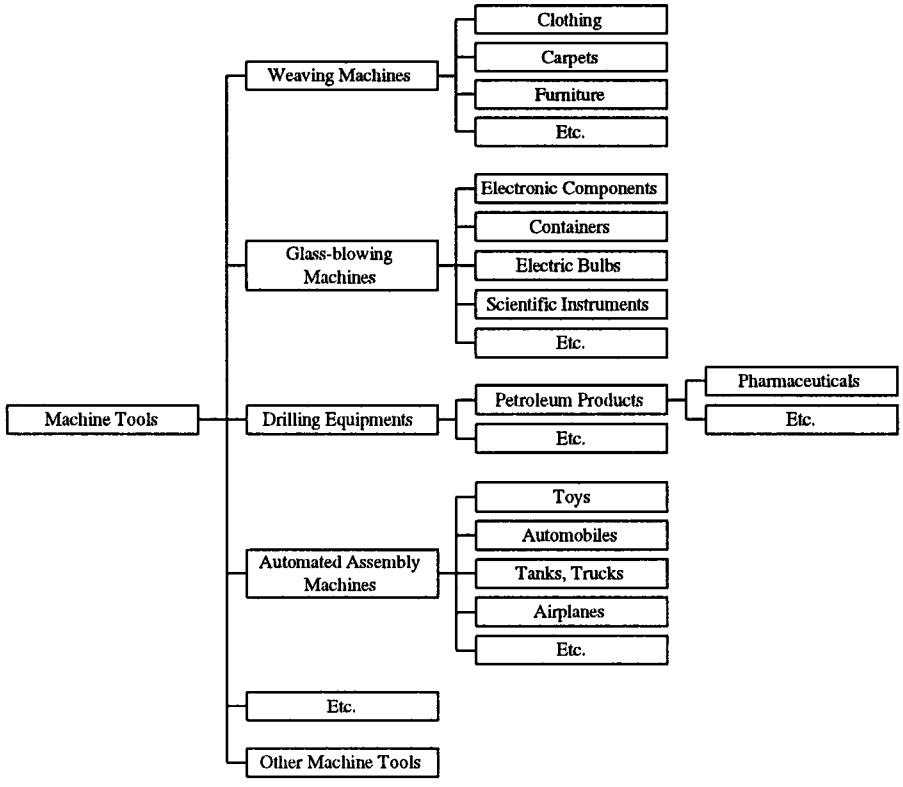

Figure 2-1 An Example of the Long-Linked Economic Impact of Machine Tools

A machine tool is defined as "a powerful device, not hand-held, which cuts, forms, or shapes metals" (The National Machine Tool Builders Association). The first machine tool, a boring mill, was invented in 1774 and enabled the completion of the first successful steam engine[1]. Since then, the machine tool industry has been of great strategic importance to the processes of economic growth and industrial development. As shown in Figure 2-1[1], virtually every major manufactured product is produced on machine tools or

on machines built by machine tools. The competitiveness of many major American industries, especially heavy industry, in both domestic and world markets relies heavily on the capability of machine tools. Due to a direct linkage with national security, military spending has been heavily invested in machine tool research and development. This investment made the numerically controlled machining possible in the 1950s. This technology is still helping us to increase manufacturing capability now. The US Cabinet Council on Commerce and Trade asserted that a healthy machine tool industry is important to the strength of the US industrial base in a recent report[2].

Historically, the U.S.'s machine tool industry maintained its leadership until the 1960's. The invention of NC machining in 1961 represented the peak of its development. However, the sliding national economy in the 1970's and the following shift in military spending forced the industry to scale down its research. Nevertheless the US still spends tens of millions of dollars every year on machine tool research. A vast amount of knowledge has been gained from those efforts including fundamental machining mechanics, vibration control skills, structural characteristics and electromechanical conversion. Unfortunately, the gained knowledge has been developed independently without a collaborative integration towards machine tool vibration control. This undermines the enormous economic impact of the research to society.

As the foreign machine tool builders develop their own machine tools researches, the technological advantages that used to be possessed by the domestic builders are diminishing quickly, or even fall into some foreign builders' hands. The machine tool industry has started to find ways to regain its competitiveness. The industry gradually adopts advanced

sensing and control systems to improve quality and productivity of machine tool performance in order to remain competitive in this highly globalized economy. The introduction of active control systems to compensate tool motion errors, while the machine tool is on operation, is one of the promising developments.

With the discovery of practical electrostrictive and piezoelectric ceramic materials, large-scale engineering applications of smart material have been focused on wide bandwidth ceramic actuators for active control systems. Its importance can be seen from the comprehensive study on this new generation of ceramic actuators sponsored by the Advanced Research Projects Agency (ARPA). The study is titled, "Synthesis and Processing of Smart Material and Structure." Its participants include universities, national research facilities and industries. This thesis represents the application area of the study with emphasis on machine tool vibration control. The goal is to search through the new technologies and knowledge in various disciplines for a right synergic solution to take full advantage of the state-of-the-art electrostrictive ceramic actuators.

2.2 Brief Review of a Lathe

Lathes are generally considered to be one of the oldest machine tools. Over time, lathes have grown to be the most common machine tools used by industry. Although lathes have become a class of machine tool with a number of variants, every lathe still shares some basic operational principles.

A typical lathe is shown schematically in Figure 2-2[3]. Several key components and their functions are worthy of mentioning. The bed supports all key components. The

carriage assembly, which slides along the ways, consists of an assembly of the cross-slide, tool post, and apron. The cutting tool is mounted on the tool post, usually with a compound rest that swivels for tool positioning and adjustments. The headstock, which is fixed to the bed, is equipped with motors, pulleys, and V-belts that transmits power to the spindle at various rotational speeds. The tailstock, which can slide along the ways and be clamped at any position, supports the other end of the workpiece.

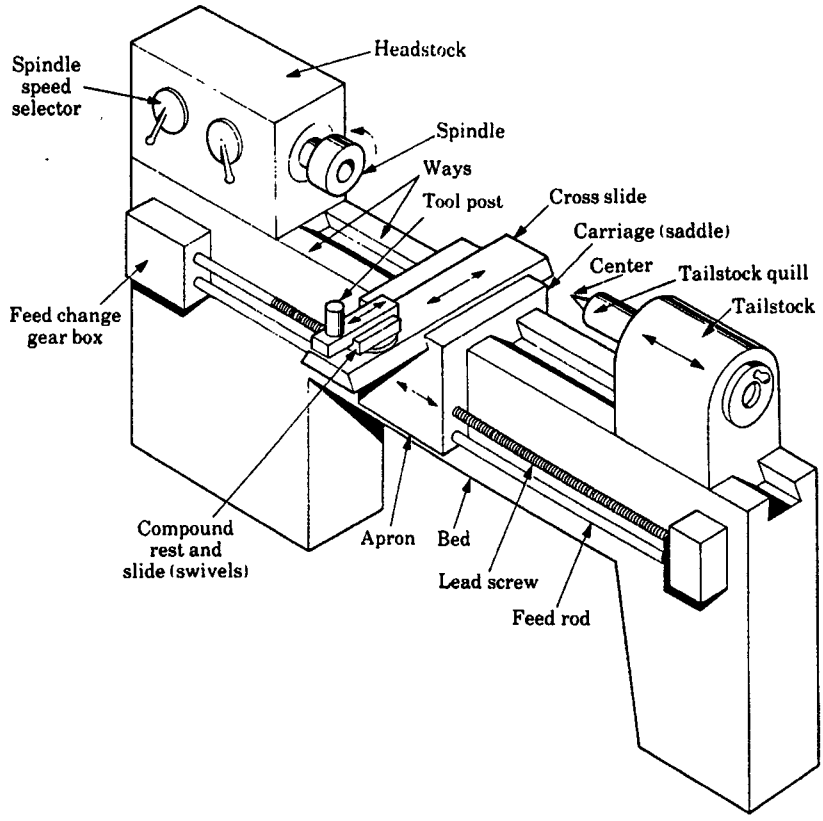

Figure 2-2 Schematic Illustration of the Components of a Lathe

2.3 Study of Dynamics Of Machining Systems

From Merritt's work[4], a machining system is identified having three major components. They are cutting process, structural dynamics, and a set of feedback paths that represent the interactions between the cutting process and structural dynamics. The block diagram proposed by Merritt in 1965 (shown in Figure 2-3) illustrates the machining system as a closed loop system.

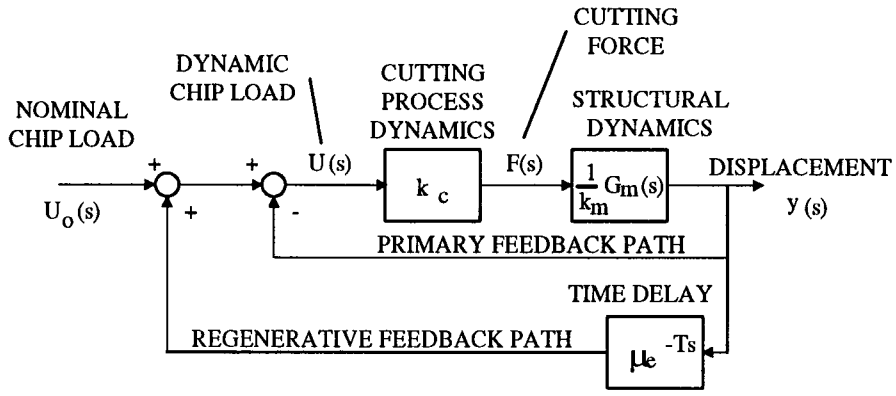

Figure 2-3 Feedback Diagram for the Dynamics of a Machining System

As illustrated in Figure 2-3, the input to the cutting process or the machining system is the chip load. Given the chip load, the cutting process generates a corresponding cutting force, which serves as the input to the machine tool structure. The machine tool structure, then, determines the tool motion based upon the input cutting force. The feedback paths modify the nominal chip load instantly by sending the tool motion back to the system input.

2.3.1 Modeling of Cutting Process

When the structural dynamics is neglected, Merchant[5] suggested that a steady-state cutting process can be characterized by a parameter called k_c, which is referred to as

cutting stiffness, or static directional cutting stiffness. The resultant cutting force, F(t), is related to the instantaneous uncut chip thickness, u(t), according to equation (2-1).

$$F(t) = k_c\, u(t) \qquad (2\text{-}1)$$

A low value of k_c may indicate that the force generated during machining is at a low magnitude. This resembles the machining of low hardness materials, small depth of cut, or both.

Since Merchant first proposed his model in 1944[5], the model has been widely accepted by the machine tool profession although the model has its limitation to characterize the machining process without error. The deviation induced by modeling comes from;

1. the negligence of cutting dynamics which influences the uncut chip thickness; and
2. the varying nature of the cutting stiffness at different speeds instead of the assumed constant value.

Unfortunately, the differential equations describing the dynamic behavior of the cutting processes have not been written from the physics of metal cutting. In fact, a definitive experimental result has not been published. Nevertheless, the deviation does not significantly affect the characterization ability of Merchant's model.

2.3.2 Modeling of Structural Dynamics

From a machine tool perspective, modeling of structural dynamics is to build a model capable of describing the dynamic characteristics of the machining system under

investigation. There are three important parameters for every dynamic model namely, mass or inertia, stiffness, and damping coefficient regardless of its actual physical layout.

In a complex dynamic modeling problem, a lump-sum model is usually used. The object may be partitioned into numbers of smaller objects with individual characteristic parameters. Then, by applying various continuity theorems, the dynamic behaviors of the smaller objects can be linked together to estimate the grand behavior of the problem. In machine tool research, the degree of partition varies widely depending upon the specific type of machine tool under study and the nature of the problem being analyzed. An n-degree-of-freedom system can be used if necessary.

2.3.3 Modeling of the Feedback Paths

The two feedback paths merely resemble the interaction between the cutting process and the structural dynamics of a machine tool. The first feedback path is called the primary feedback path which characterizes the relative position of the tool with respect to the workpiece being machined. Intuitively, the instantaneous thickness of cut decreases as the cutting tool moves away from the preset depth of cut relative to the workpiece.

The second feedback path is called regenerative path which represents how much material was left over from previous cutting action. The effective residual material from previous action is the product of the percentage of overlap between two consecutive actions and the amount of residual material from the first action. This concept agrees with the fact that there is no residual material from the previous revolution in machining a thread.

Therefore, the momentary uncut chip thickness is the sum of two components. The first component is the difference between the preset depth of cut, $u_0(t)$, and the current position of the cutting tool, y(t). The second component is the amount of residual material from T units of time ago, $\mu y(t-T)$. The mathematical expression for the relationship is shown in equation 2-2.

$$u(t) = u_0(t) - x(t) + \mu x(t-T) \qquad (2\text{-}2)$$

where μ is the overlap factor ranging from 0 to 1.

2.4 Vibration and Chatter

Vibration and chatter are problems to metal cutting and can happen on any chip-producing machine tool. Besides deteriorating the surface quality and dimensional accuracy, severe vibration and chatter will reduce tool life and machine tool life. Thus, machine tool vibration or chatter control has been studied by many researchers and engineers. So far, the advancement is still very limited because vibration and chatter are complex phenomena. This understanding in cutting operations suggests that there are two types of vibration occurring in cutting: forced vibration and self-excited vibration.

Forced vibration is generally caused by some periodic exciting force present in a machine tool. Such an exciting force may come from gear drives, imbalance or misalignment of the machine tool components, or motors and pumps. Other causes can be related to the nature of individual machining task such as turning a shaft with a keyway[6].

Different solutions to forced vibrations have been proposed. For instance, if resonance occurs between the forcing element and a component of the machine tool system,

one of the natural frequencies may be raised or lowered. The amplitude of vibration can be reduced by increasing the stiffness or damping the system. Besides structural modifications, changing the cutting speed and the tool geometry can reduce tool vibration too. It is because changing the cutting speed has an effect on changing cutting stiffness while changing the tool geometry has an effect on the built-up edge formation.

Generally called chatter, self-excited vibration is caused by the interaction of the chip-removal process and the structure of the machine tool. Self-excited vibrations usually have a relatively high amplitude. Chatter typically begins with a disturbance in the cutting zone. Such disturbances include lack of homogeneity in the workpiece material or its surface condition, and changes in type of chips produced. The most important type of self-excited vibration in machining is regenerative chatter. It is the effect of the regenerative feedback discussed early.

Many theories have been proposed to explain self-excited chatter in the past, but the complexity of chatter prevents a simple comprehensive mathematical analysis that will lead to chatter prediction and prevention. However, from experience, it has been pointed out that by increasing the stiffness between workpiece and cutting tool the danger of chatter is decreased. At the same time, as every production engineer knows, chatter is often eliminated by easing some of the locks of machine tool slides and thus increasing the structural flexibility. Designers are aware that some flexible machines appear to suppress chatter better than similar machines with appreciably greater stiffness. Researchers suggest that damping also plays a highly important role in the chatter phenomena. In some cases, a loss

of stiffness may be accompanied by an increase of damping, resulting in an elimination of chatter.

However, regardless of the specific approach, the sole purpose is to shift the borderlines of stability until the operating speed of the machine tool falls in the stable region. The exact mathematical solution to the three borderlines of stability for a one degree-of-freedom structure was found by Tobias and Fishwick[8]. They also developed the concept of penetration rate to account for the region of stability at lower speed. A typical stability chart for a machine tool is shown in Figure 2-4[7]. Later on, more papers have been published. However, these techniques are computationally inconvenient to apply until Merritt published his first paper on the theory of chatter[4].

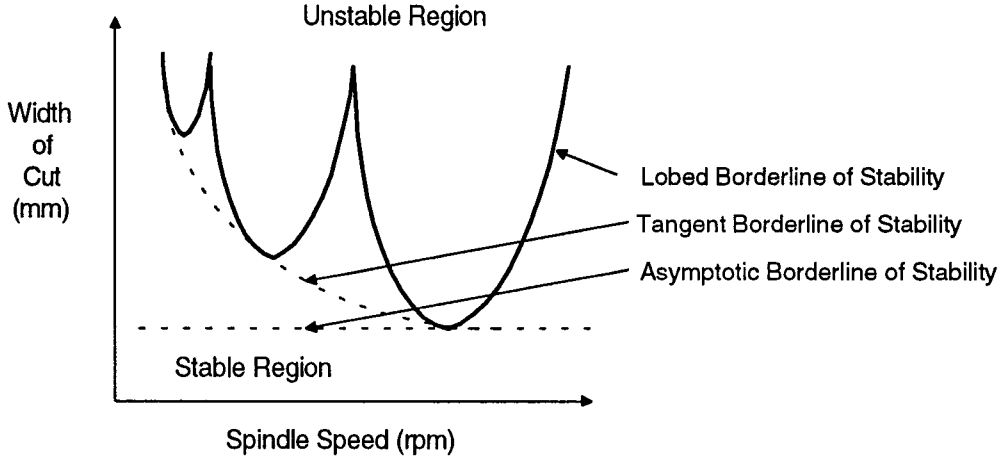

Figure 2-4 Stability Chart for a Machine System

Therefore, vibration and chatter are determined by three factors: kinematics motion, tool geometry, and chatter. However, control over kinematics motion will constrain productivity and control over tool geometry is almost impossible in a dynamic machining environment. Thus, chatter of a machine tool should be under control.

2.5 Vibration Control

Engineers have tried different methodologies to either eliminate, or suppress undesirable vibration in various applications. Even in applications where vibration is desirable, for example, source of power, engineers still need to make vibration behave in a desired way. Concerning vibration control, there are two fundamental approaches; namely passive vibration control and active vibration control[9,10,11].

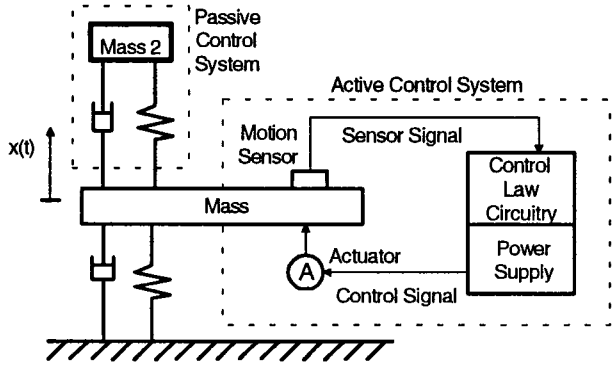

Figure 2-5 Active and Passive Control Systems

2.5.1 Passive Vibration Control

In passive vibration control, as illustrated in Figure 2-5, designers will choose an optimal setting of mass, damping, and stiffness for a model under a specific operating environment. The settings of these parameters determine the behavior of the model. The major weaknesses of this approach are difficulty of implementation and lack of robustness.

Considering the hassle of changing the mass or stiffness of a model after the materials are selected for a given model, or even after the model is already installed at a site. In addition, a less-than-optimal performance can be expected when the actual operating

environment deviates from the designed environment. Therefore, a more responsive vibration control scheme is needed for a performance critical model under a changing environment and this is the prime motivation of having active vibration control.

2.5.2 Active Vibration Control

Active vibration control uses an external active device, called an actuator, to provide a force to the model under control. Depending upon the desired performance, preferably including the system transfer function of the model, a control law is constructed. A complete active control system includes a device used to apply the force (i.e., the actuator), together with a sensor and a signal processing unit (Figure 2-5). The sensor is used to measure the response of the system and to forward the information to the signal processing unit for data processing. According to the control law, an appropriate signal is sent to the actuator to achieve desired system response. To date, a multitude of control systems hardware and a variety of control laws are available for use in vibration control.

A simple illustration of the active control for a single-degree-of-freedom system is followed. In such an isolation design, the state feedback consists of the acceleration of the system. A signal processing unit performs integration over the signal to obtain velocity and position information. The controller then provides a command to the actuator proportional to measured velocity and displacement (also called PD control or position and derivative control). The actuator generates a desired force to the system of the form

$$u = -g_1 x - g_2 \dot{x} \tag{2-3}$$

where g_1 and g_2 are called gains.

The gains g_1 and g_2 depend upon the designer's choice of control law. The equation of motion for a single-degree-of-freedom oscillator with PD control given by (2-3) becomes

$$m\ddot{x}+(c+g_2)\dot{x}+(k+g_1)x=0 \tag{2-4}$$

Consequently, the closed-loop equation (2-4) has two more parameters (i.e., g1 and g2) than the passive system, which can be adjusted to ensure that the response has the desired form.

2.5.3 Vibration Control Using a Smart Structure

Over the years, researchers and engineers have tried both passive and active control schemes in machine tools with some success, but the vibration attenuation is often limited to individual cases with narrow operating ranges. Among all attempts, active control schemes usually result in greater vibration attenuation than passive control schemes do. The main barrier for active control schemes to a full success is the lack of quick response actuating elements with high power to volume ratio and sufficient dynamic stiffness.

Since the discovery of piezoelectric materials, many researchers in vibration domain have begun to use the materials as sensors because of the high stiffness and compact size natures of the piezoelectric sensors. As researchers gain more experience in using the materials, they start to explore other usage of the materials. One usage is to reverse the materials' functionality from sensing to acting; making the actuators to expand and contract as commanded.

A structure embedded with those special actuators can integrate sensing, actuating, and processing elements to enable self-awareness, action, and adaptation in response to

environmental stimuli. It is recognized as a smart structure because the structure is capable of responding intelligently.

The advantage of using a smart structure is that it has an integrated function of sensing and actuating. Thus, detailed knowledge of state can be obtained in a rather simple and explicit manner. Also, it has a higher adaptability and wider fault-tolerance. The structure can even correct minor manufactured defects by itself. In addition, the response of the structure is impulse free and instinctive. Therefore, smart structure is an appealing candidate to a lot of engineering applications, especially to machine tool applications where weight, size, and cost are of primary importance.

2.6 Smart Material Made Actuators

2.6.1 Fundamentals of Actuators

The smart actuator examined in this thesis work is an electroactive device made of an electrostrictive ceramic material: lead-magnesium-niobate (PMN). The actuator is smart because it has the ability to sense and to react to its environment. In fact, an electroactive device is broadly defined as a device that produces a non-electrical output, given an electrical input, or vice versa. Although not all devices can operate bidirectionally, the PMN-made smart actuator is a special kind of electromechanical device that can convert the energy in both directions.

As illustrated in Figure 2-6, an actuator can be a single-layer device. The amount of displacement the device can achieve is proportional to the voltage per unit length of the material (that is the electric field, V/m). It is preferable to have a thin layer device because

it provides more displacement than a thick layer device per unit length under a given applied voltage. In other words, thinner layers allow lower voltage operation. To maximize total displacement, and minimize operating voltage, several single layer devices are usually stacked together to produce a multi-layer device. The PMN actuators used in this thesis work are multi-layer ceramic actuator (MCA), or simply called smart actuators. The construction of the smart actuators is basically stacking hundreds of single layers on top of each other. This is mechanically similar to putting hundreds single layer ceramic actuators in series although they are electrically connected in parallel as illustrated in Figure 2-6.

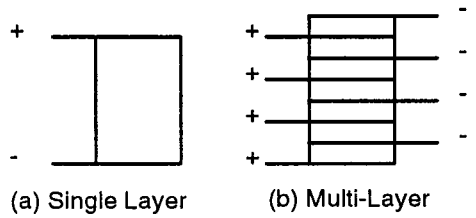

Figure 2-6 Single Layer and Multi-layer Ceramic

2.6.2 Electrostrictive and Piezoelectric Materials

The material used to construct an actuator determines the nature of its output response. The two basic categories of smart materials are electrostrictive and piezoelectric. Both materials belong to the class of polar dielectrics. This class of materials is the one whose crystal structure contains a unique axis, along which an electric dipole will exist. All crystals possessing such a unique axis will show the phenomena of "pyroelectricity" (the release of charge with application of stress). In addition, the orientation of the polar axis can be changed by applying an electric field of sufficient magnitude to the crystal.

The fact that the orientation of the polar axis in the smart materials can be changed by the application of a field has a very important consequence. If a polycrystalline body is made of a polar material, then the crystal axes is likely to be randomly oriented and the body will possess no net polar axis. It cannot, therefore, show either piezoelectricity or pyroelectricity. However, if a large electric field is applied to the body, the polar axis within the grains will tend to be reoriented to align with the applied field, as shown in Figure 2-7. This process is called "poling" and is illustrated in Figure 2-8. The resulting ceramic is polar and will show both piezoelectricity and pyroelectricity.

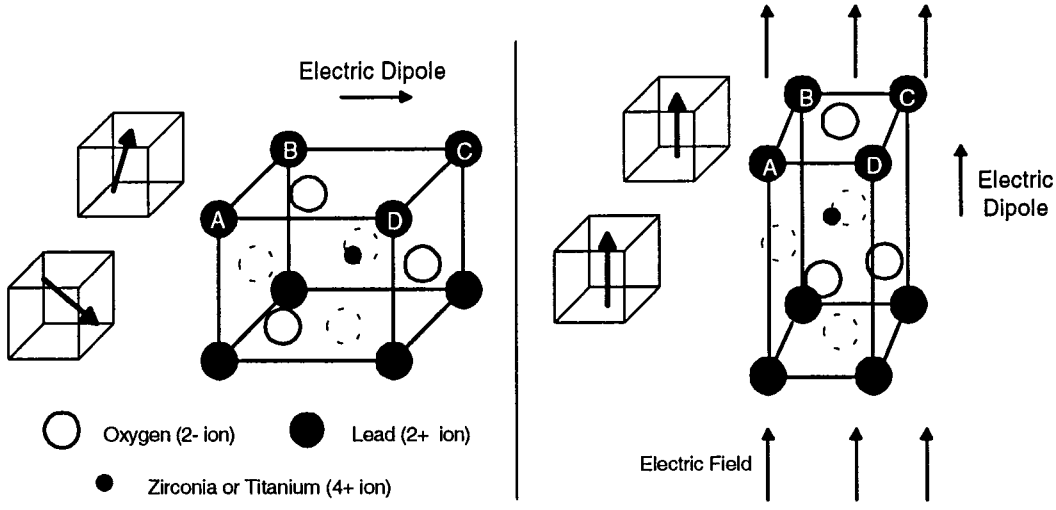

Figure 2-7 Piezoelectric Poling Mechanism

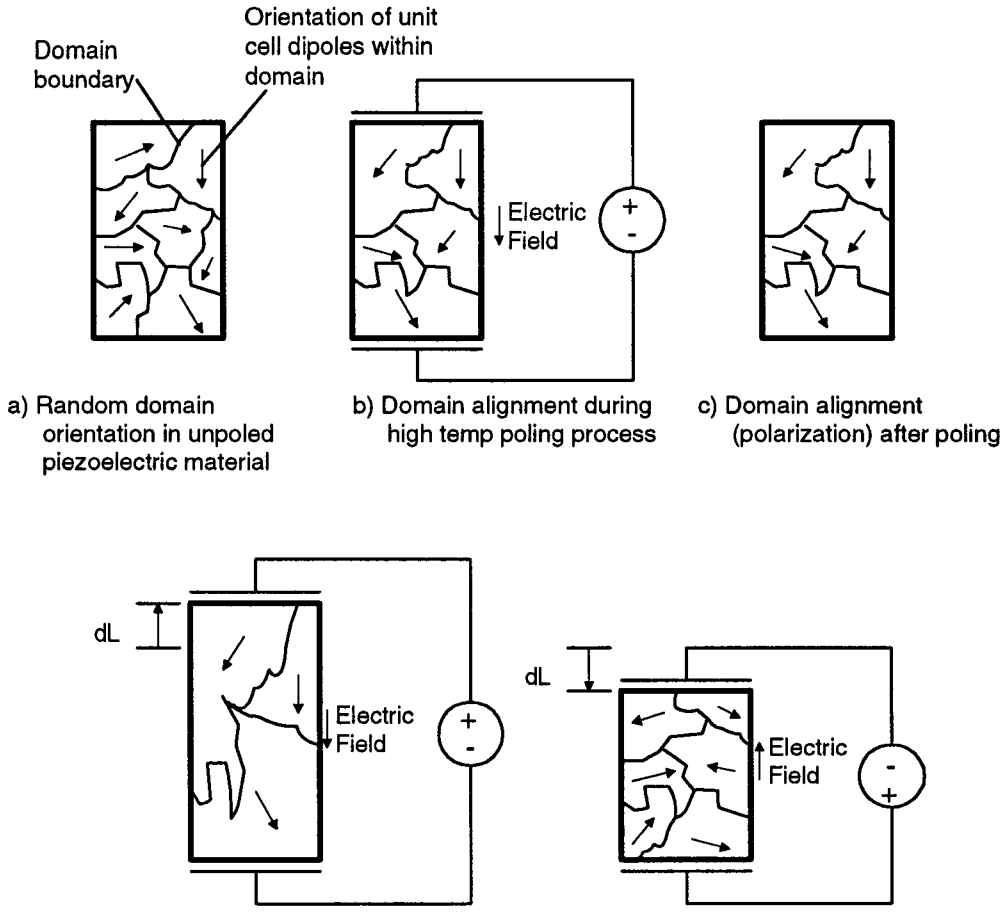

Figure 2-8 Poling Process and Piezoelectric Phenomenon

Although all smart materials generally behave in the manners described above, the electrostrictive materials possess a unique characteristic. As illustrated in Figure 2-9, an electrostrictive material always elongates when it is subjected to external voltage. This behavior is contrary to the piezoelectric materials' behavior that those materials elongate and contract depending upon the polarity of the applied voltage. As a summary, the displacement of the actuator vs. applied voltage for both types of smart materials are sketched in Figure 2-10.

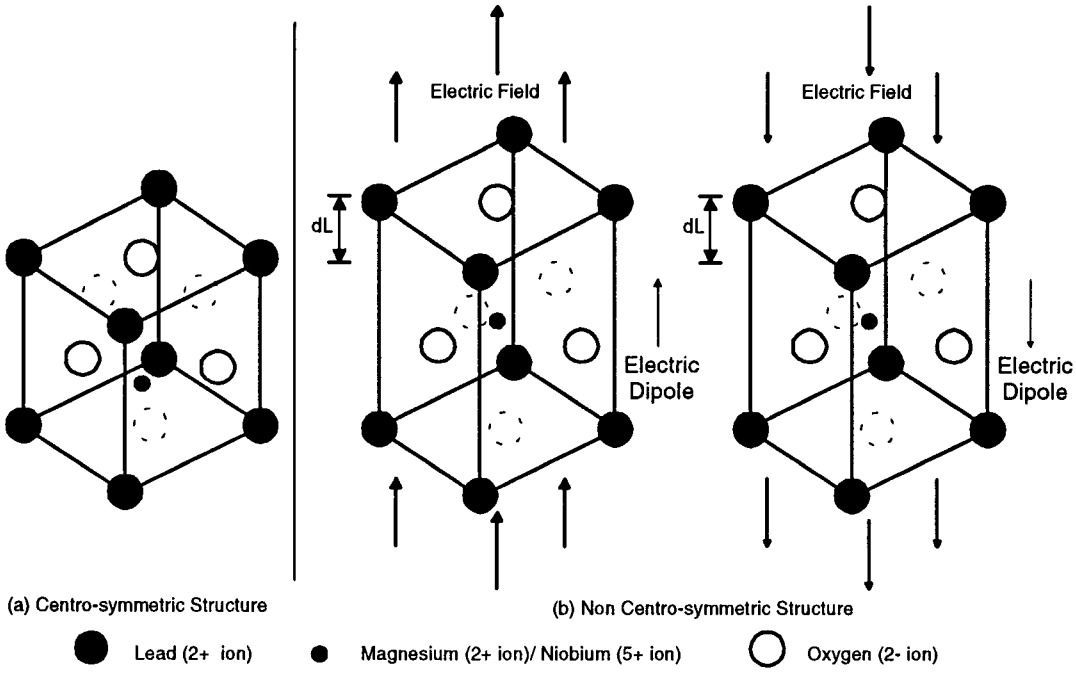

Figure 2-9 Primary Electrostrictive Response Mechanism

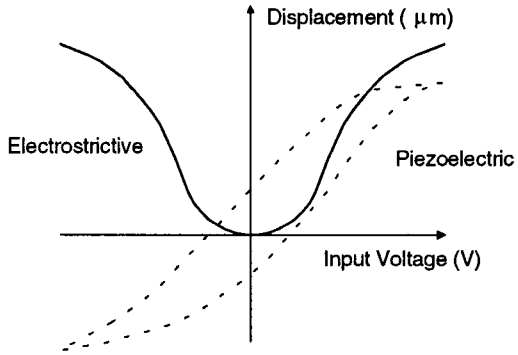

Figure 2-10 Typical Stress-Strain Relationships for the Two Types of Actuators

2.6.3 Actuator Performance Specifications

The performance of the actuators made of those two materials are compared and summarized in Table 2-1. Also, typical parameters for a 6mm diameter, 20mm length, cylindrical actuator stack are shown in Table 2-2 [16].

Table 2-1 Performance Comparison between Electrostrictive and Piezoelectric Actuators

	Electrostrictive	Piezoelectric
Example	lead magnesium niobate (PMN).	lead zirconate titanate (PZT).
Unit Cell's Microstructure	Perovskite Structure; Centro-Symmetric.	Perovskite Structure; Non Centro-Symmetric.
Net Material Polarization	Before Usage, No. During Usage, Yes. After Usage, No.	Yes All the Time.
Poling before Service	No.	Yes. Electric field is applied to the heated sample. Domains are realigned from relocation of cell ions. (Figure 2-7, Figure 2-8)
Operating Principle	The cations and anions are displaced in the electric field. The net result is a distortion of the unit cell with an unbalanced charge distribution. (Figure 2-9)	Application of an electric field of the same polarity as the poling field will increase domain alignment. It causes a physical elongation. Contraction can be caused by applying opposite polarity. (Figure 2-8)
Displacement vs. Applied Field	Quadratic	Linear
Displacement Resolution	High Precision	Low Precision
Hysteresis*	Obvious.	Not Serious.
Creep*	Insignificant	Significant
Operating Temp.	Narrow	Wide
Capacitance	High	Low
Force	High	Low

* Note: Hysteresis is defined as the difference in device output resulting from different input conditions.

Creep is defined as the change in displacement over time under constant electric field.

Figure 2-11 Illustration of the Half-Stroke Operation for PMN actuators

Table 2-2 Typical Actuator Parameters

	Electrostrictive	Piezoelectric
Maximum Displacement (μm)	18	16
Capacitance (μF)	6	1
Dissipation Factor (%)	4.5	3
Maximum Frequency (Hz)	100	100
Force (N)	3,000	1,300
Hystersis (%)	2	15
Creep (Max. after 24 hours)	2%	15%
Operating Temperature (°C)	10 to 50	-20 to 80
Thermal Coeff. of Expansion	<1 ppm/°C	<2 ppm/°C
Modulus (N/m^2)	9.6e10.	6.0e10.
Response Time	<100μs	<10μs

2.6.4 Current Practice of Applying Smart Actuator

As shown in Figure 2-10, characteristics of the PMN type smart actuators includes saturation at high voltage and reversal stroke at 0 volt. From operation point of view, it is best to operate at $\max(\frac{\partial d}{\partial V})$ when the signal is small. When a full-stroke operation is needed, a bias at half-stroke point becomes necessary.

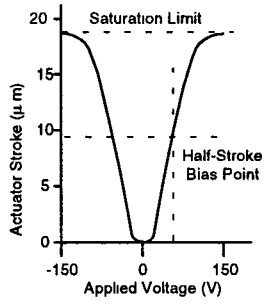

Figure 2-11 Illustration of the Half-Stroke Operation for PMN actuators

The actuator will be bias at half-stroke point. The tangent line at the bias point will describe the behavior of the linear model. The actuator signal will be from -53V to +101V. The key operation parameters for a typical 6mm diameter, 20mm long PMN type smart actuator is shown in Table 2-3.

Table 2-3 Operation Parameters for the PMN Type Smart Actuators

Item	
Bias Voltage (Vo)	53 V (D.C.)
Control Voltage (Vc)	-53 to 101 V (D.C.)
Linearized Transductance (q)	0.179 μm/V
Actuator Stroke Limit	±9.25 μm

In summary, electrostrictive actuators are more suitable to be used in the smart tool post application than piezoelectric actuators. Mainly it is due to the wider operation range and precise displacement. Half-stroke bias operation scheme is useful for large-signal operation. Attention has been paid to avoid saturation and reversal stroke which may be caused by the large signal. Although the dynamic behavior of the actuator is not linear over its entire operation range, nonlinearity has little effect below saturation. A simple (tangent) linearization is effective up to 80% stroke.

2.7 Constructing a Smart Material Model

A mathematical model which predicts the performance of the smart materials is essential for efficient and effective usage of the materials and their associated structures. A study of crystallography on the microscopic level is necessary for a sound theoretical model.

However, a macroscopic study of material properties will allow building a model for most practical uses.

2.7.1 Modeling of Smart Materials

For non-isotropic materials (different properties along different directions, including most crystalline materials) the relationship between electric flux density {D} and electric field {E} can be written as

$$\{D\} = [\varepsilon]\{E\} \tag{2-5}$$

where [ε] is a 3x3 dielectric constant matrix.

For ideal actuator materials $\varepsilon_{ij} = 0$, when $i \neq j$, so that only ε_{11}, ε_{22} and ε_{33} are non zero but they are not necessarily equal. Their stress strain relationship in the absence of an electric field can be expressed as

$$\{T\} = [c]\{S\} \tag{2-6}$$

where {T} and {S} are 6x1 stress and strain vectors respectively and [c] is a 6x6 elastic constant matrix. The elements along the main diagonal c_{ii} are the longitudinal and shear moduli. The others are cross coupling terms.

The piezoelectric effect depends on the direction of the electric field and applied stresses with respect to the crystal lattice. The relationship between strain {S} and 3x1 electric field {E} in the absence of stress is

$$\{S\} = [d]\{E\} \tag{2-7}$$

where [d] is a 6x3 piezoelectric constant matrix. Equation (2-7) establishes the cross relation between the electric field and the strain field. Equation (2-5) can also be written as

$$\{E\} = [\beta]\,\{D\} \tag{2-8}$$

$$\text{where} \quad [\beta] = [\varepsilon]^{-1} \tag{2-9}$$

and equation (2-6) can be replaced by

$$\{S\} = [s]\,\{T\} \quad \text{where } \{s\} = [c]^{-1} \tag{2-10}$$

In general, the total strain due to stress and electric field can be

$$\{S\} = [s]_E\{T\} + [d]_T\{E\} \tag{2-11}$$

where the stress-strain relationship must be measured with the electric field set equal to zero (terminal short circuited) as indicated by the subscript E and the strain-electric field relationship is measured with stress equal to zero (free) as indicated by subscript T.

A reciprocal relationship exists between electric flux density {D} and stress {T}

$$\{D\} = [d]^t\{T\} \tag{2-12}$$

where $[d]^t$ is a 3x6 matrix which is the transpose of [d] matrix in equation (2-7), and which is measured in the absence of electric field.

With externally applied electric field and stress the total electric flux density can be obtained by combining equations (2-5) and (2-12), namely,

$$\{D\} = [\varepsilon]\{E\} + [d]^t\{T\} \tag{2-13}$$

Equations (2-11) and (2-13) are called the equations of state for the piezoelectric material. However, actual strain in ceramics is induced in much more complicated ways. Strain changes associated with the domain reorientation are often superimposed on the

piezostriction, leading to hysteresis during an electric field cycle. Therefore, an empirical model deriving from experiments is a more practical and ready-to-go approach.

2.7.2 Modeling of Actuators

The work on evaluating piezoelectric actuators' performance under various boundary conditions has been done by some piezoelectric material producers [14,16]. The general characteristics are summarized in Figure 2-12.

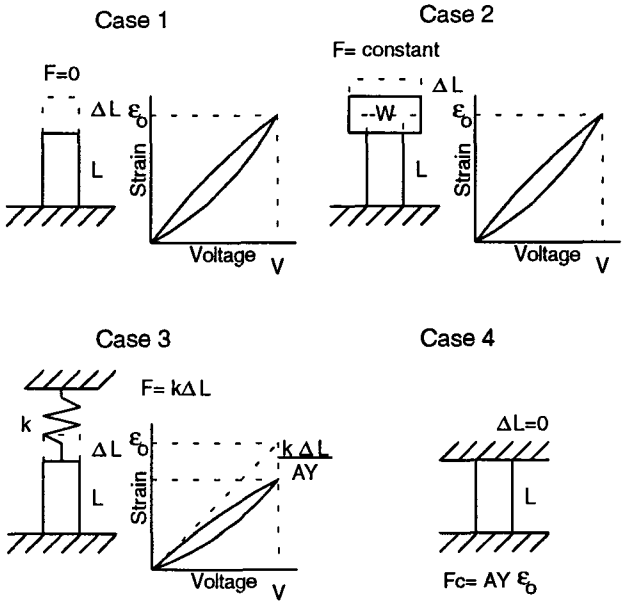

Figure 2-12 Effects of Various Loadings on Smart Actuators

In Figure 2-12, four fundamental loading cases are shown. For each loading case, a diagram is used to describe the conditions graphically. Also, whenever applicable, each diagram is associated with a plot that demonstrates the relation of the applied voltage and the resultant strain of the actuator. The strain is defined as the ratio of the change in dimension to the original dimension.

In case 1, the actuator is subjected to a voltage with both ends free. Although there is no external force to change its dimension, the applied voltage induces an internal strain to the actuator and changes the dimension of the actuator. In case 2, the actuator is subjected to a deadweight. The strain induced by the applied voltage is still the same as the one obtained in case 1. In case 3, the actuator is subjected to a variable load which increases its magnitude along with increment in the strain of the actuator. The induced strain is reduced by the amount induced by the external force. In case 4, the actuator does not show any deformation when it is subjected to an applied voltage. However, there are forces that are proportional to the applied voltage generated at both of the actuator's ends.

Models have been developed by piezoelectric materials manufacturers [14,16]. Mostly, those models are based on single layer configuration. For a multi-layer configuration, they usually suggest users to approximate its behavior by simply multiply the performance parameters for single layer by the number of layers. However, the accuracy of the approximation is not high enough to meet some of the applications where accuracy is a major concern. Therefore, researchers have developed models for multi-layer configuration.

A constitutive model of multi-layer ceramic has been developed by the Smart Material Synthesis (SMS) team that is formed under the ARPA's technology reinvestment program [17]. The uniaxial behavior of the ceramic material subjected to a stress σ, polarization P, and electric field E is described by two mechanical and electrical formulas.

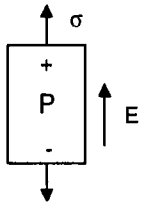

$$\text{Mechanical} \quad \sigma = Y\varepsilon - YQ_{11}P^2 \tag{2-14}$$

$$\text{Electrical} \quad E = -2Q_{11}\sigma P + \frac{1}{k}\arctan h(\frac{P}{Ps}) \tag{2-15}$$

where σ is stress, Y is Young's Modulus, ε is total strain, P is polarization strength, E is the electric field, P_s, Q_{11} are coefficients obtained from experiments.

Basically, both equations are based on the theoretical model and are developed for engineering applications. The first term in the mechanical formula is coming from Hooke's law, $\sigma = Y\varepsilon$. The second term, $Q_{11}P^2$, is the electrically induced strain. In the electrical formula, the converse effect caused by the electromechanical coupling is demonstrated by the $-2Q_{11}\sigma P$ term. The second term in the electrical formula, $\frac{1}{k}\arctan h(\frac{P}{P_s})$, represents the stress-free dielectric behavior.

When the actuator was subjected to pre-stress and alternating voltage, the response of the actuator changed accordingly. The sketches of the experimental and predicted responses are shown in Table 2-4. The qualitative agreements between the predicted and experimental responses validate the effectiveness of the empirical model.

Table 2-4 Smart Actuator Performance under Various Boundary Conditions

Boundary Conditions	Dielectric Response	Induced Axial Strain
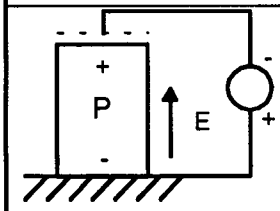	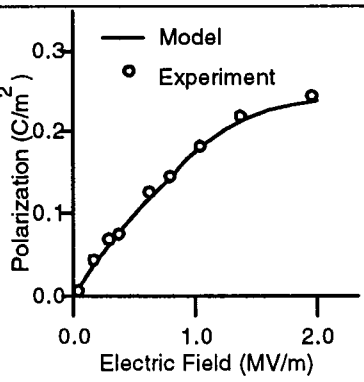	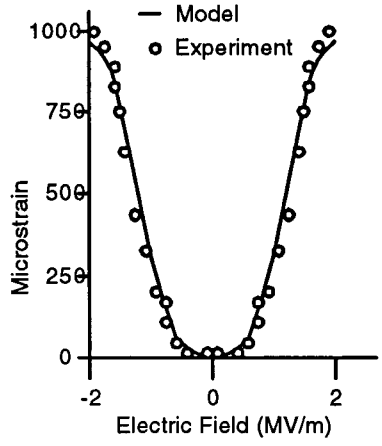
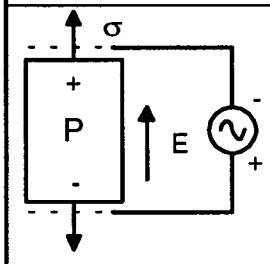	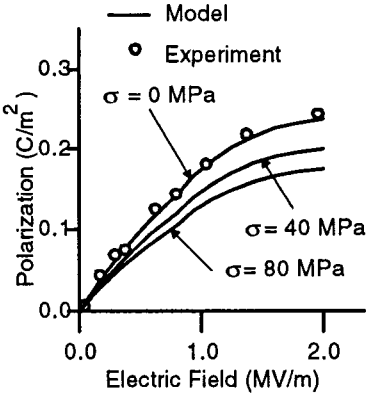	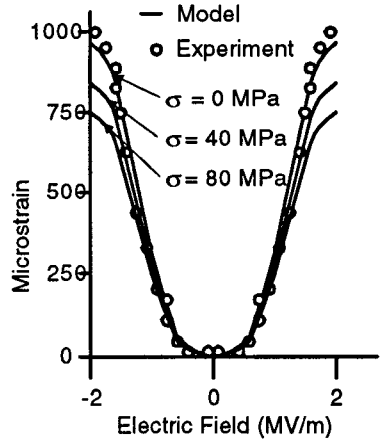

3. Modeling of a Machining System

The primary objective is to investigate the implementation guidelines of a vibration control system to a conventional lathe so as to provide crucial information for developing a vibration control system to machine tools.

3.1. System Overview

In this thesis work, the systems engineering approach guides the progress of the overall investigation although several other engineering approaches are used for individual technical analyses. The main aspect of this investigation is the operating environment for the proposed add-on system. A virtual system model is built for rapid experimentations. Based on the experimental results, critical operating parameters for the vibration control system wll be identified and established.

Machining systems cover a wide range of operations, such as turning, miling, grinding, etc. As the first attempt of this investigation, the focus is given to turning. Turning is a fundamental and the most common material removal process used in industry. In addition, a lathe shares a lot of characteristics with other machining systems. The knowledge gained from this study will be applicable for developing vibration control systems for other machine tools in general. Therefore, a turning process on a conventional lathe is selected for this thesis work.

Besides focusing only on the turning process, the analysis will be limited in a one-dimensional space: the radial direction as illustrated in Figure 3-1, although the cutting tool

motion during machining is best dealt with by a three-dimensional vector. The reason for this simplification is the effect of the tool's radial movement which is dominate in machining accuracy and surface quality. In addition, the similarity in vibration control between the other two directions and the radial direction is expected to be close. Therefore, results obtained from this study can be further deduced to other machining systems in interests.

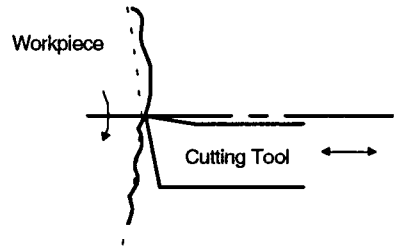

Figure 3-1 Surface Generation

3.2. Machining Environment

The environment that a turning machining system faces is a typical manufacturing environment, which is illustrated in Figure 3-2. Since this study focuses on vibration control, our attention will be given to the noise presented in the system and its environment.

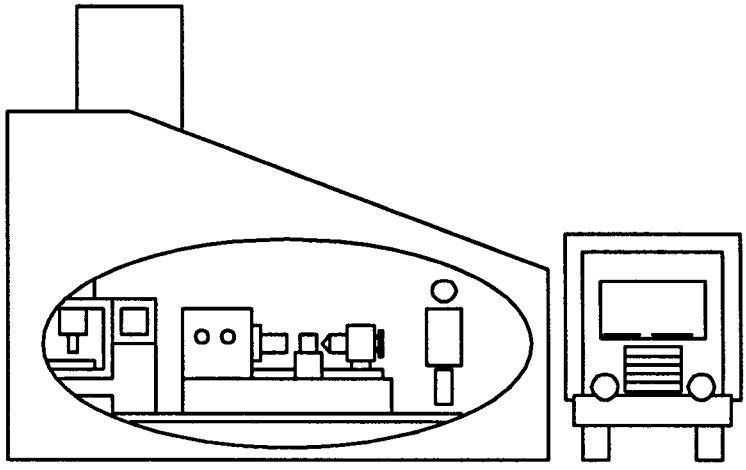

Figure 3-2 Lathe and its Environment

Figure 3-3 presetns the sources of noise. As indicated in the figure, some of the noise comes from the machining process while some of the noise comes from the vibration of other machinery on the shopfloor, motorized equipment and instruments (10 to 500 Hz), acoustic vibrations (above 20 Hz), street traffic (5 to 100 Hz), swaying of tall buildings (0.1 to 5 Hz), and ground and upper floor building resonances (5 to 50 Hz).

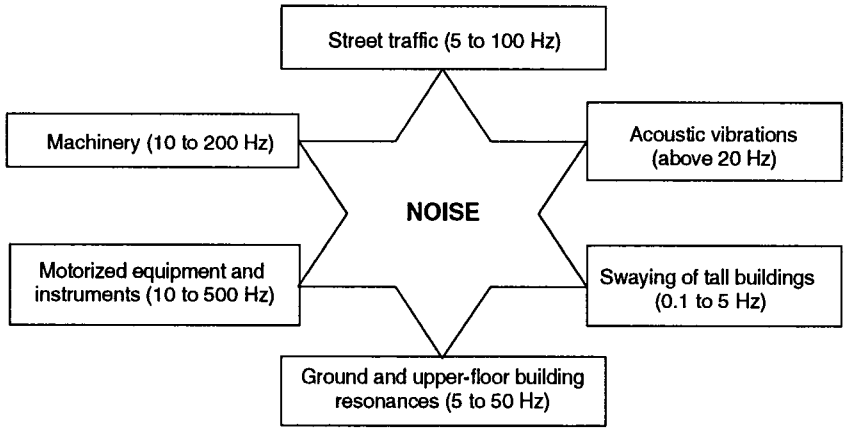

Figure 3-3 Sources of Noise

The machining system by itself presents several noise sources. Two of them are associated with coolant conditions and chip formation. Although coolants can improve surface finish while chips reflect the quality of surface finish, both of them have indirect effects on vibration. As a reminder, vibration and chatter are results of forced and self-excited vibrations which are mainly caused by varying disturbance. The disturbance comes from the feedback paths in the cutting process, the inversely proportional relationship between cutting speed and cutting force and other uncontrollable factors such as the heterogeneous material properties of the workpiece and the existence of build-up edges.

3.3. Performance Criteria

There are two key performance criteria to assess the effectiveness of the vibration control. The first performance criterion is dimensional accuracy, and the second performance criterion is surface finish. These two criteria are correlated to each other. A smooth surface on a machined part assures a high dimensional accuracy achievable. In other words, a machined part must have a satisfactory dimensional accuracy first. Among the two possible nonconforming dimensions in a machining operation, removing more than desired material is usually worse than removing less. It is because the excess remaining material can be removed later through other means and it is usually impossible to recover the lost material from the part.

The second performance criterion is the quality of machined surface because the main reason to have a vibration control system installed is to improve machining quality. The measurement of surface roughness involves the determination of the average linear deviation of the measured surface from the nominal surface. There is a direct relationship between the dimensional tolerance and the permissible surface roughness on a part. Evidently the variations introduced by surface roughness should not exceed the tolerance placed on the dimension. Otherwise, the measurement of the dimension will be subject to an uncertainty that is greater than the required tolerance as illustrated in Figure 3-4. The standard method of measuring surface roughness involves the determination of the average deviation from the mean value. The peak-to-valley of the surface roughness is usually approximately four times the measured average surface roughness in micrometers. This factor will vary somewhat with the character of the surface under consideration.

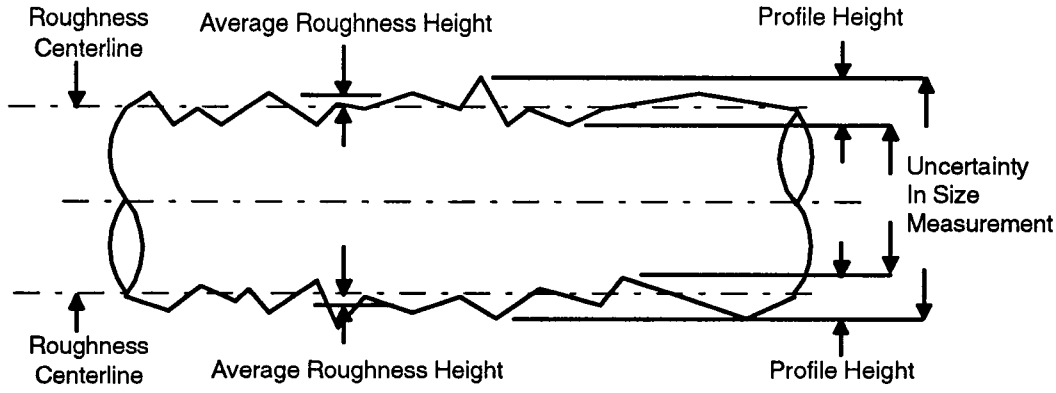

Figure 3-4 Uncertainty in Dimensional Measurement(ASA B46.1-1962)

From these considerations it follows that if the average surface roughness specified on a part exceeds one eighth of the dimensional tolerance, the whole tolerance will be taken up by the roughness height. Thus, it is necessary to specify a suitably small surface roughness, less than one eighth of the dimensional tolerance, in order that useful dimensional measurement can be made.

A typical machined surface profile is shown in Figure 3-5. A corresponding three dimensional surface topography image is reconstructed in Figure 3-6.

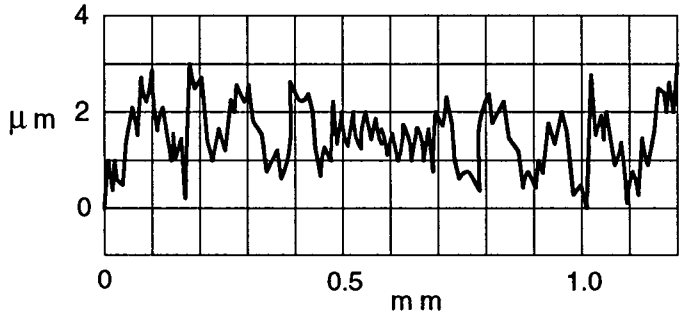

Figure 3-5 Profile Figure

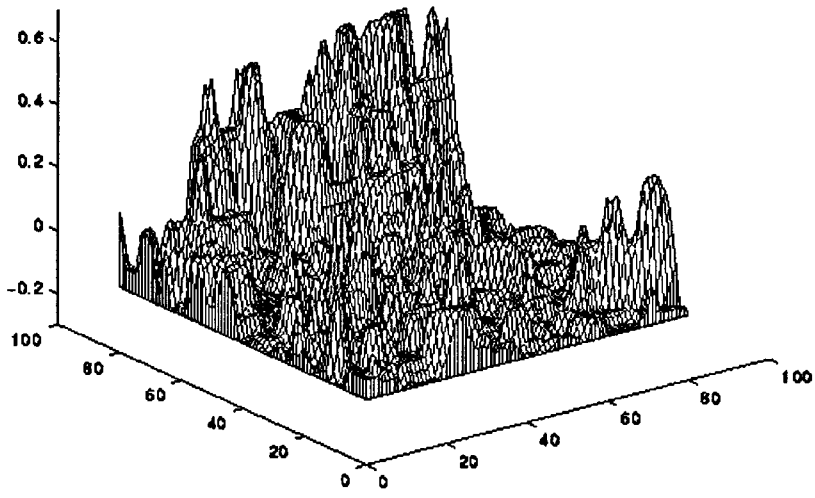

Figure 3-6 3-D Topography Figure

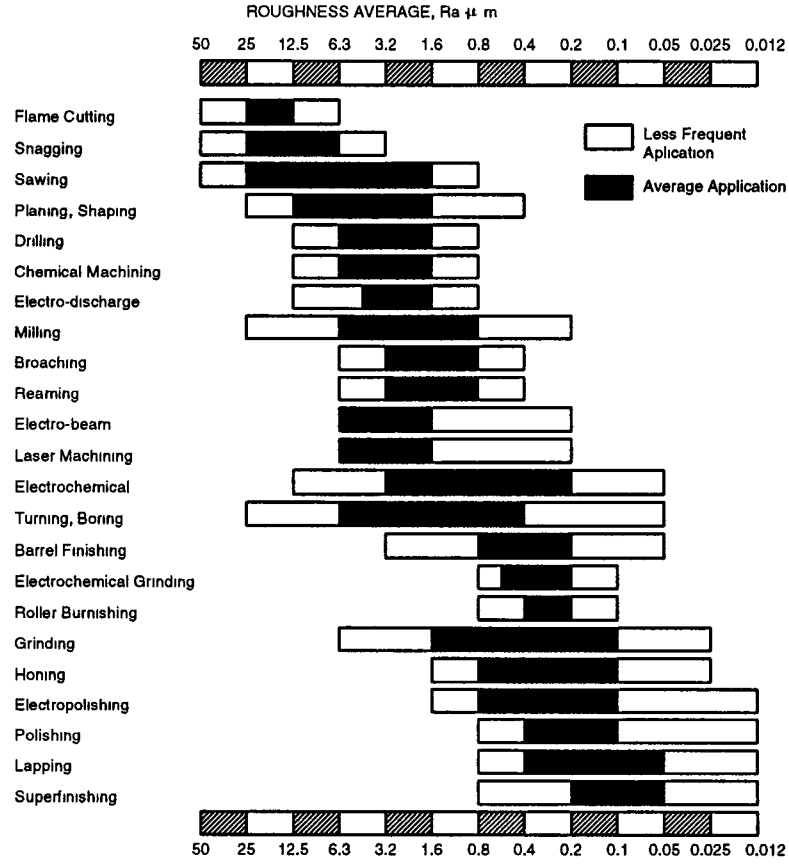

Figure 3-7 Surface Roughness Produced by Common Production Methods

The quantitative values for the surface finish under various machining methods are shown in Figure 3-7 [15]. Generally speaking, the peak-to-valley value is in the magnitude of a micrometer. That means the system should be able to control the amplitude of vibration and chatter in a scale of 10^{-7} m to qualify as sucessful. If the system fails to achieve a better machined surface, there is no need to discuss other performance indicators because nobody will install an add-on system to deteriorate the original system's performance.

Besides the two key performance criteria, other performance indicators will be identified as the system develops in later stages.

3.4. Machining System Modeling (I)

A successful model not only demonstrates a good understanding of the physical system under study, but also provides a convenient virtual testbed for various system testing and evaluation in the later stages.

3.4.1. Considerations and Platform for Building the Model

Since the model should be valid throughout the whole project, there are several considerations which can help to ensure the usability and maintainability of the model;

- graphical user interface
- rich built-in functional library
- minimal programming needs
- high portability

Among available options, an X-Windows based graphical user interface extension of Matlab for model simulation is selected to run on a Sun SparStation. The extension is equipped with various special tools for virtual simulation purposes. In addition, it can

interact with the powerful tool boxes developed for Matlab to facilitate the model building process.

3.4.2. Model Partition and Development

For a complex system, such as a machining system, the virtual system model is prone to be inappropriate and can be extremely difficult. Fortunately, Merritt's model for a machining system has been shown to be a reliable one.

As illustrated in Figure 3-8, the model can be viewed as an integration of four subsystems. The subsystems are external force subsystem, dynamics subsystem, primary subsystem and regenerative subsystem. Models for these subsystems are discussed as follows and all of them are built as a state-space model with the state variable X designated as [dx_1/dt; x_1] where x_1 is the displacement of the cutting tool tip.

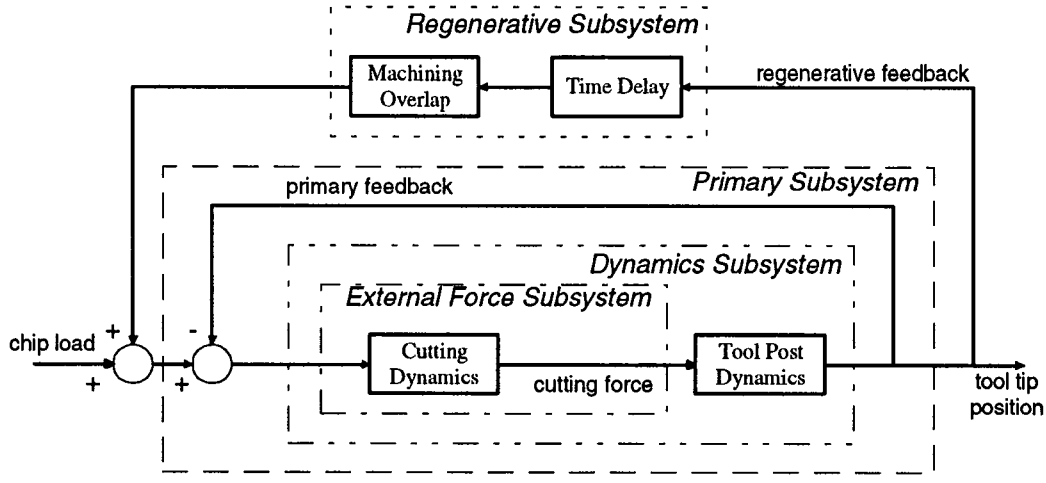

Figure 3-8 Divisions of Merritt's Machining System Model

3.4.3. Cutting Dynamics (Cutting Process)

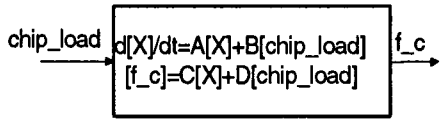

Figure 3-9 Block Diagram for Cutting Dynamics

The cutting process is modelled based on the work of Merritt mentioned in section 2.2.1. A linear model which generates output proportional to its input is used. The state space model for the process is expressed as;

$$A = [0] \qquad B = [0] \qquad C = [0] \qquad D = [k\_c]$$

where k_c is the cutting stiffness and its value, which depends upon the cutting tool, workpiece material and machining conditions, is available in machining data handbook [15].

3.4.4. Toolpost Dynamics

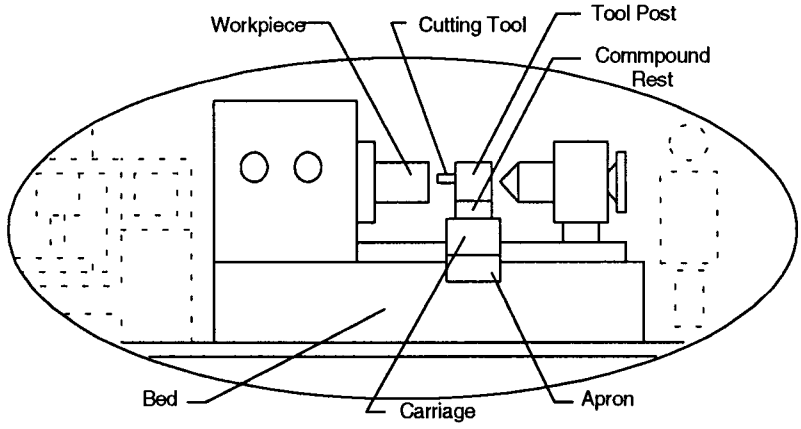

Figure 3-10 Major Structural Components in a Lathe

By examining a lathe, the structural dynamics of a lathe can be viewed as a system dynamics contributed by its components. As illustrated in Figure 3-10, there are five structural components in the lathe structure. They are the tool post, the compound rest, the carriage, the apron, and the bed. According to theories in dynamics, the dynamic characteristics of a system is dominated by the element with the lowest stiffness and smallest inertia. For a lathe, such an element is the cutting tool. In other words, most of the vibration effect will be observed at the linkage between a cutting tool and a tool post. This agrees with observations made on the shopfloor, especially during finish cutting that cutting force is in relatively small magnitude. The vibration is mainly observed in a localized area. Therefore, a lump-sum model having two components to characterize the system rigidity and damping is an appropriate representation of the dynamic behavior of the lathe in the machining system (Figure 3-11).

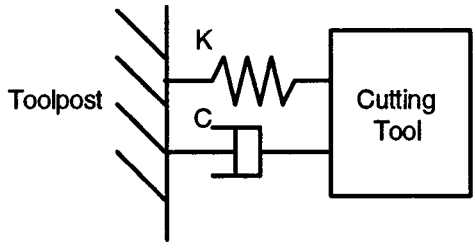

Figure 3-11 Schematic Diagram for the Joint between a Toolpost and a Cutting Tool

As a result, the state-space model of the toolpost structural subsystem is modelled as a one degree-of-freedom dynamic system. The input to the subsystem is the cutting force generated from the machining. The output is the tool tip position relative to the workpiece. The block diagram of the model is shown in Figure 3-12 and the exact expression of the model coefficients are obtained from section and are presented below;

$$A=\begin{bmatrix} -\frac{C_1}{m_1} & -\frac{k_1}{m_1} \\ 1 & 0 \end{bmatrix} \quad B=\begin{bmatrix} \frac{1}{m_1} \\ 0 \end{bmatrix} \quad C=[0 \quad 1] \quad D=[0] \qquad X=[x]$$

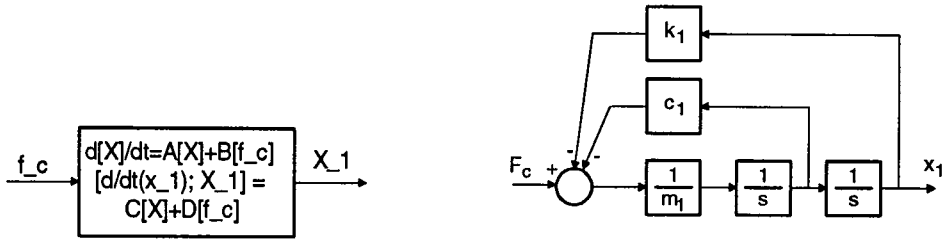

Figure 3-12 Block Diagram for Tool Post Dynamics

3.4.5. Dynamic Subsystem

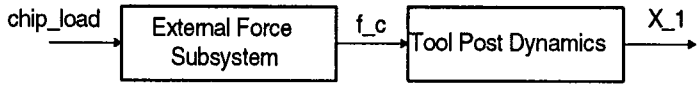

Figure 3-13 Block Diagram for Dynamic Subsystem

A dynamic subsystem is a subsystem containing all the vital information about the dynamic characteristics of the overall system excluding detail feedbacks. It is formed by connecting the external force subsystem in series with the tool post dynamics. This dynamic subsystem takes the chip load as well as the tool tip position as its inputs and generates the next tool tip velocity and tool tip position as its outputs.

3.4.6. Primary Subsystem

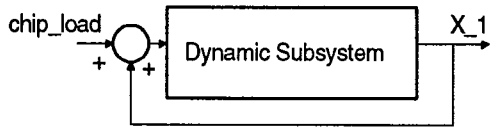

Figure 3-14 Block Diagram for Primary Subsystem

The primary subsystem is named as it contains the primary feedback path of a machining process. It is done by feeding the complement (or negative) of the second output (tool tip position) of the dynamic subsystem into its first input which is the chip load.

3.4.7. Time Delay

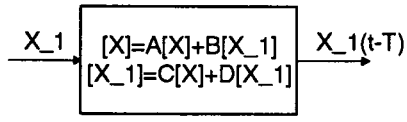

Figure 3-15 Block Diagram for Time Delay

The time delay is due to the repetitive nature of a turning process. The amount of time delay is equivalent to the amount of time elapse for one revolution, 60/n, when n is the turning speed of the machining process expressed in revolution per minute (rpm). Since there is no exact mathematical expression for a time delay process in a state space format, Pade approximation is used to model the time delay.

Pade approximation is a mathematical approximation for a time delay. The Pade approximation can be developed by writing the transfer function for a time delay as

$$e^{-t_d s} = \frac{e^{-t_d s/2}}{e^{t_d s/2}} \tag{3-1}$$

then expanding the exponential functions in both the numerator and denominator in a Taylor series. The desired accuracy determines the number of orders of expansion used. For the first-order Pade approximation, the truncation at each series is after the linear terms

$$e^{-t_d s} = \frac{1-(t_d/2)s}{1+(t_d/2)s} \tag{3-2}$$

A comparison of the exact and first-order approximate transfer function indicates that the gain curve is correct but that deviations start to occur in the phase curves at values of $t_d\omega$ greater than about 0.75. The deviation point is shifted to approximately 2.0 for the second-order approximation model[10]. As an initial trial, a third order Pade approximation model is built.

3.4.8. Machining Overlap

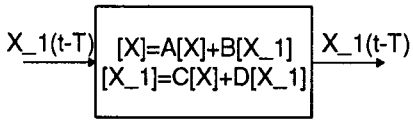

Figure 3-16 Block Diagram for Machining Overlap

The machining overlap is simply used to express the interaction effect between feed and width of cut. Therefore, the state space model is

$$A = [0] \qquad B = [0] \qquad C = [0] \qquad D = [\mu]$$

where μ is the overlap factor ranging from 0 to 1.

3.4.9. Regenerative Subsystem

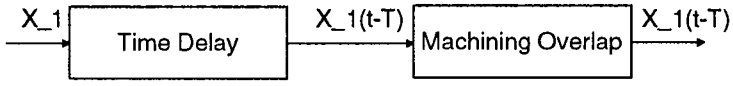

Figure 3-17 Block Diagram for Regenerative Subsystem

The regenerative subsystem is to represent the memory of a machining process. As discussed in section 2.3.3, the amount of chip load is the sum of the preset chip load and the residual material from the previous cut. For turning, if the cutting tool moves away from the

workpiece during the previous revolution as a result of its vibration, the cutting tool will leave certain amount of workpiece uncut. In that case, the cutting tool will have to cut those uncut material and the preset amount of material so as to achieve desired finish dimension. Therefore, the subsystem is constructed by connecting the time delay and the machining overlap in series.

3.4.10. Overall System

The overall system is a complete model to represent the lathe, the physics behind a machining process and the interactions between them. It is by feeding the second output of the primary subsystem to the input of the regenerative subsystem and then directing the output of the regenerative subsystem back to the first input of the primary subsystem.

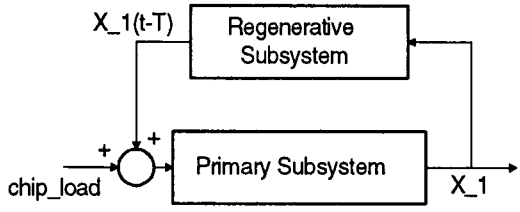

Figure 3-18 Block Diagram for Overall Machining System Model

3.4.11. Results

The virtual model of the system is implemented in Matlab and the schematic diagram for the system in Matlab is shown in Figure 3-19. At the same time, a Matlab script file is written for defining variables. The script file is listed in the Appendix section. An arbitrary set of values (Table 3-1) is used for testing the model and sample output from the model is shown in Figure 3-21.

Table 3-1 Simulation Settings

Variable	Value
preset chip load	0.0001m
mass	0.9kg
stiffness	$1x10^8$N/m
damping factor	0.09
cutting stiffness	$1x10^6$N/m
time delay	0.001sec
overlap factor	0.8

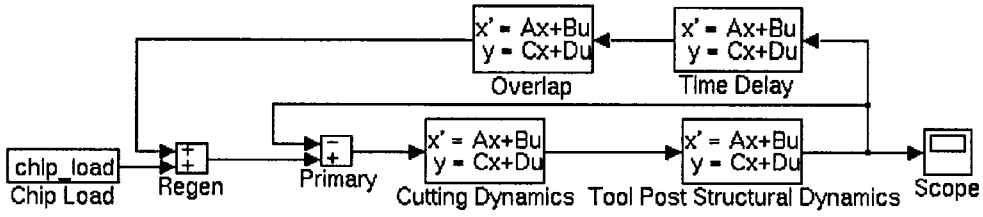

Figure 3-19 Schematic Diagram for the Machining System in Matlab

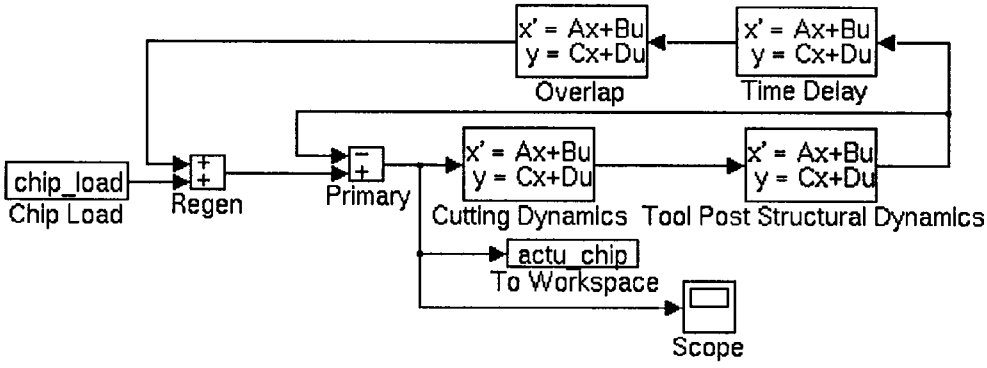

Figure 3-20 Modified System Layout for Data Acquisition

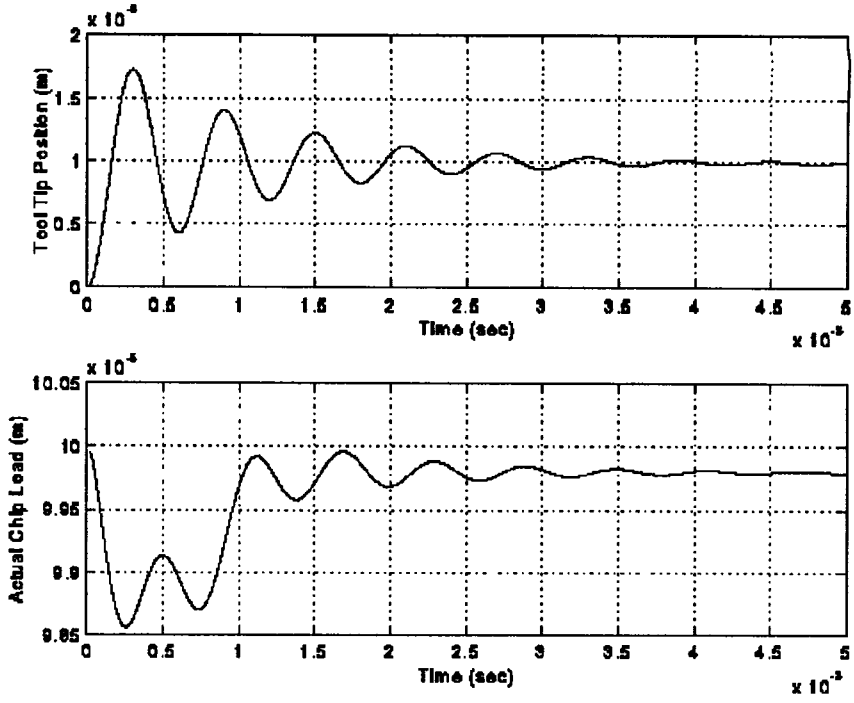

Figure 3-21 Sample Simulation Results (tool tip position:top; actual chip load:bottom)

3.5. Machining System Modeling (II)

Having the basic machining system model built, the vibration control model is built and integrated to the basic model. The purpose is to examine the effectiveness of vibration control under various control schemes. The complete system is partitioned into six subsystems as shown in Figure 3-22. The six major subsystems are smart tool post structural subsystem, actuator subsystem, controller subsystem for the actuators, cutting dynamics subsystem, overlap subsystem, and time delay subsystem. Among the six subsystems, only the actuator subsystem and its controller subsystem are new to the previous machining system model. Details about the new subsystems are followed.

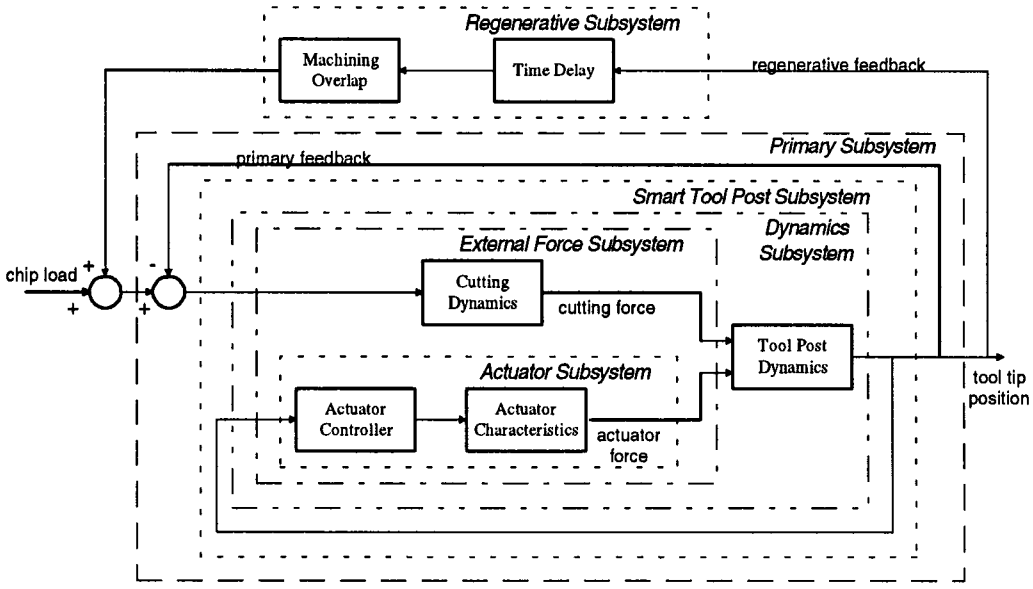

Figure 3-22 Complete Layout for the Vibration Control Model

3.5.1. Actuator (Characteristics)

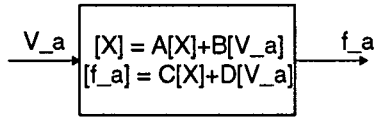

Figure 3-23 Block Diagram for the Actuators

The actuator is a simplified linear model. The relationship between its input, voltage supplied from the controller, and its output, actuating force is directly proportion to a constant, Ka. The Ka is the slope of the linear range of the actuator force vs. applied voltage graph obtained from experiment. The same method is used to build the model for cutting dynamics model.

The actuator is first modeled as a linear model which shows that an actuator has a nearly linear characteristics over a normal operating range. Thus, the model in its state space format is

[A] = [0] [B] = [0]

[C] = [0] [D] = [k_a]

where k_a is the ratio of force to input voltage for a particular type of actuator.

3.5.2. Controller

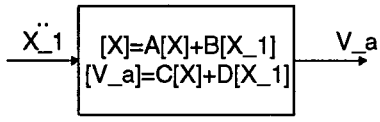

Figure 3-24 Block Diagram for the Controller

The controller is modeled to generate its output based on the acceleration at the tool tip position. Since searching for an optimal control scheme is not the objective at this stage, a simple proportional-plus-integral-plus-derivative (PID) controller model is used. The simplicity of such a model helps to keep the building process manageable although the PID control scheme is unlikely the optimal model. The state space model for this model is

$$[A]=\begin{bmatrix}0 & 0 & 0\\ 1 & 0 & 0\\ 0 & 1 & 0\end{bmatrix} \quad ;[B]=\begin{bmatrix}1\\ 0\\ 0\end{bmatrix} \quad ;[C]=[kd\ \ kp\ \ ki] \quad ;[D]=[0]$$

$$X=\begin{bmatrix}\dot{x}_1\\ x_1\\ \int x_1\end{bmatrix} \quad ;U=[\ddot{x}_1] \quad ;Y=[\,V\,]$$

where kd is the derivative gain, kp is the proportional gain, ki is the integral gain and V is the voltage used to drive the actuator.

3.5.3. Actuator Subsystem

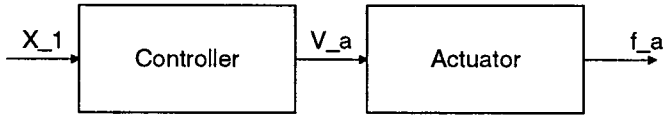

Figure 3-25 Block Diagram for the Actuator Subsystem

The actuator subsystem is composed of the actuator and its controller. By connecting the two components in series, an actuator subsystem is formed. The tool tip position is the input while the actuator force is its output.

3.5.4. External Force Subsystem

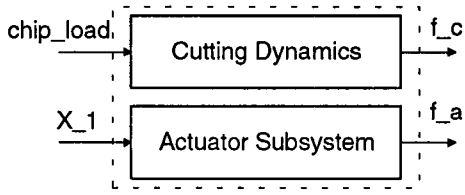

Figure 3-26 Block Diagram for the External Force Subsystem

The external force subsystem is formed by appending the cutting dynamics model and actuator subsystem together. It represents all the external forces acting on the tool post structure. The inputs are chip load and tool tip position while the outputs are cutting force and actuator force.

3.5.5. Structural Dynamics (Tool Post Dynamics)

The tool post structural subsystem is a state-space model for a two degree-of-freedom structure. The change from the one degree-of-freedom structure to the two degree-of-freedom structure is to examine the effect of the structural dynamics to the machining

system. The two inputs to the subsystem are the cutting force generated from the machining process and the actuating force generated by actuators. The two outputs are the tool tip position and its velocity.

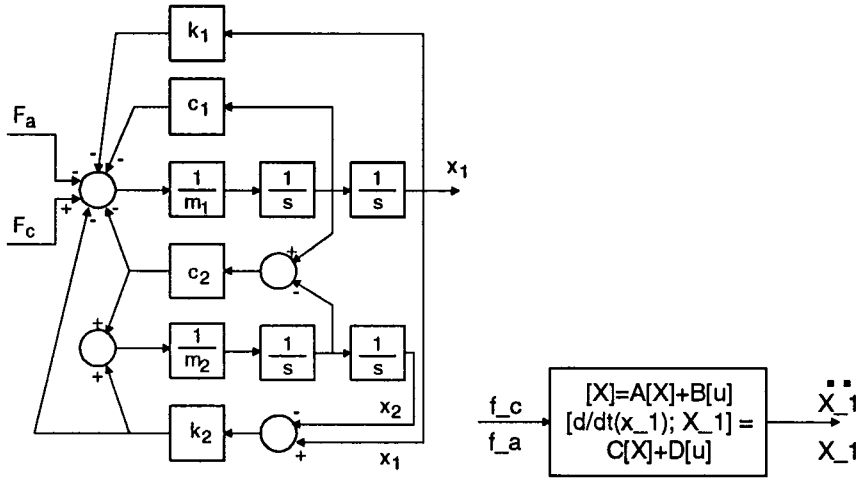

Figure 3-27 Block Diagram for the Structural Dynamics

The tool post dynamics is modeled according to a two degree-of-freedom system which is subjected to two external forces which are represented by an external force subsystem.

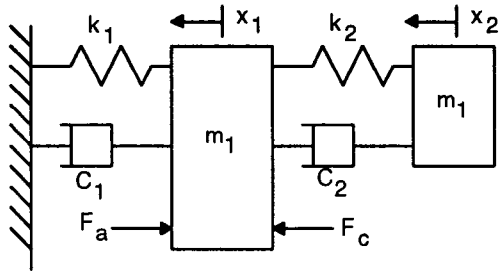

Figure 3-28 Schematic Diagram for the Two Degree-Of-Freedom System under Study

The schematic diagram for the dynamic model is shown in Figure 3-28. It consists of two rigid masses connected in series with an ideal spring and a damper. The m_1, k_1, C_1

represent the mass, stiffness and damping coefficient for the primary structure. The m_2, k_2, C_2 represents the mass, stiffness, and damping coefficient for the secondary structure. Assumption is made that the primary structure is the one subjected to external forces. The equations of motion that characterize the dynamics of the system are derived as follows.

Based on Newton's law, $\Sigma F = ma$, two equations are obtained to described the dynamics of the masses individually.

$$k_2(x_1 - x_2) + c_2(\dot{x}_1 - \dot{x}_2) = m_2 \ddot{x}_2 \tag{3-3}$$

$$F_c - F_a - k_1 x_1 + k_2(x_2 - x_1) - c_1 \dot{x}_1 + c_2(\dot{x}_2 - \dot{x}_1) = m_1 \ddot{x}_1 \tag{3-4}$$

Therefore,

$$\ddot{x}_1 = -\frac{(c_1 + c_2)}{m_1}\dot{x}_1 - \frac{(k_1 + k_2)}{m_1}x_1 + \frac{c_2}{m_1}\dot{x}_2 + \frac{k_2}{m_1}x_2 + \frac{F_c}{m_1} - \frac{F_a}{m_1} \tag{3-5}$$

$$\ddot{x}_2 = \frac{c_2}{m_2}\dot{x}_1 + \frac{k_2}{m_2}x_1 - \frac{c_2}{m_2}\dot{x}_2 - \frac{k_2}{m_2}x_2 \tag{3-6}$$

From these two equations, the state space model which represents the dynamic characteristics of the system is expressed as follows.

$$\dot{X} = AX + BU \tag{3-7}$$

$$Y = CX + DU \tag{3-8}$$

where $X = \begin{bmatrix} \dot{x}_1 \\ \dot{x}_2 \\ x_1 \\ x_2 \end{bmatrix}$; $U = \left[(F_c - F_a)\right]$; $Y = \begin{bmatrix} \ddot{x}_1 \\ x_1 \end{bmatrix}$;

$$A = \begin{bmatrix} -\frac{C_1 + C_2}{m_1} & \frac{C_2}{m_1} & -\frac{k_1 + k_2}{m_1} & \frac{k_2}{m_1} \\ \frac{C_2}{m_2} & -\frac{C_2}{m_2} & \frac{k_2}{m_2} & -\frac{k_2}{m_2} \\ 1 & 0 & 0 & 0 \\ 0 & 1 & 0 & 0 \end{bmatrix} \tag{3-9}$$

$$B = \begin{bmatrix} \frac{1}{m_1} \\ 0 \\ 0 \\ 0 \end{bmatrix} \tag{3-10}$$

$$C = \begin{bmatrix} \frac{-(c_1 + c_2)}{m_1} & \frac{c_2}{m_1} & \frac{-(k_1 + k_2)}{m_1} & \frac{k_2}{m_1} \\ 0 & 0 & 1 & 0 \end{bmatrix} \tag{3-11}$$

$$D = \begin{bmatrix} \frac{1}{m_1} \\ 0 \end{bmatrix} \tag{3-12}$$

3.5.6. Results

The model of the new system is implemented in Matlab and the scematic diagram for the system built in Matlab is shown in Figure 3-29. At the same time, a Matlab script file is written for defining variables. The script file is listed in the Appendix section. A set

of values (Table 3-2) which is similar to the set of values used in the previous model is used for testing the model and sample output from the model is shown in Figure 3-30.

Table 3-2 Simulation Settings

Variable	Value
preset chip load	0.0001m
mass 1	0.9kg
mass 2	0.1kg
stiffness k_1	$1x10^8$N/m
stiffness k_2	$1x10^6$N/m
damping factor	0.09
cutting stiffness	$1x10^6$N/m
time delay	0.001sec
overlap factor	0.8
kd	0.01V/(m/s)
kp	1V/m
ki	1V/(ms)
Actuator Characteristics	1N/V

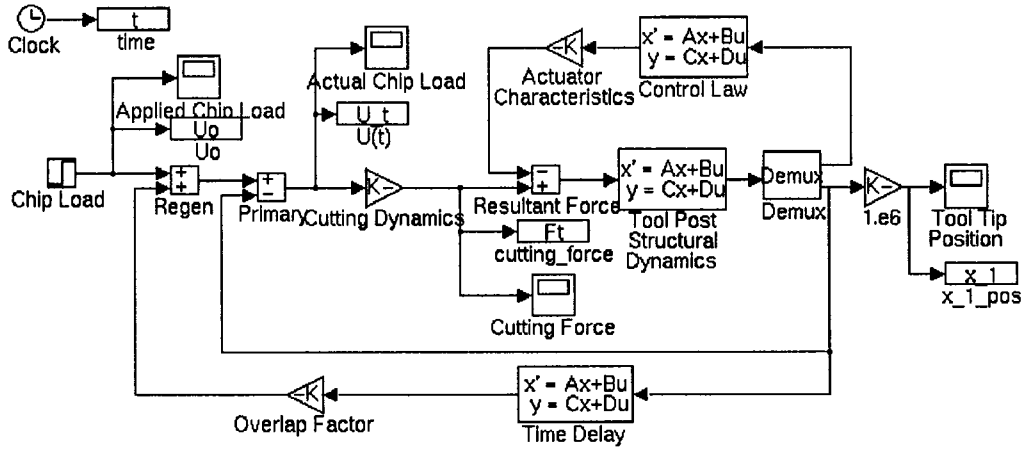

Figure 3-29 Schematic Diagram for the Complete Vibration Control System

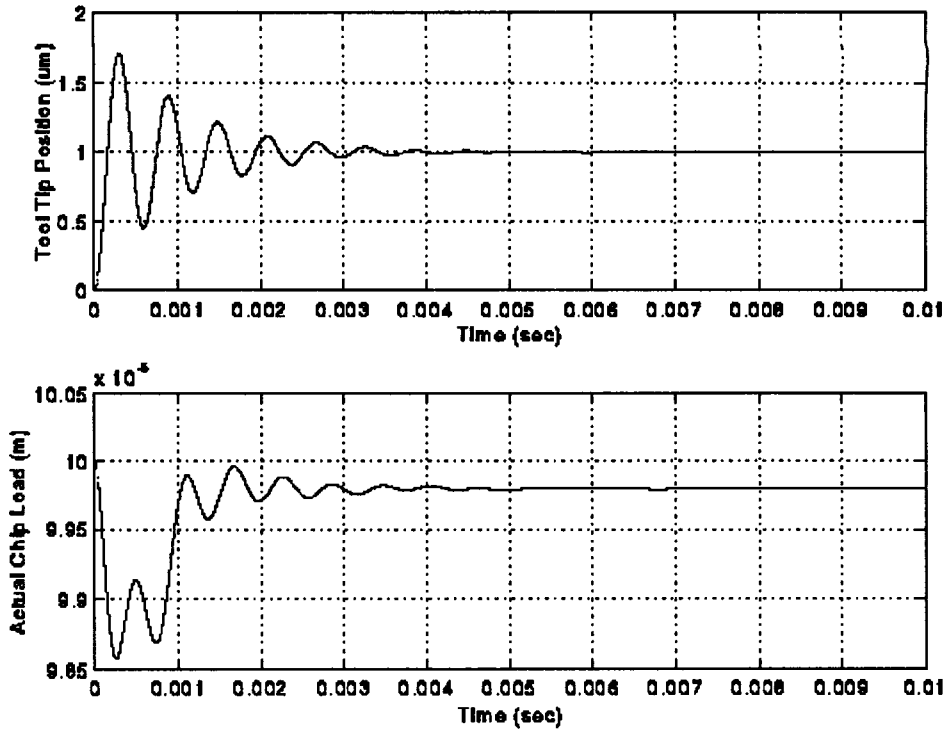

Figure 3-30 Sample Simulation Results (tool tip position:top; actual chip load:bottom)

3.6. Summary

The model is completed satisfactorily. From the simulation results, the tool tip displacement matches the dynamic characteristics of the assumed tool post structure. In addition, the irregular changes in the actual chip load is as expected caused by the feedbacks in the system model. Therefore, the model is suitable for testing and evaluating the vibration control system in the later stages.

4. Formalization of the Design Concepts

After reviewing the development in machine tool related technologies and examining the operations of a machining system, an effort is put into summarizing all the findings and their contributions to machine tool vibration. The work presented in this chapter is related to identifying the keys of solving the problem and to formalize the outlines of an ideal vibration control system applied to machine tools.

4.1. Design Specifications

Before exploring in detail, there are several specifications that the final designed machine tool vibration control system must meet so as to perform properly. The specifications are listed as follows:

1. Natural frequency of the first mode should be, at least, 500 Hz to cope with the observation that the spectrum of the cutting force generally spans up to 400 Hz.

2. The static stiffness has to be high enough to ensure that the tool vibration to be compensated during machining is limited to a range that linear approximation can be applied with satisfaction.

3. The flexibility has to be sufficient so that the anti-vibration force exerted by the actuators is at an order which is comparable to the order of the vibration force induced during machining. This means that the mechanical stucture should give the authority to the actuators for vibration compensation.

4.2. Keys to the Solutions of the Problem

Based upon the study of machine tools and the machining system simulation, there are three major causes of tool vibration. They are dynamic variation of the cutting force, dynamic characteristics of the machine tool structure, and the interaction between cutting force and structural dynamics. The complications and difficulties of dealing with these three causes are shown by the long existence of the problem. Researchers were used to isolate the causes and to deal with one cause at a time. This narrow-scope approach downplays the significance of the machining system running as an integrated entity. Thus, the results obtained so far have had limited minimal improvement in the vibration suppression capability.

From a system engineering perspective, attention should be paid not only to the components in a system, but also to the interactions between components in order to ensure a satisfactory overall system performance. By taking this view, a systemwide characteristic of the three vibration causes is identified.

The common characteristic nature among the three causes is their vibration energy generation nature. A machine tool is usually stable and predictable over a period of time after the initial cut because of the presence of damping in the system. The continuous tool vibration is mainly due to a continuos supply of vibration energy during machining.

About possible solutions to this situation, there are two basic approaches. One approach is to discontinue the supply by removing the undesired vibration energy source, but it is almost impossible to implement in practice. For example, the non-homogeneous material properties which cause variations in the cutting force always exist in the real life

practice. The other approach is to remove the undesired energy as soon as it appears. Although energy cannot be destroyed, energy can be absorbed and dissipated. As a result, the vibration control system should be designed following either one or both of these two strategies; vibration energy absorption and vibration energy dissipation(Figure 4-1).

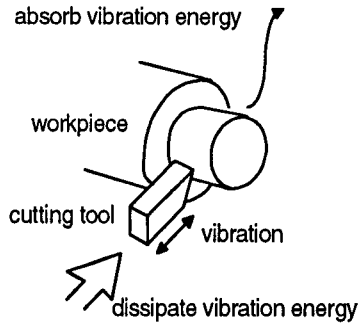

Figure 4-1 Vibration Control Concepts to be Followed

In summary, the key to solve the machine tool vibration problem is to build a vibration control system which is capable of removing the vibration energy entering the machining system at a rate fast enough to avoid the occurrence of vibration. In an ideal situation, the removal process will be implemented in real time without delay. In other words, the faster the designed system responds, the better the vibration attenuation the system can achieve.

4.3. System Design

Since the speed of the system response is crucial to the success of the system, the machine tool vibration control system must be able to identify its stimulus and to respond to it in a timely manner. In addition, the system must be capable of attenuating a wide frequency spectrum of energy because the vibration energy in machining system varies over

a wide frequency range. Under these two guidelines, it is conceivable why the reported results for active vibration control generally have better performance than the results from passive vibration control. The active control system can sense the state of the system under control and react to it based upon a control law. Therefore, the layout for the design concept of the system is similar to an active control system as illustrated in Figure 4-2.

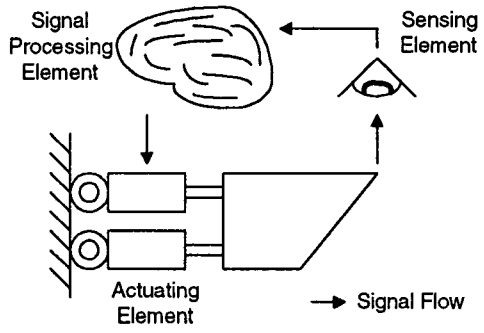

Figure 4-2 Schematic Diagram for the Design Vibration Control System

As shown in Figure 4-2, the vibration control system will consist of a sensing element, a signal processing element, and actuating elements. With this setup, the system will be capable of implementing a wide range of control laws. However, besides the components in a typical active control system, there is one important element in the schematic diagram, that is the cutting tool.

As discussed earlier, the overall system performance cannot be optimized unless steps are taken to deal with not only the components in a system, but also the whole system. From the system layout, the cutting tool which represents the machine tool apparently plays a significant role besides its contribution to the structural dynamics in the machining system. If the tool is fixed to the ground (theoretically speaking), the actuating elements will not be able to respond to the vibration force generated during machining because they are

essentially separated by a wall. On the other hand, a loosely held cutting tool cannot do the job either because the low stiffness of the structure affects the structural dynamics of the machining system adversely.

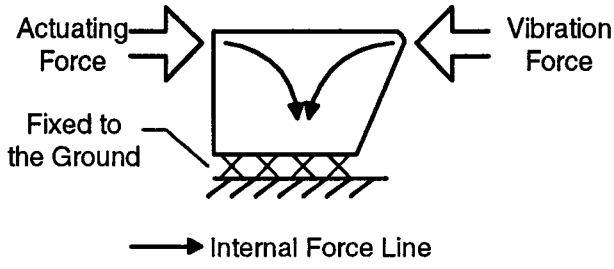

Figure 4-3 Force Line in the Fixed Cutting Tool

4.3.1. System Reliability and Backup System

Besides the system performance, the reliability of the system is also an important issue. Considering the system complexity presented and the environment under which the system operates, it is unavoidable to have one or more components in the system failed from time to time. Since the components interact in a serial manner, the failure of a single component will cause a systemwide breakdown. Therefore, it is necessary to add a redundant vibration control system to the current system layout.

Although it is possible to add an additional component in parallel with or as a backup unit for each system component to increase the overall sytstem reliability, this is a rather costly solution. In addition, the overall system reliability still relies on the reliabilities of the same types of components. Given the fact that mechanical components generally have higher reliability than other kind of components, a simple mechanical secondary vibration control system is preferable.

Since an active vibration system is usually more complex and marginal performance is usually acceptable for a backup system, a simple passive vibration control system is considered. The desired backup system is a simple system with acceptable vibration attenuation ability. One common way is to fine tune the primary system parameters to minimize vibration in the first place with the active vibration control system disabled. The other common way is to impose an attachment to the primary system with a hope that the attached system absorbs the dominant vibration energy. The success of this vibration absorption system hinges on the efficiency of the absorption process as well as the identification of the dominant vibration energy. Since both passive measures are highly feasible to implement, both measures will be carried out in the system design layout.

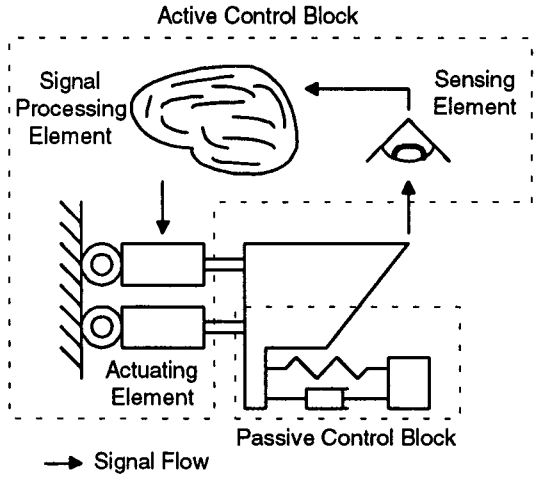

Figure 4-4 Schematic Diagram for the Final System Layout

Consequently, the final system design layout is shown in Figure 4-4. The uniqueness of this fundamental design concept is the implementation of both active and passive vibration control schemes in a machining system. Although the fine tuning measure

is not shown in the schematic layout, it will be carried out when the design optimization stage is reached.

4.4. Realization of the Design Concept — Smart Tool Post

Although the design concept is formalized, there is another question which remains unanswered. The question is what the execution method is. Since the current study focuses on the mechanical portion of the system, the question will be how to design a mechanical structure which meets the defined objective of an effective vibration control. As indicated in the analysis of machining system, the vibration phenomenon is mostly observed at the cutting tool area. Thus, the control system is best to be implement as close to the cutting tool as possible. Knowing that the linkage between the cutting tool holder and the bed of the lathe is the weakest joint in the overall machine structure, implementing the control system at the tool post is a natural choice. Since the new design of the tool post is a smart structure, the designed vibration control system for a lathe is called smart tool post.

4.4.1. Mechanical Realization - Attempt #1

Taking the design concept as the foundation, the first mechanical design was made at the beginning of 1994 and its schematic diagram is shown in Figure 4-5. The design consists of four main parts; a cutting tool holder, a vibration absorber, bearing bars, and a case. The cutting tool holder and the vibration absorber are connected together through springs and actuators while the bearing bars provide precision linear motion guidance as well as support for two aluminum parts. Having two linear bearings built in each block, each block can move freely along the rod. One of the blocks has a cutting tool installed to

act as a cutting tool holder. Another block is simply a mass which is connected to the tool holder block through a spring. In that way, the block becomes a vibration absorber for the tool holder block. A casing is used to support the bars and contain all the parts. The controller is a separate device and is connected to the actuators through electrical means. Since the controller is planned to be an electronic component, its design will not be discussed here.

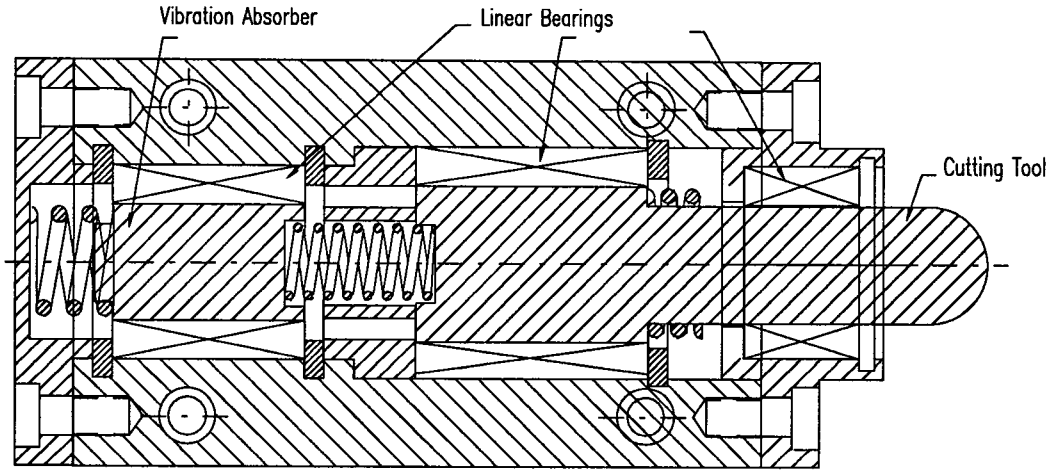

Figure 4-5 First Mechanical Design for the Vibration Control System

The uniqueness of this design approach includes its simplicity and flexibility. Two simple metal blocks function as a tool holder and a vibration absorber as well. Although the blocks are simple, the precision of their movements are guaranteed by the linear bearings and shafts installed. In addition, the tool holder block is designed with a standard size tool accommodation. This can assure the interchangeability of cutting tools between the new tool post and the conventional tool post. Thus, a potentially huge re-tooling cost following the adoption of the vibration control system can be avoided.

Another cost saving comes from the extensive use of off-the-shelf products for high production cost components. The linear bearings, shafts, and springs are commonly available as standardized components, so their quality and price are always competitive. Besides these, the easy access to the blocks and springs can ease the adjustment task during both testing and operation stages. Having all these merits and implementing both active and passive vibration control schemes, the design is expected to perform satisfactorily until the discovery of a fatal weakness in the design.

The fatal weakness in the design is the unknown dynamic behavior of the system under a cyclic small displacement (usually in micrometer scale) during machining. Although the friction between linear bearings and bearing shafts is usually low and uniform, the low and uniform friction phenomenon is under the condition that the two objects have relative motions to each other. The magnitude of friction changes abruptly when switching between static and dynamic states. Given that the blocks are going to have a sinusoidal motion throughout the whole machining operation, it is equivalent to the blocks switch between the static and dynamic states. It makes the dynamic characteristics of the system unpredictable.

Several attempts were made at that time to modify the design to avoid the uncertainty brought by friction, but in vain. Therefore, a complete redesign of the vibration control system was sought immediately afterwards and the result of the redesign effort is the current design of the vibration control system that follows.

4.4.2. Mechanical Realization - Attempt #2

The redesign of the vibration control system represents a breakthrough from the first design. The redesigned system consists of four main parts; namely a cutting tool, a vibration

absorber, membranes, and a case. The adoption of membrane components leads to a significant reduction of the overall size of the tool post structure by more than 50%. This change is a highly favorable because it can minimize the installation space needed. Given that the valuable working area is fixed for a machine tool, less space is occupied by the vibration control system, more working area can be utilized for production.

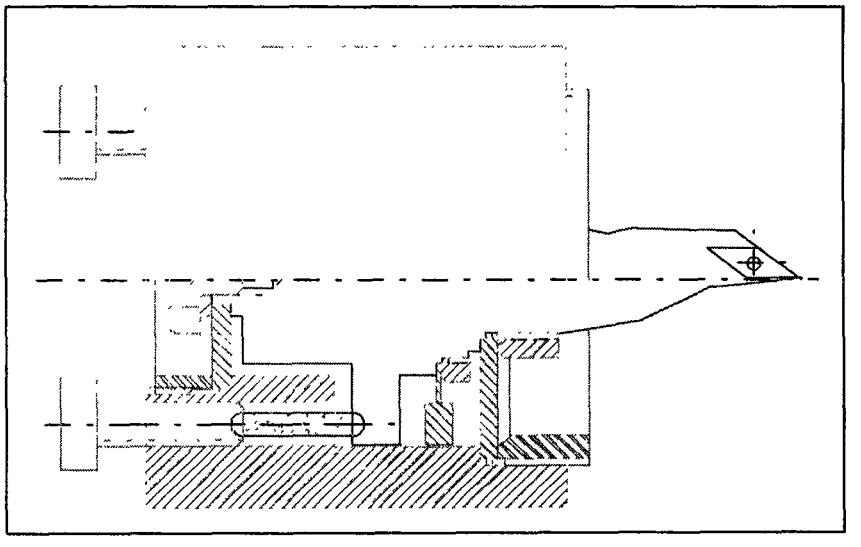

Figure 4-6 Cross Section of the Smart Tool Post

Although the new design is smaller in the overall size, there is no compromise made in terms of its functionality. On the contrary, the new design has more merits over the original design besides the reduction in size. For instance, the integrated actuator housings with the smart tool post casing eliminates the relative movement between the two elements. Reducing the number of moving parts in a structure can increase the structural stiffness as well as simplify the mathematical analysis of the structure.

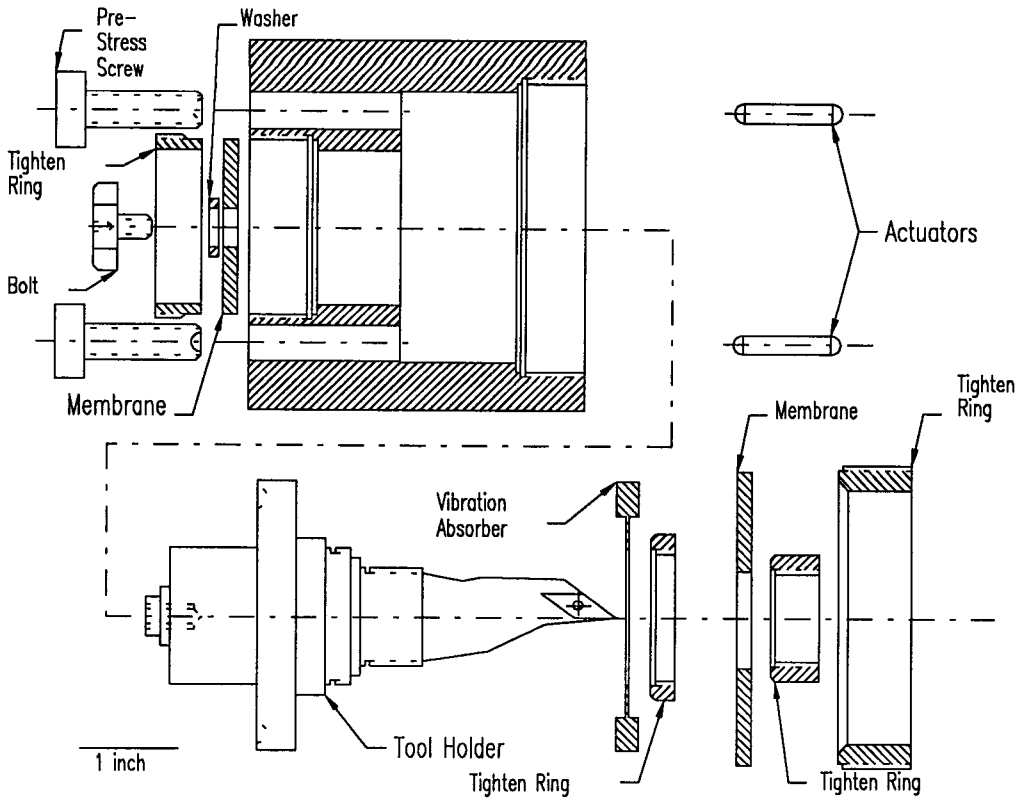

Figure 4-7 Smart Tool Post Layout

4.4.2.1. Major Changes in the Design

4.4.2.1.1. Membrane structures

Replacing springs with membranes is one major change in our design approach. This change has provided great rewards in terms of dynamic behavior and overall size of the system. As illustrated in Figure 4-8, a membrane can be viewed as a diaphragm which is being supported along its edge to withstand loading applied on its surface from an engineering perspective. The uniqueness of a membrane includes its low axial stiffness, but relatively high transverse stiffness. Consequently, the membrane can replace the bearing bars and its supports perform in the preliminary design to support the cutting tool holder and

the vibration absorber. Besides providing transverse supports, the membrane can maximize the authority of the actuators while keeping the integrity of the structural dynamics of the machining system. The relatively low stiffness along the actuating force direction allows actuating force to react to the vibration force. Removing the bearing bars alone reduces the overall dimension by over 30%.

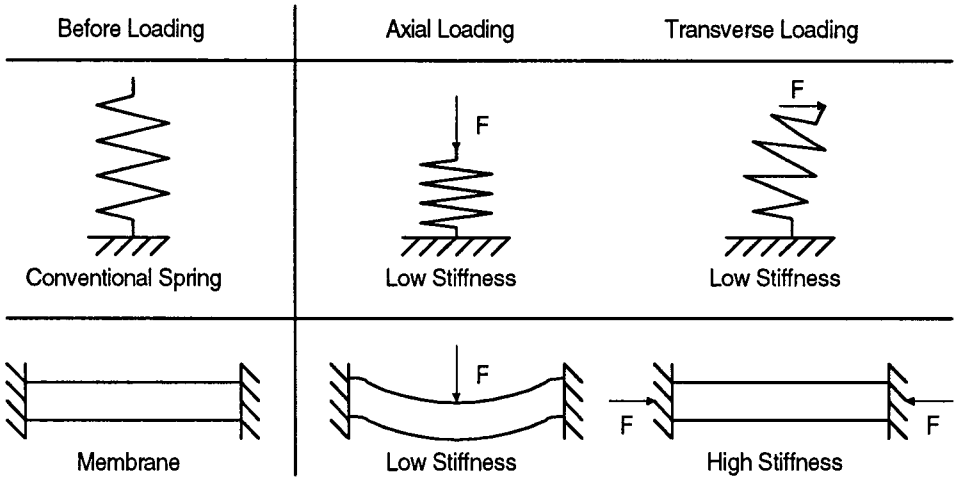

Figure 4-8 Characteristics of a Membrane Structure vs. a Spring

4.4.2.1.2. Cylindrical-shaped components

The second major change is that most of the components in the final design are in cylindrical shape contrary to the blocks found in the first design. This change is partially due to the introduction of membrane structures to the design. However, this change is mainly due to a consideration of realizing a uniform load distribution on cylindrical objects. Figure 4-9 illustrates how the actuators can take advantage of the six designed actuator housings in vibration control. This design change offers three alternative ways to provide anti-vibration force. Alternatives 1, 2, and 3 utilize two, three, and six actuators

respectively. It is evident that the current cylindrical-shape can reduce the occurrence of local stress concentration. Loading produced by machining is distributed uniformly. Without the existence of torque and local stress concentration, the mathematical structural analysis becomes easier to handle. As a result, a mathematical model which better describes the tool post performance can be built.

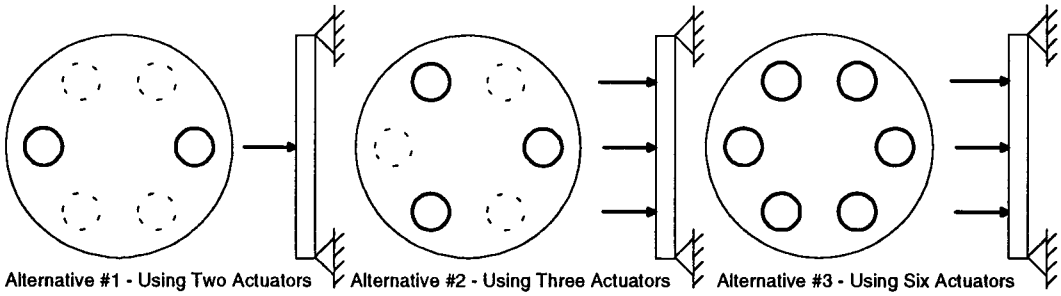

Figure 4-9 Alternatives for Actuator Arrangement

4.4.2.1.3. Tightening rings

The third change is that the components are tightened together by tightening rings. As illustrated in Figure 4-10, the components can be positioned in a desired way and adjusted before tightening together by screwing in tightening rings. If the components are screwed together without the ring structure, the components will be randomly positioned and may be different in their relative positions to each other every time they are tightened.

In addition, the design is more fault-tolerant. As shown in Figure 4-10, even when the membrane is in an oval shape(shaded area), the assembly will still be able to maintain an acceptable contact boundary(pointed by arrows). As long as the interior dimensions of the base and the tightening ring are close to each other, the contact boundary will be a circular ring.

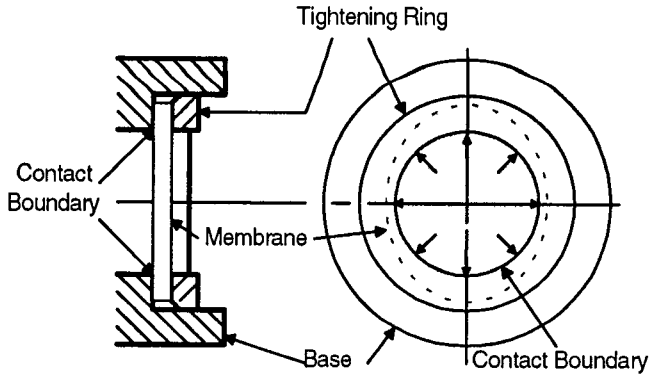

Figure 4-10 Illustration of the Fault-Tolerant Character of Using Tightening Rings

4.4.2.1.4. Change in Vibration Absorber

The forth major change is a modification of the vibration absorber. The vibration absorber in the final design is about 90% lighter and smaller than that in the first design while maintaining its functionality to the vibration control system. This significant improvement demonstrates the realization of the physics of a vibration absorber. The absorber is capable of absorbing vibration energy from the object to which it is attached mainly because the natural frequencies of the absorber and the object are very close to each other with the natural frequency of the absorber which is always in the lower side. The current design uses a smaller mass with lower stiffness to achieve the natural frequency requirement. In addition to a smaller size, a by-product of the lighter design is a faster response due to its small inertia.

4.4.2.2. Precautions Taken During Design Formalization

As discussed above, the concept of system optimization is considered in the redesign process. However, the uncertainty about the behavior of system components during

operation also presents a potential danger to call for another cycle of redesign. In addition, another challenge in the redesign process is to decide whether an optimal design of the mechanical structure will provide an optimal or a favorable pre-condition for the controller design. Special attention has been paid to the redesign process to these new challanges, and precautions are taken to ensure that the designed mechanical structure offers a comfortable environment to the controller design and possesses the desired adoptability when it is operated under a variety of machining conditions.

The two precautions taken are listed as follows:

1. six actuator housings are designed which are uniformly distributed on the base of the smart tool post structure. This arrangement offers three alternative ways to provide a balanced anti-vibration force. The first way is to place two actuators in diagonal. The second way is to place three actuators along the circumference with an empty housing right next to each actuator. The last way is to place six actuators in all available housings. These alternatives make it possible to offset the vibration force in an adjustable manner which is very effective and efficient vibration. However, this compensation method has its limitation. When the vibration force is either too small, or too large, then all the three alternatives may fail to do the job.

2. The system rigidity is designed to be capable of making changes. In order to do so, circular membrane components are used to function as the energy conservation devices. By varying the thickness of the circular membranes, the system rigidity can vary in a relatively large scale.

The combination of this two precautions accomplishes an initial stage of design optimization which provide a very effective way to optimize the system.

4.5. Summary

Major considerations for designing the mechanical structure of the smart tool post have been presented in this chapter. Efforts have been made to ensure that the design specifications are met and the designed mechanical structure has laid a solid foundation for the controller design. It should be admitted that the mechanical structure design is not an optimal one due to the system complexity and the uncertainty about the behaviors of some components. However, careful pre-cautions have been taken to keep the possible negative impact at its minimal level. As evidenced in the discussion, the finalized mechanical structure embodies the considerations of fine-tuning on the properties of each system component and a mechanical vibration absorber. The product of this design concept development stage is an intermediate mechanical structural design of the system. The next stage in this investigation will be a set of experiments to characterize the performance of certain critical components in the system. The experimental confirmation will further enhance the understanding of the smart tool post design.

5. Characterization of the Key Mechanical Components

Although qualitative information about each component is available, quantitative information to characterize their performance is generally not available. Because of the lack of theoretical work and variation of the methods used to characterize their performance, uncertainty is evidently present. Since it is extremely important to calibrate the system parameters, studies are carried out to characterize the key components in the system under study. The smart actuators and membrane structure represent two focal points in this investigation. In this thesis, characterization efforts of these two components are presented.

5.1. Actuator Characterization

5.1.1. Experimental Investigation of Characteristics of MCA

Among all elements in the formalized system design concept, the smart actuators are the least understood. The difficulty involved in the applications of smart actuators includes the large deviation in performance among different production batches. Similar to other ceramic materials, the production of smart materials is highly labor intensive. A lot of material handling is involved. This increases the chance of contamination as well as variation in production condition significantly. Thus producing a consistent conforming smart actuators is a research topic itself.

Consequently, a series of extensive experiments is performed to characterize the smart actuators. The focus is on the dynamic characteristics of the smart actuators. The

measures in interest include the magnitude of applied voltage, the frequency of the applied voltage, the displacement of the actuators and the generated force from the actuators.

5.1.1.1. PMN and PZT Under Low Frequency (1Hz) Power Supply

The objective of this experiment was to gain experience in operating multilayer ceramic actuators by verifiying the displacement of an actuator under low frequency power supply. According to the data provided by the producer of the actuators, both actuators should elongate its axial dimension when a positive voltage is applied. For PZT type actuators, the elongation will change to contraction when the polarity of the voltage is reversed. However, the PMN type actuators always elongate no matter what the polarity of the voltage is.

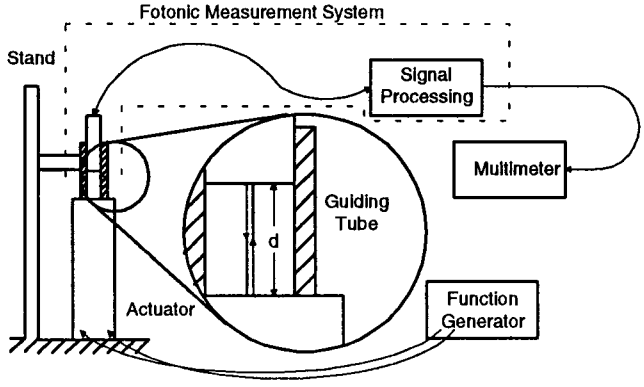

Figure 5-1 Experiment Setup for Characterising Displacement under DC Voltage

The experiment setup is shown in Figure 5-1. The setup includes a stand, a guiding tube, a function generator, a multimeter and a Fotonic displacement measurement system. The actuator under testing is fixed to the ground and subjected to a 1 Hz sine wave signal from the function generator. A low frequency signal is used because of the non-conductive nature of the actuators under DC power supply. The corresponding displacements of the

actuators at various applied voltage levels were measured and recorded using a Fotonic measurement unit. Two types of smart materials were examined; a solid PMN cylindrical actuator and a hollow PZT cylindrical actuator. After the system was calibrated (refer to the Appendix section), the experiment was carried out and the results for the PMN type actuators were shown Figure 5-2.

The results plotted in Figure 5-2 showed that both actuators changed their dimensions when a DC voltage was applied across their two ends. However, the changes were different for different materials in terms of both the magnitude and the direction. Among the two materials, the PMN actuators expanded along its axial direction under any polar orientation of the applied voltage, but the PZT actuators expanded along its axial direction under a specific polar orientation and contracted when the orientation was reversed. Both observations agreed with the prediction.

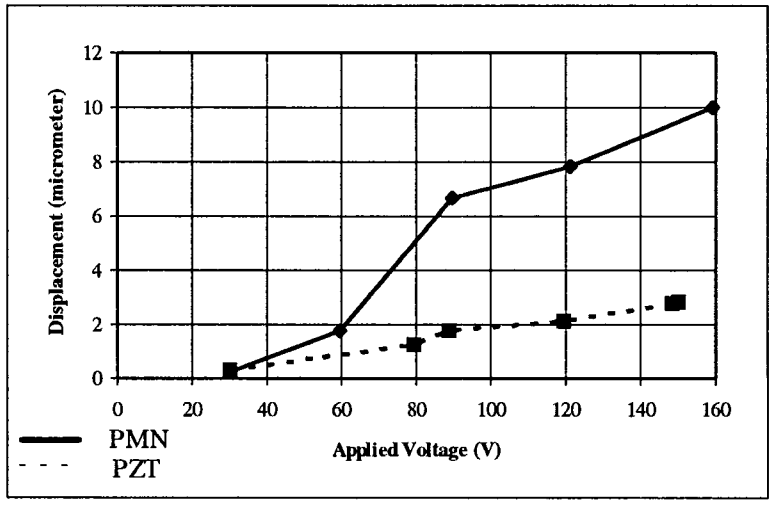

Figure 5-2 Applied Voltage vs. Displacement of Smart Actuators under 1Hz Signal

Besides the agreement with prediction, an important observation made during the experiment was that the response time of an actuator for contraction was much longer than

the time for elongation. One possible explanation would be the fact that the actuator requires time to remove the stored charges which cause the actuator to elongate at the first place. However, it does not take as much time for an actuator to store additional charges to elongate further. This capacitor-like behavior is caused by the actuator's structural similarity to a capacitor.

5.1.1.2. Frequency Reponse of the Ceramic Actuators

The objective of this experiment was to characterize the behavior of an actuator under AC power. Based on the experience and results obtained from the DC power environment, the smart actuators used in this project seemed capable to meet the system performance requirement. Nevertheless, since the system would be operated in a dynamic environment, the frequency response of the actuator is critical to the success of the system. Under this phase of testing, the actuators were subject to 60Hz line power at different amplitude levels ranging from 0V to 140V. With one end of the actuator fixed to a base, the displacements of the actuator along its axial direction were measured and recorded while subjecting to four different voltage levels. The experiment setup using an optical interferometry method was shown in Figure 5-3.

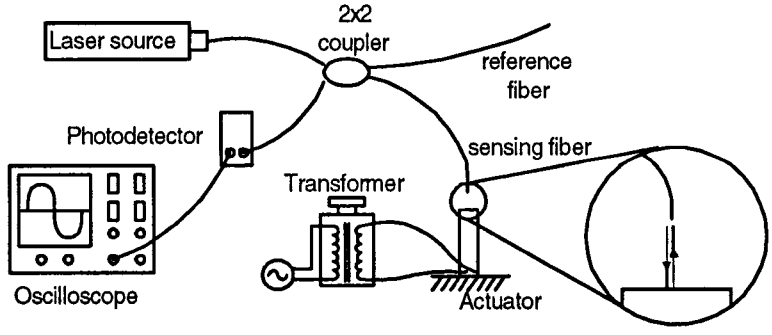

Figure 5-3 Experiment Setup for Frequency Response Test

The reason of using optical interferometry method to measure the displacement is to immute the measurement system from the noise which mainly comes from the power supply (60Hz). In fact, the same noise was present in the fotonic optical measurement system used in the earlier static measurement too. However, the noise could be filtered out without too much difficulty given the fact that any high frequency component in a static measurement can be treated as noise. On the other hand, the same 60Hz component in a frequency response measurement may be the true system response instead of noise. Therefore, the optical interferometric measurement system was selected because of its noise free nature.

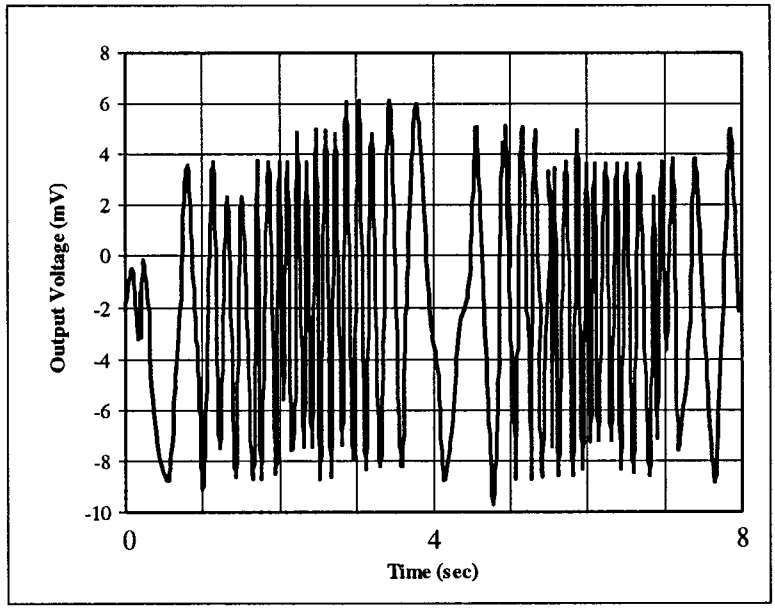

Figure 5-4 A Typical Fringe Patterns Obtained in the Experiment

The optical interferometry method takes advantage of the interference of light wave when two light wave meet together with different phase shift. The relationship is that each change of constructive interference to destructive interference or vice versa is equivalent to a $\lambda/4$ (in this experiment, 0.317μm) displacement. Since the wavelength of of the laser source is a known constant (independent of power supply), the actuator displacement can be

measured to within a fraction of the wavelength by counting the the number of fringe shifts for a given applied voltage.

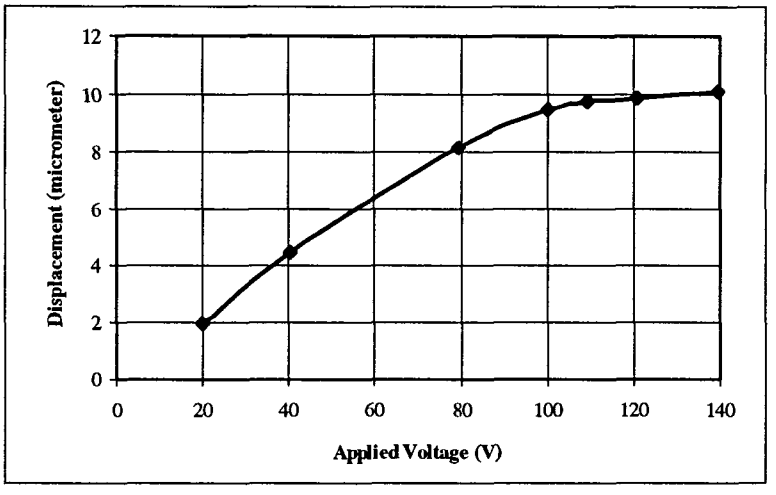

Figure 5-5 Applied Voltage vs. Displacement of PMN Type Actuator under 60Hz AC

5.1.1.3. Pre-stress Effect on Performance of Actuator

Under normal operational conditions, the actuators are pre-stressed in order to perform properly. This set of experiments is to investigate the performance of an actuator under pre-stressed condition. The performance measures between the previous experiments and this experiment are different. In the previous experiments, the displacements of the actuators were recorded. In this experiment set, the magnitudes of the force generated by the actuators were recorded instead. It is because the actuators have to consume a certain amount of energy to overcome the initial induced stress (or strain). During this stage, the actuators do not have any displacement (or work done). Thus, the amount of displacement does not represent how much load is applied to the actuator, or generated by the actuator. On the contrary, the force applied across the actuator indicates the level of loading applied on the actuator.

The setup for the experiments was shown in Figure 5-6. During the experiment, the actuator was subjected to a constant strain induced by a clamping mechanism. A force gage which was powered by a DC power unit was placed underneath the actuator. The signal from the gage was conditioned by a bridge amplifier, displayed and recorded on an oscilloscope.

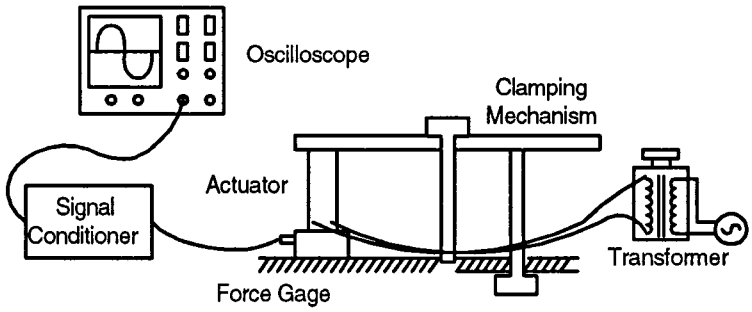

Figure 5-6 Experiment Setup for Examining Pre-stress Effect on Smart Actuators

This set of experiments include the study of the relationship between applied voltage and generated force, relationship between generated force and time, and, lastly, the waveform of the generated force.

5.1.1.3.1. Relationship between Applied Voltage and Generated Force

The relationship between applied voltage and generated force observed from the experiments are shown in Figure 5-7 and Figure 5-8. An important observation was the verification of the general behavior of an actuator under two different boundary conditions; both ends fixed, and one end fixed with the other end connected to a spring because a large clamping force resembles the fixed ends conditions while a small clamping force, which is not strong enough to eliminate all the clearance in the system, resembles a spring connected condition. As shown in Figure 2-10 in section 2.7.1, the actuator under testing did not

generate as much force as it was fixed at both ends. It is because part of the energy is stored as strain energy of the spring, 0.5x(spring force)x(displacement). The amount of force generated would be the product of the stiffness of the spring and its displacement. On the other hand, the actuator with both of its ends fixed delivered a larger force than the actuator with free ends. This is because all the power was used to generate force.

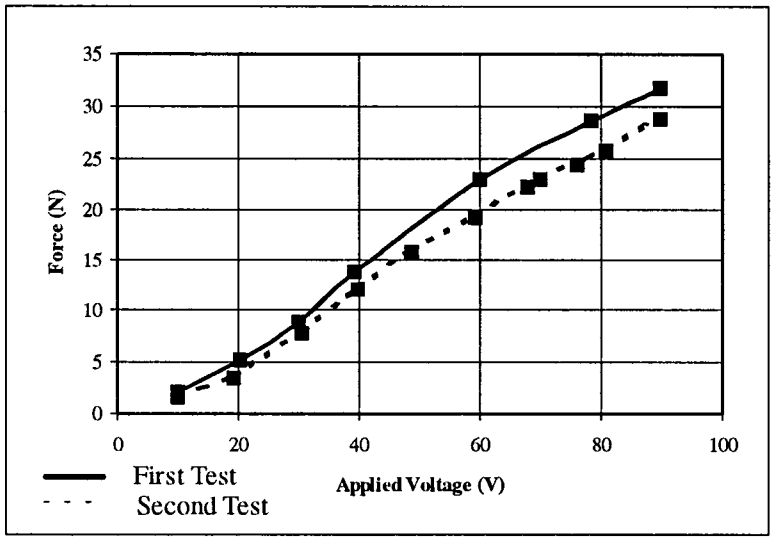

Figure 5-7 Applied Voltage vs. Generated Force under Small Pre-Stress

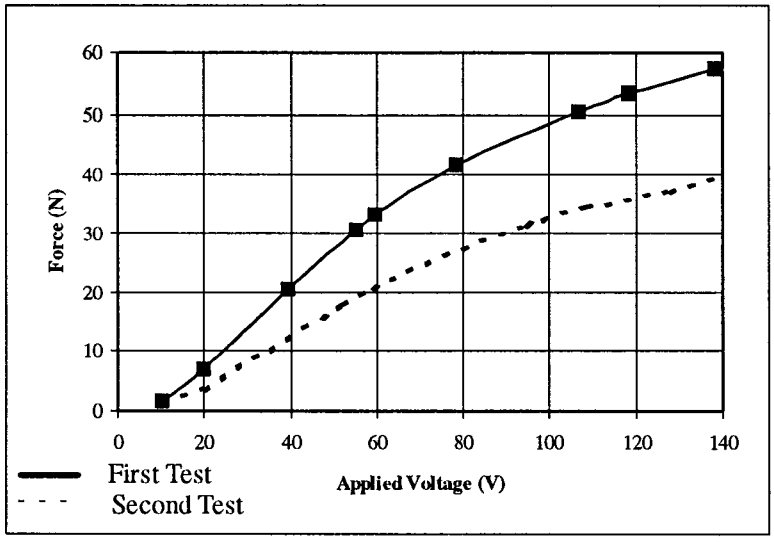

Figure 5-8 Applied Voltage vs. Generated Force under High Pre-Stress

5.1.1.3.2. Relationship between Generated Force and Time

As indicated in section 2.6, the smart material made actuators possess the creep characteristic. The magnitude of the force generated by the actuator is going to reach its maximal value shortly after a voltage is applied to the actuator. Then, the magnitude of the force decreases until it reaches the steady-state force level. This change in the force generated over time is common to all the smart material made actuators and is important to the development of the controller for the actuators. Therefore, this experiment is devoted to investigate the creep phenonmenon on the smart actuators used in this project.

The results were obtained by keeping the applied voltage at 80VAC and an pre-stress force of 20 lb over a period of time while the force magnitude was recorded. The results are shown in Table 5-1 and plotted in Figure 5-9.

Table 5-1 Generated Force vs. Time for a Smart Actuator Subjected to 80VAC

Time (min.)	0	10	20	30	40
Force (lb)	6.17	5.9	5.78	5.66	5.66

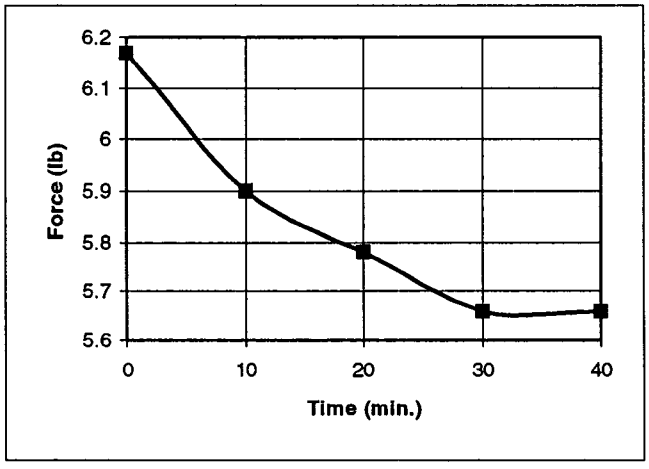

Figure 5-9 Generated Force vs. Time

Besides the effect of initial boundary conditions, the loading history of an actuator also had significant effect on its performance. The PMN actuator generates a larger force when it has not been used for hours than when it was used shortly before. Even during operation, the actuating force of an actuator is also time dependent. The general characteristic about the actuating force was that the force reached its maximum value right after the voltage was applied. Then, it started to be smaller and smaller and reached a lower-force steady state. The time taken in the experiment ranged from 30 to 40 minutes.

5.1.1.3.3. Waveform Information

Besides the force magnitude, the waveform of the actuator response also plays a key role in determining the effectiveness of the actuators. The waveforms of the actuator response at three different settings were recorded and presented in Figure 5-10, Figure 5-11, and Figure 5-12.

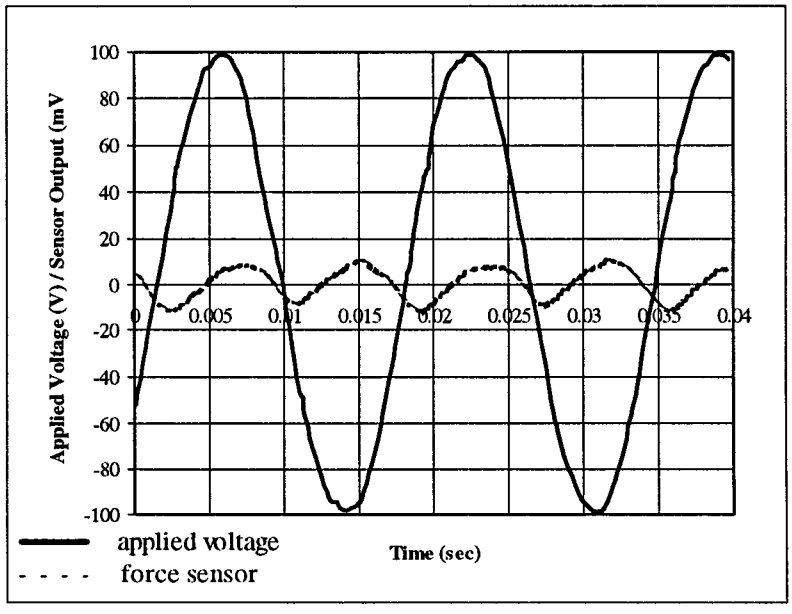

Figure 5-10 Response of a PMN Type Smart Actuator Subjected to 80 VAC

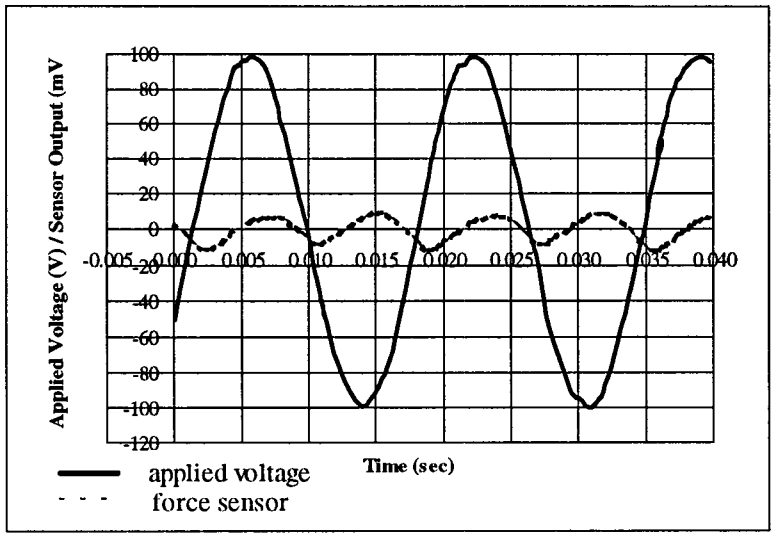

Figure 5-11 Response of a PMN Type Smart Actuator Subjected to 100 VAC

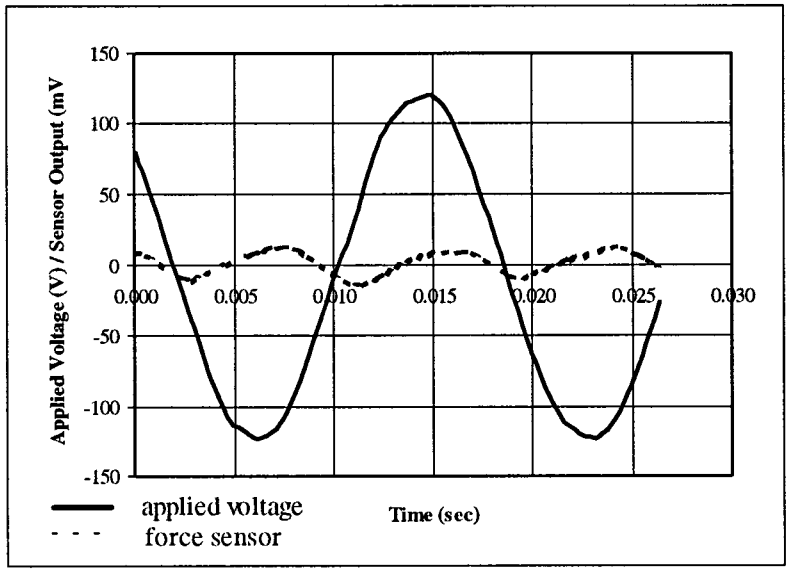

Figure 5-12 Response of a PMN Type Smart Actuator Subjected to 120 VAC

Observations were made from the recorded force waveforms. First of all, the characteristic of the PMN type smart actuator under examination was clearly shown. The actuator expanded its size independent of the polarity of the applied voltage. Thus, the

frequency of the force signal was doubled the frequency of the applied voltage. Another observation made was the approximate 90° phase shift between the applied voltage and the output force signal. The phase shift was probably caused by the capacitance of the actuator. (The capacitance has a 90° phase lead to the resistance.) In addition, the waveform of the actuating force was not exactly in sine waveform. The possible reason was the charge and discharge characteristics of a capacitor.

5.2. Characterization of Membrane Structure

Membrane structures are under the thin plates category. The purpose of plates in engineering applications is to cover, generally, a rectangular or circular area and to support concentrated or distributed loading normal to the plane of the plate. "Thin" is a relative term which indicates that the thickness of the material is small compared with the overall geometry, a ratio of 10:1 or greater being the criterion. A further factor which affects the nature of the analysis is the range of deformation, again in qualitative terms referred to as "small," or "large."

5.2.1. Analytical Format

Since a membrane is a common mechanical component, its characteristics, or analytical solution, have been formulated and listed in engineering textbooks and handbooks[20]. The solution given by a representative book authored by Benham will be examined and compared with the solutions obtained through different approaches.

5.2.1.1. Assumptions

Followings are the assumptions for small deflections of thin plates:

1) No deformation in the middle plane of the plate, i.e. a neutral surface.

2) Points in the plate lying initially on a normal to the middle plane of the plate remain on the normal during bending.

3) Normal stresses in the direction transverse to the plate can be disregrarded.

5.2.1.2. Formulation

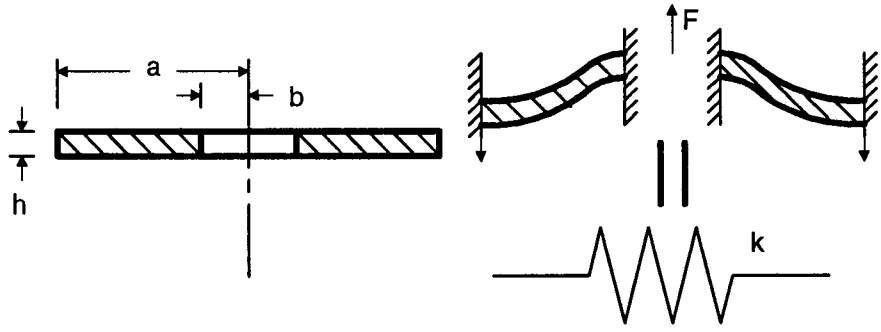

Figure 5-13 Geometric Representation of the Variables Used in the Formulas

The maximum deflection can be represented by the following relations:

$$w_{max} = c' \frac{pa^4}{Eh^3} \quad \text{or} \quad w_{max} = c' \frac{Fa^2}{Eh^3} \qquad (5\text{-}1)$$

where c' is a factor involving the ratio a/b and Poisson's ratio.

The maximum stresses can also be expressed by formula as follows:

$$\sigma_{max} = c'' \frac{pa^2}{h^2} \quad \text{or} \quad \sigma_{max} = \frac{c'' F}{h^2} \qquad (5\text{-}2)$$

where c'' is also a factor as defined above. Values of c' and c'' for v = 0.3 and a/b in the range 1.25 to 5.00 are given in table.

Table 5-2 Table of Coefficients for Membrane Structure

a/b	1.25	1.50	2.00	3.00	4.00	5.00
c'	0.00129	0.0064	0.0237	0.062	0.092	0.114
c''	0.115	0.220	0.405	0.703	0.933	1.13

5.2.2. Experimental Evaluation of Membrane

5.2.2.1. Stiffness

The objective of this experiment was to determine how well a theoretical formula predicted the stiffness of a membrane. The experiment setup was shown in Figure 5-14. A membrane was held tight in a special designed membrane holder. Weights were added to the membrane in various levels. The corresponding displacements were measured and recorded by a fotonic optical measurement system.

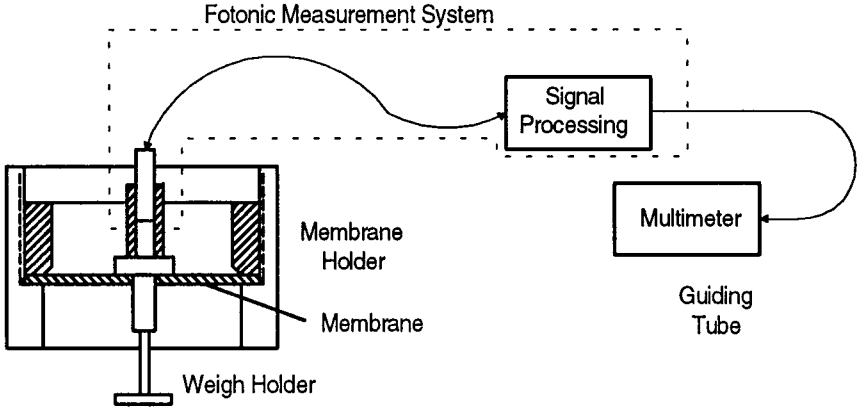

Figure 5-14 Experiment Setup for Membrane Test Using Fotonic Measurement System

The results were plotted in Figure 5-15. From the graph, the displacement was directly proportional to the load. The equivalent stiffness was 7.81MN/m.

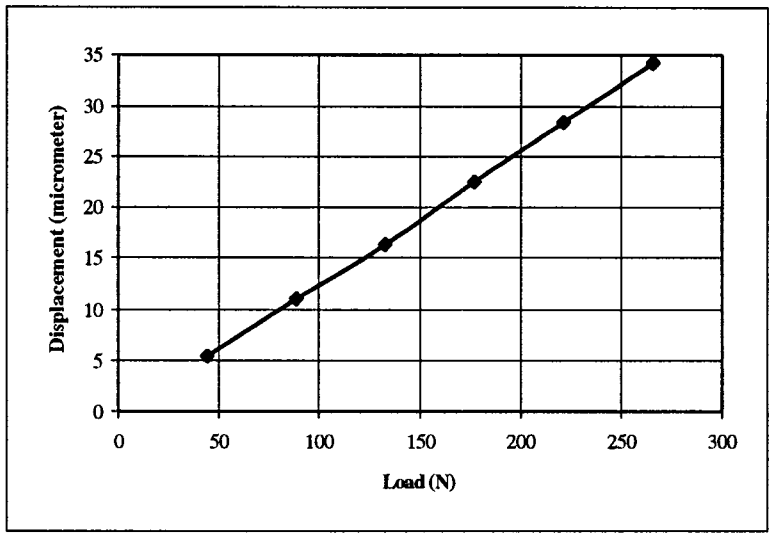

Figure 5-15 Displacement of the Membrane under Various Load (using Fotonic system)

To double check the measurement, a micrometer was used to replace the fotonic system. The results were plotted in Figure 5-16. The equivalent stiffness was 7.62 MN/m which was only 2.4% different than the one obtained from fotonic system.

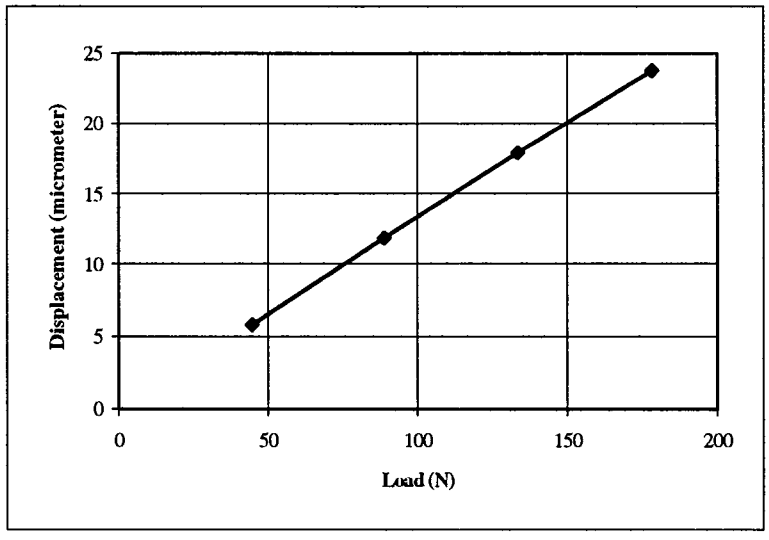

Figure 5-16 Displacement of the Membrane under Various Load (using a Micrometer)

5.3. Summary

The two key components are examined and verified on their performance. The PMN type smart actuators generate more power than the same size PZT type actuators do. However, as noted in section 2.6 and the results from the frequency response experiments done for the PMN type actuators, PMN type actuators always expand in sizes under the influence of electric field regardless of its polarity. Thus, the controller for the PMN type actuators must be carefully designed. Otherwise, the whole smart tool post system will not only fail, but also cause disasterous damage to the machining system.

In addition, the linearity of the stiffness of a membrane structure is verified to be valid, at least under a restricted operating range. This property confirms that the replacement of springs with membrane structures is appropriate. Also, the analytical work on the smart tool post system and the controller design can be simplified because of the linear stiffness.

6. Test and Evaluation of the Smart Tool Post Performance

Experiements were performed with two purposes, namely, observing the performance of the fabricated smart tool post and estimating the system parameters to verify the accomplishment of the design objective. In this chapter, the information about the experimental setup and the experimental procedure for the verification is presented.

6.1. Fabrication of the Smart Tool Post

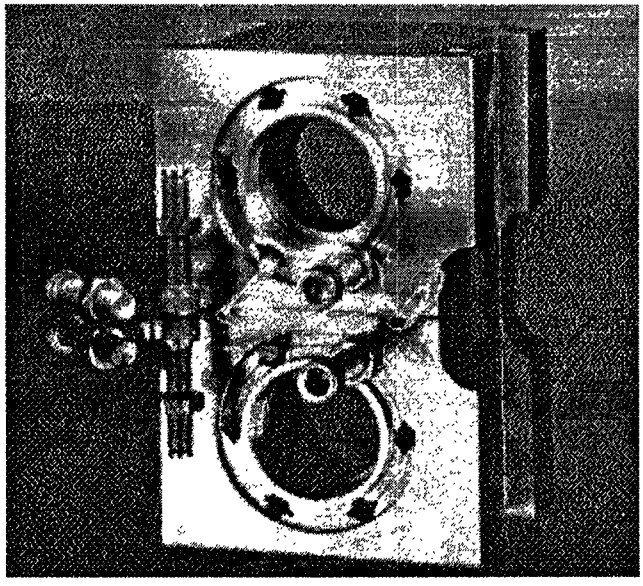

Figure 6-1 Picture of the Smart Tool Post Mechanical Structure

The smart tool post is built based on the analysis performed and the structure designed. Although the design is expected to comply with all the requirements, there are certain factors affecting the final performance of the smart tool post, such as natrual production imperfections, deviation from the defined assembly procedure, and others.

Therefore, a series of testings is prepared to quantify the overall effect of those factors on the performance of the smart tool post.

Testings of the smart tool post are intended to answer the following three questions:

1. What is the natural frequency of the structure? Does it comply to the design objective?
2. How well does the mathematical model describe the behavior of the smart tool post structure?
3. What is the general pattern of frequency response in terms of the gain and phase of the smart tool post against the applied force at various frequencies?

By answering these three questions, a better understanding of the behavior of the structure in the real world can be obtained. In addition, the testing results will provide information which is important to identify part of the feedback path. Furthermore, the data obtained are used to calibrate the mathematical model to improve the model prediction accuracy. Therefore, the series of experiments is crucial to the success of the project.

6.2. Dimension Measurement of the Smart Tool Post Structure

The objective of this measurement is to provide the actual dimensions and other physical properties of the smart tool post prototype for later analytical uses. The measurement data are listed as follows:

Item	Tool Holder	Vibration Absorber	Membrane (thick, large)	Membrane (thin, large)	Membrane (thick, small)	Membrane (thin, small)
Mass(g)	833.2	74.0	93.6	51.8	36.1	20.3

Item	Outer Contact Radius for Membrane #2	Inner Contact Radius for Membrane #2	Outer Contact Radius for Small Membrane	Inner Contact Radius for Small Membrane	Outer Contact Radius for Small Membrane	Inner Contact Radius for Small Membrane
Radius (mm)	52.17	40.64	19.05	6.35	35.56	21.25

6.3. Experiment #1 -- Impulse Test

The main objective of this test is to identify the natural frequencies of the smart tool post structure at various physical arrangements. In addition, the damping characteristic can be obtained based on the experiment results.

The response of a structure reaches its peak value at its natural frequency. Due to the various possible physical arrangements of the smart tool post structure, a detailed examination of the structure's natural frequency for each of these arrangement is important to provide a general picture of the structural dynamics of the system.

6.3.1. Impulse Test

The method used is an impulse test. In an impulse test, the structure is given an impulsive load by being hit with a hammer. An accelerometer attached to the structure picks up the response of the structure subjected to the loading. Since an impulsive load is a wide frequency spectrum load, the structure is essentially subjected to a load over a wide frequency range. Therefore, a power spectrum analysis on the responses of the structure can identify all the natural frequencies possessed by the structure.

Note that in section 5.2 the maximum deflection for a thin circular plate with fixed inner and circumference boundary under loading along its edge can be represented by:

$$w_{mas} = c' \frac{Fa^2}{Eh^3}$$

where c' is a coefficient, w_{max} is the maximum deflection, E is the Young's modulus, h is the thickness of the plate, F is the applied load, a is the outer radius.

Note that the stiffness is defined as the ratio of force to displacement, the stiffness for the thin circular plate can be expressed by

$$k = \frac{Eh^3}{c' a^2} \tag{6-1}$$

For the large membrane used in this study, the inner contact radius is 21.25mm and the outer contact radius is 35.56mm. For the small membrane, the corresponding radii are 6.35mm and 19.05mm, respectively. Thus, c' is approximately 0.0064 for the large membrane and is 0.062 for the small membrane.

Substituting E_{steel} = 208GN/m^2 and corresponding dimensions into Equation (6-1) gives:

k_{large} = 86.74 MN/m k_{small} = 31.20 MN/m for the 1.5mm thin membrane

k_{large} = 693.94 MN/m k_{small} = 249.60 MN/m for the 3.0mm thick membrane

Since these membranes are placed in series, the overall stiffness of the assembly should be the sum of their stiffnesses of the membranes. For the 1.5mm thin membrane, the equivalent stiffness of the assembly is given by

$$k_{equivalent} = k_{large} + k_{small} = 117.94 \text{ MN/m}.$$

For the 3.0mm thin membrane, the equivalent stiffness of the assembly is given by

$$k_{equivalent} = k_{large} + k_{small} = 943.54 \text{ MN/m}.$$

Regarding the equivalent mass of the tool holder, it should be approximately equal to the sum of the mass of the tool holder and its associated membranes because the equivalent mass of a spring is about 1/3 of its normal mass and the mass of the membrane is incomparable to the mass of the tool holder. Consequently, for the 1.5mm thin membrane, the equivalent mass is given by

$$m_{equivalent} = m_{tool\ holder} + m_{large} + m_{small} = 905.30 \text{ g}.$$

For the 3.0mm thin membrane, the equivalent mass is given by

$$m_{equivalent} = m_{tool\ holder} + m_{large} + m_{small} = 962.9 \text{ g}.$$

The natural frequency for an object is equal to $\sqrt{\frac{k}{m}}$. The natural frequency for the smart tool post with 1.5mm thin membranes should be given by

$$\omega_n = 11413.91 \text{ rad/s} \quad \text{or} \quad f_n = 1816.58 \text{ Hz}.$$

The natural frequency for the smart tool post with 3.0mm thin membranes should be given by

$$\omega_n = 31303.26 \text{ rad/s} \quad \text{or} \quad f_n = 4982.07 \text{ Hz}.$$

In a similar manner, the natural frequency for the vibration absorber should be given by

ω_n =18819.91 rad/s or f_n = 2995.28 Hz.

In the above calculations, an assumption has been made that the actuators used in the smart tool post are not in place. The natural frequency of the structure will be increased when the actutators are in place. When the smart tool post is in use, the actuators are connected to the structure in parallel with the membranes. Based on structural analysis principles, the system stiffness will change with the presence of the actuators. The overall stiffness should be the sum of stiffnesses of all parallel elements. Given that there are three identical actuators in place (alternative 2 in Figure 4-9), the quantitative increment in the natural frequency for the 1.5mm thin membrane is given by

$$\omega_n = \sqrt{\frac{k_{eq}}{m}} = \sqrt{\frac{3k_{actuator} + k_{membrane}}{m}} = 43928.13 \text{ rad/s} \quad \text{or} \quad f_n = 6991.38 \text{ Hz.}$$

For the 3.0mm thin membrane, we have ω_n =51688.09 rad/s, or f_n = 8226.41 Hz.

Besides the change in natural frequencies, the overall damping factor of the structure may also vary. The damping characteristic should be able to be identified through the transient response of a system, which can be described by

$$\frac{d^2x}{dt^2} + 2\zeta\omega_n \frac{dx}{dt} + \omega_n^2 x = \frac{C}{m}\delta(t) \tag{6-2}$$

The solution to equation (6-2) is given by

$$x = \frac{ce^{-\zeta\omega_n t}}{m\omega_n\sqrt{1-\zeta^2}} \sin \omega_n \sqrt{1-\zeta^2}\, t \tag{6-3}$$

and its second derivative which represents the acceleration of the system is given by

$$Accel(t) = \frac{d^2x}{dt^2}$$
$$= \frac{c\omega_n e^{-\zeta\omega_n t}}{m\sqrt{1-\zeta^2}}(-\sin\omega_n\sqrt{1-\zeta^2}\,t + 2\zeta^2\sin\omega_n\sqrt{1-\zeta^2}\,t - 2\zeta\sqrt{1-\zeta^2}\cos\omega_n\sqrt{1-\zeta^2}\,t)$$

(6-5)

Since all sinusodial functions have the same angular velocity, the acceleration will reach its local maxima every period, T. The ratio between those local maximal can be expressed as

$$\frac{Accel(t)}{Accel(t+nT)} = \frac{\frac{c\omega_n e^{-\zeta\omega_n t}}{m\sqrt{1-\zeta^2}}}{\frac{c\omega_n e^{-\zeta\omega_n (t+nT)}}{m\sqrt{1-\zeta^2}}} = e^{\zeta\omega_n nT} \tag{6-6}$$

Therefore, the damping factor can be expressed in terms of the ratio of two local maximal readings obtained in an impulse test and the natural frequency obtained earlier;

$$\zeta = \frac{1}{\omega_n nT}\ln(\frac{Accel(t)}{Accel(t+nT)}) \tag{6-7}$$

A special note about the formula (6-7) is that only the ratio of the accelerations matters. Thus, in experiments, there is a freedom in the choice of the unit of measurement for the acceleration provided that the unit of measure is proportional to the actual acceleration.

6.3.2. Experimental Setup

The experiment is set up as shown in the figure below. The testing is performed at two different settings. The setting is to screw the smart tool post tightly on a table with a 1.5mm thick membrane installed.

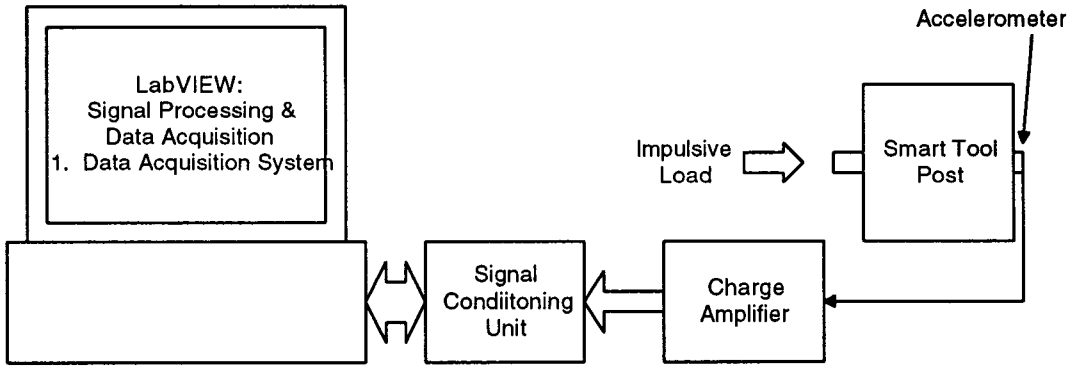

Figure 6-2 Impulse Test Setup

6.3.3. Results

The power spectrum results for the structure with thin membranes are shown as follows. However, a special note about the results is that there were a 10 Hz low frequency noise from the surroundings and a 500Hz high frequency noise from the circuitry in the computer system. The results shown were after passing through a 20Hz high-pass filter. Most of the plots are with the 500Hz frequency unfiltered because of the possibility of lossing important information about the system. Nevertheless, in each group of tests, a duplicate set of data that was passed through a 500Hz high-pass filter is also shown for better illustration of the system response.

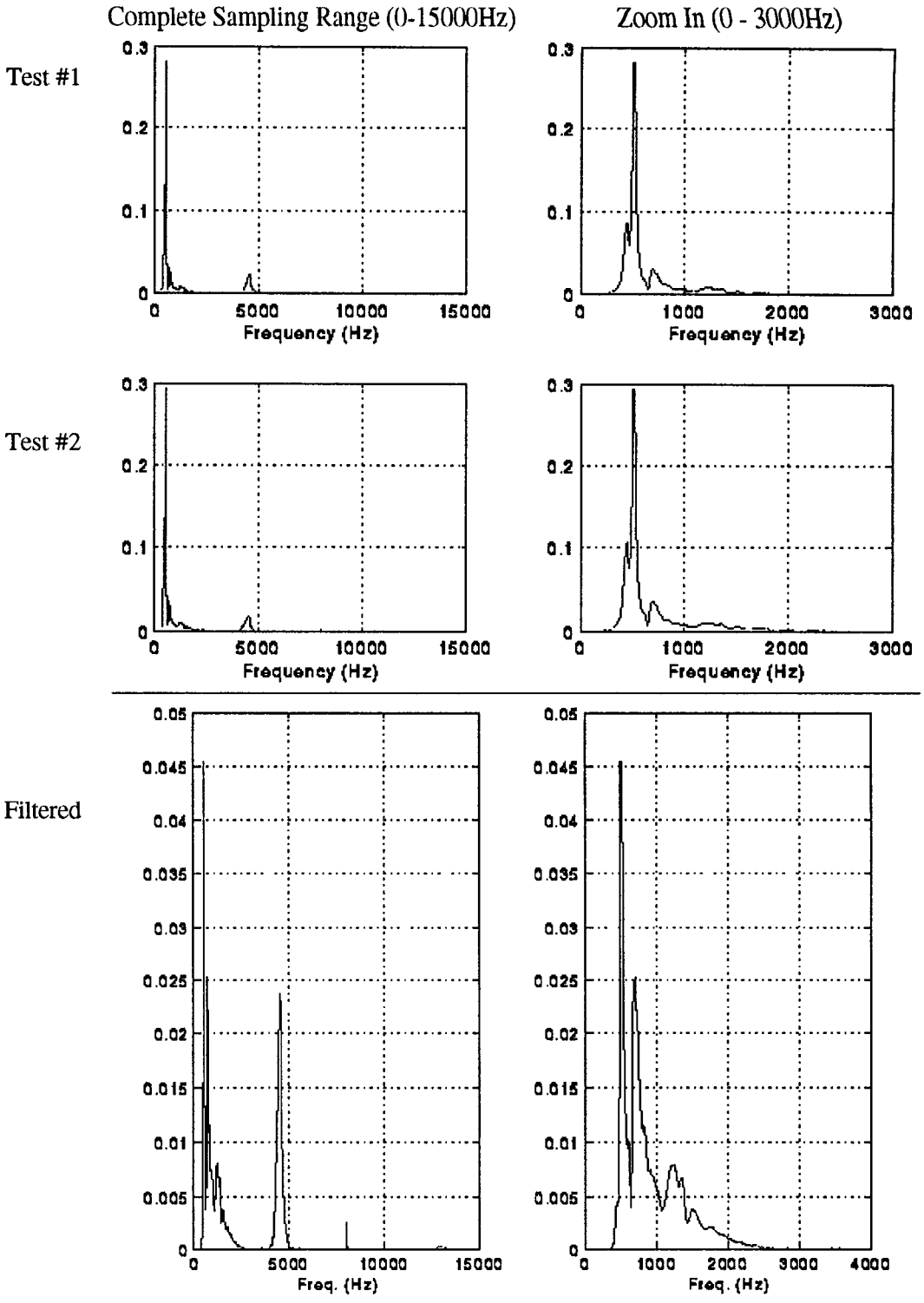

Figure 6-3 Power Spectral for the Tool Post without Actuators(along the axis)

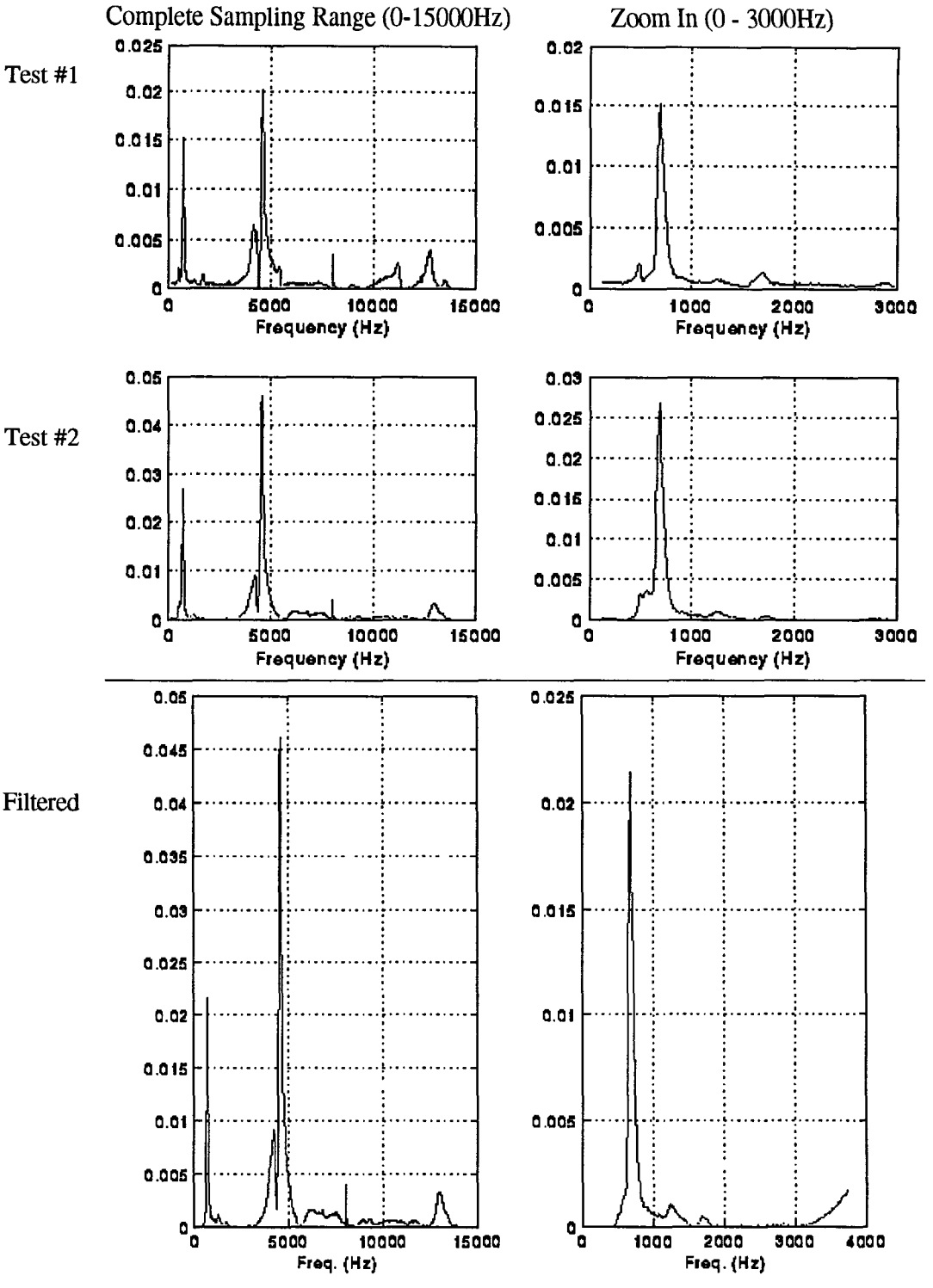

Figure 6-4 Power Spectral for the Tool Post without Actuators(from the top)

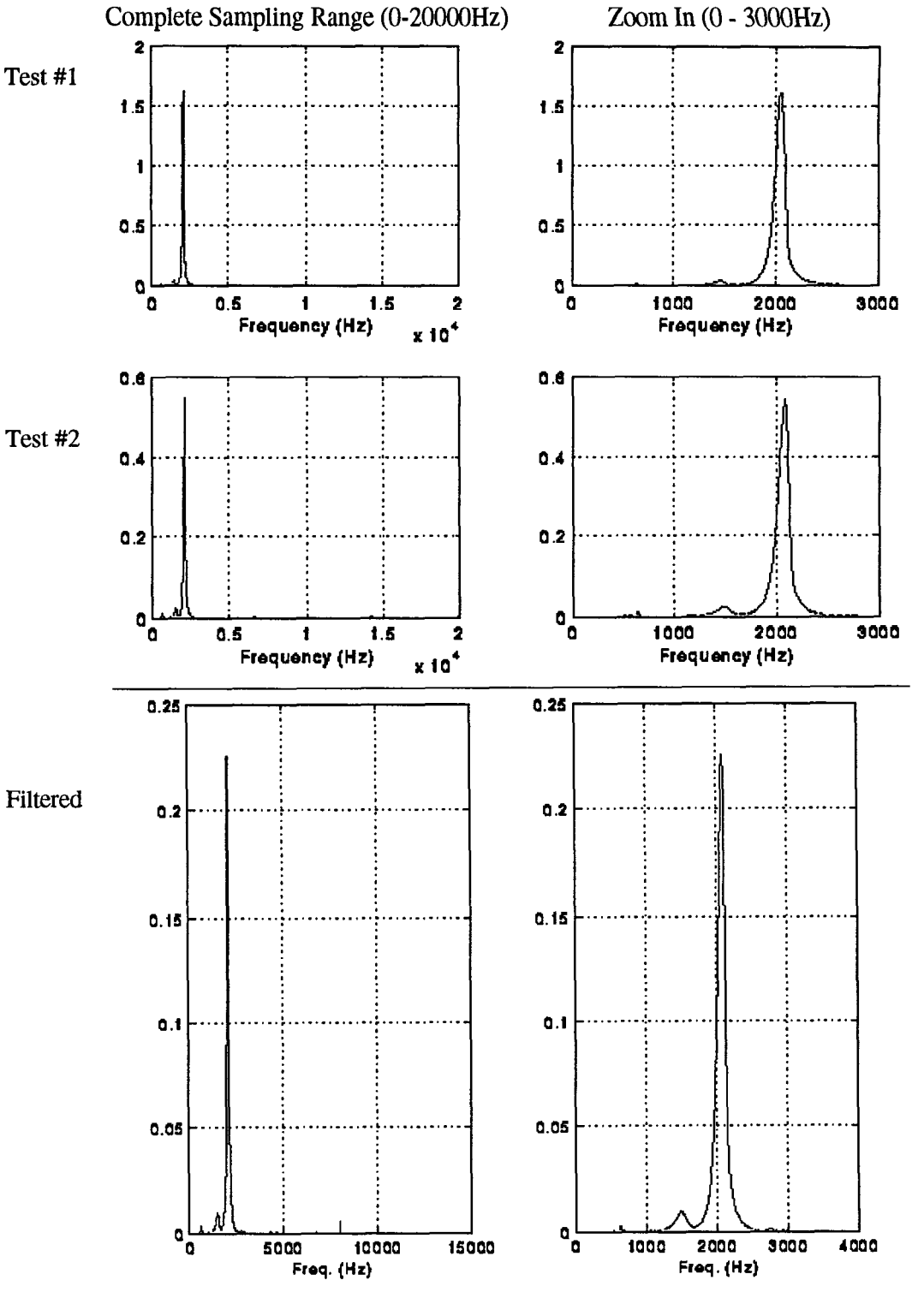

Figure 6-5 Power Spectral for the Tool Post with Open-Circuit Actuators(along axis)

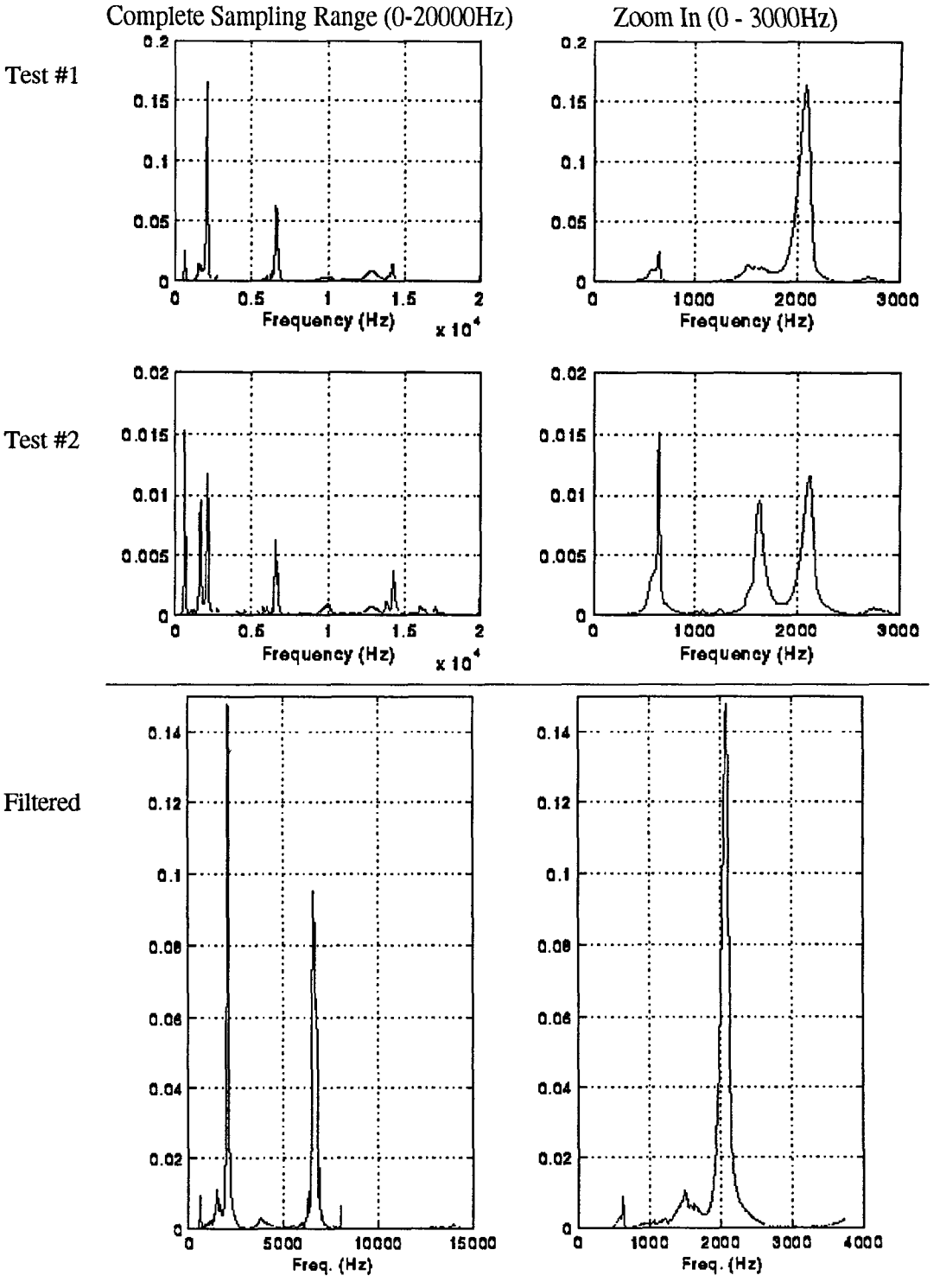

Figure 6-6 Power Spectral for the Tool Post with Open-Circuit Actuators (from top)

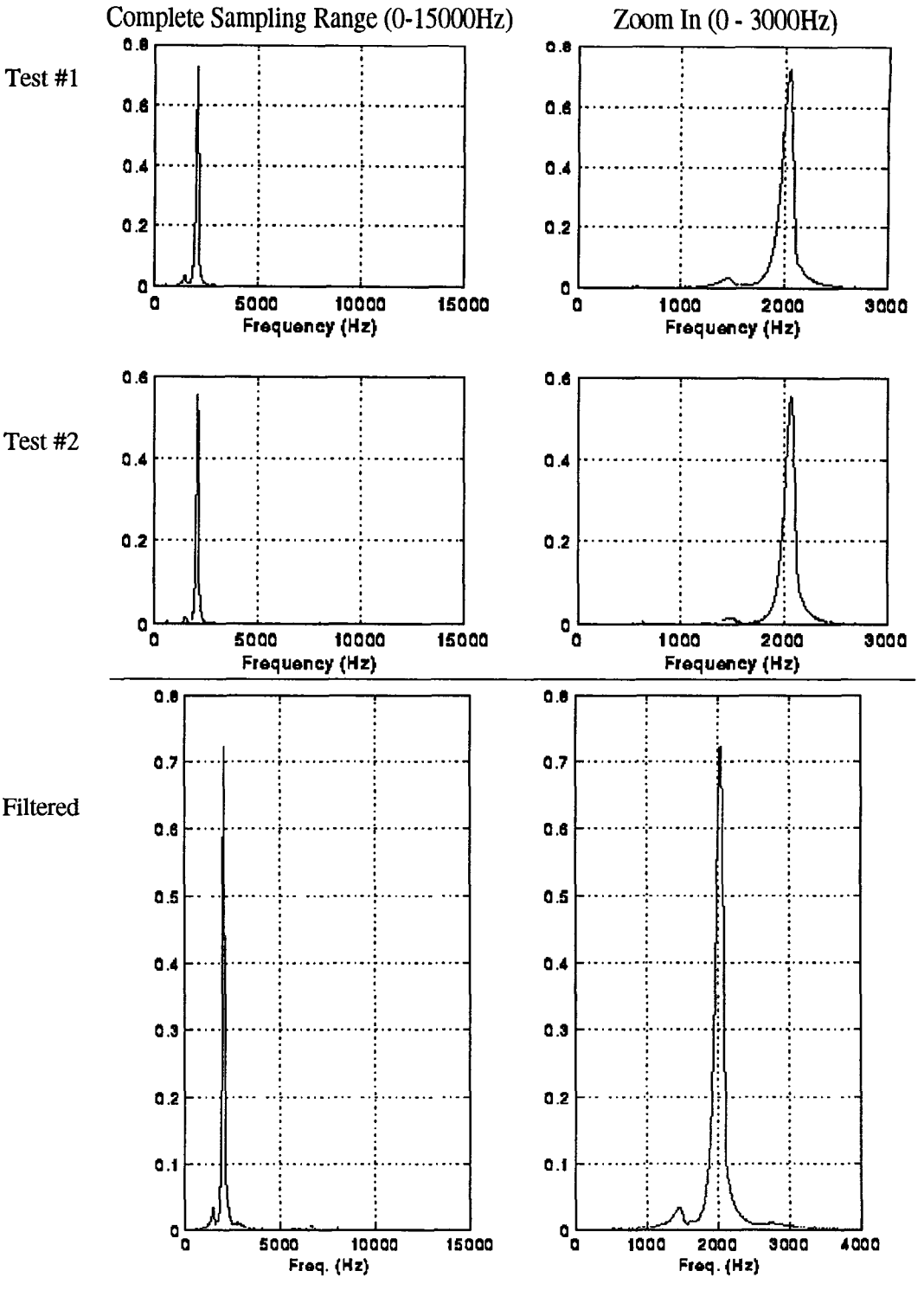

Figure 6-7 Power Spectral for the Tool Post with Short-Circuit Actuators(along axis)

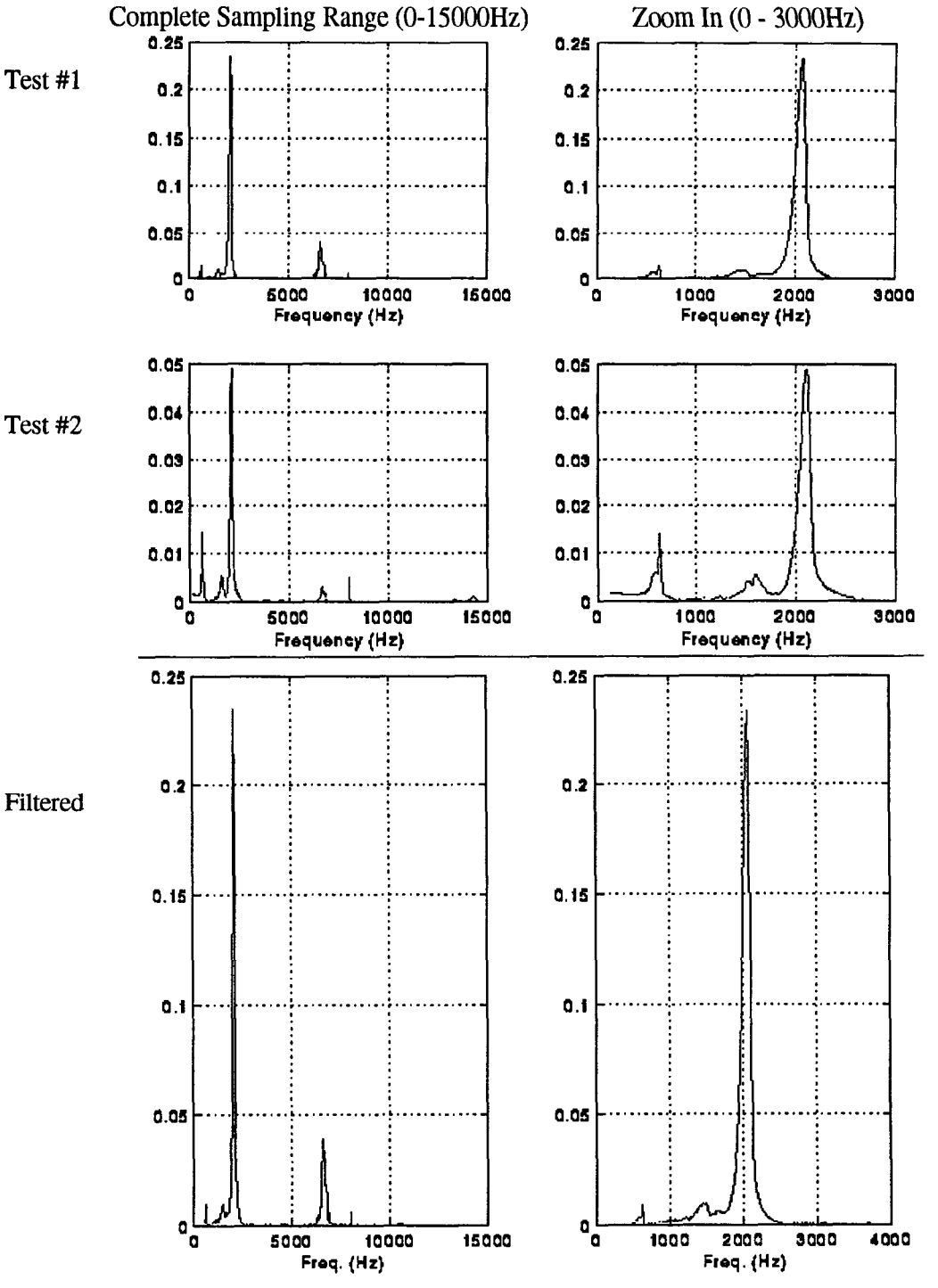

Figure 6-8 Power Spectral for the Tool Post with Short-Circuit Actuators(from top)

The experiment conditions for the results shown in Figure 6-3 were applying a horizontal load to the thin-membrane smart tool post which has no actuator installed. By examining the plots in the figure, the peak around 500Hz showed up in the plot even after it had been filtered by a 500Hz high-pass filter. Thus, it had a natural frequency at 500Hz. The next peak appeared in the region over 3000Hz was the one at about 4600Hz. This observation was consistent across the two duplicate tests.

The experiment conditions for the results shown in Figure 6-4 were applying a vertical load to the thin-membrane smart tool post which has no actuator installed. The peak around 500Hz showed up in the plot even after the data had been filtered by a 500Hz high-pass filter. Thus, it had a natural frequency at 600Hz. In addition, there was a peak at 1700Hz under the 3000Hz region. The next peak appeared in the region over 3000Hz was the one at about 4800Hz. This observation was consistent across the two duplicate tests and similar to the results obtained in the test with horizontal load. However, the peak at the horizontal impulse test was about 100Hz lower than the peak at the vertical impulse test.

The experiment conditions for the results shown in Figure 6-5 were applying a horizontal load to the thin-membrane smart tool post which has open-circuit actuators installed. After neglecting the 500Hz noise, there were peaks at 1500Hz and 2050Hz under the 3000Hz region. There was no peak appeared in the rest of the sampling region (0-20000Hz). This observation was consistent across the two duplicate tests.

The experiment conditions for the results shown in Figure 6-6 were applying a vertical load to the thin-membrane smart tool post which has open-circuit actuators installed. After neglecting the 500Hz noise, there were peaks at 1600Hz and 2050Hz under the

3000Hz region. The next peak appeared in the region over 3000Hz was the one at about 6500Hz. This observation was consistent across the two duplicate tests, but was different from the results obtained in the test with horizontal load.

The experiment conditions for the results shown in Figure 6-7 were applying a horizontal load to the thin-membrane smart tool post which has short-circuit actuators installed. After neglecting the 500Hz noise, there were peaks at 1500Hz and 2050Hz under the 3000Hz region. There was no peak that appeared in the rest of the sampling region (0-15000Hz). This observation was consistent across the two duplicate tests and similar to the results obtained (Figure 6-5) when the actuators were open-circuit.

The experiment conditions for the results shown in Figure 6-8 were applying a vertical load to the thin-membrane smart tool post which has short-circuit actuators installed. After neglecting the 500Hz noise, there were peaks at 1600Hz and 2050Hz under 3000Hz region. The next peak appeared in the region over 3000Hz was the one at about 7000Hz. This observation was consistent across the two duplicate tests, but was different from the results obtained in the test with horizontal load. However, the results were similar to the results obtained (Figure 6-6) when the actuators were open-circuit.

In order to assure the sampling rate was high enough to capture the true system response, four experiments were carried out at either a higher or lower sampling rate. The results would give the same conclusions as their corresponding data sets at different sampling rate when the sampling rate used was sufficiently high. Otherwise, a different conclusion would be resulted. The results obtained in this series of experiments were followed.

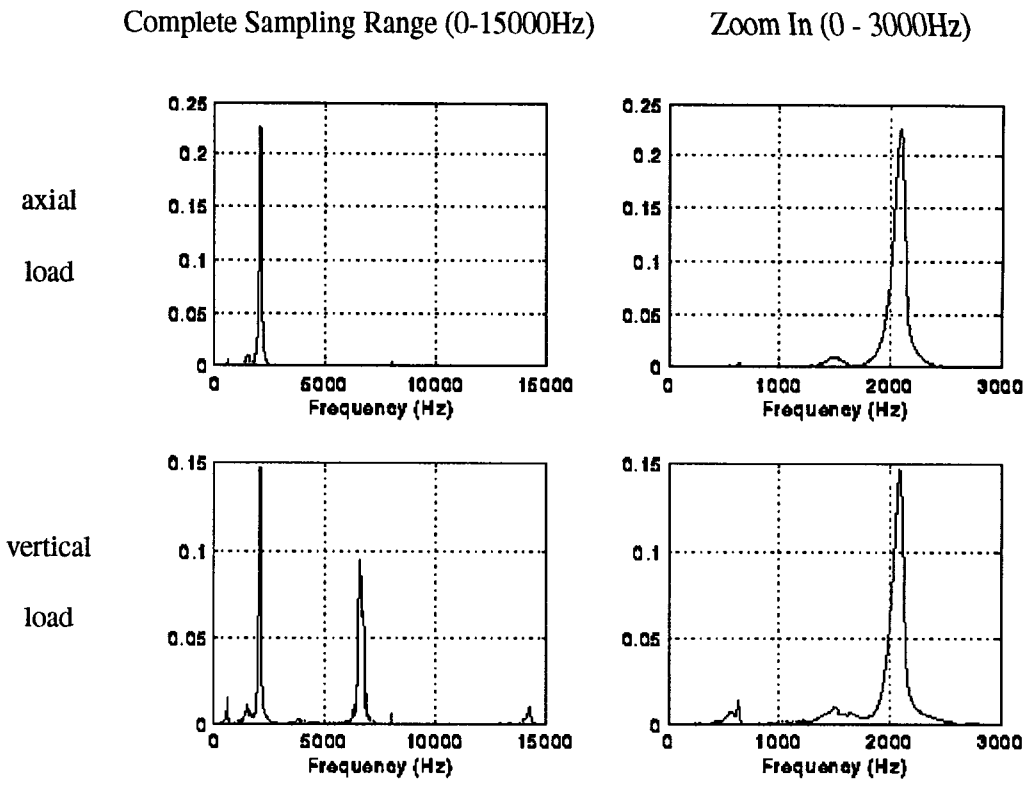

Figure 6-9 Power Spectral for Tool Post with Open-Circuit Actuators at 30kHz

The experiment conditions for the results shown in Figure 6-9 were the same as the two experiments presented in Figure 6-5 and Figure 6-6 except using a lower sampling rate. As shown in the figure, the results obtained in the three experiments matched each other. Therefore, the observations made were the true pictures of the system.

In a similar manner, the experiment conditions for the results shown in Figure 6-10 were the same as the two experiments presented in Figure 6-7 and Figure 6-8 except using a higher sampling rate. Once again, the results obtained in the three experiments matched each other. Therefore, the observations made earlier were the true system response.

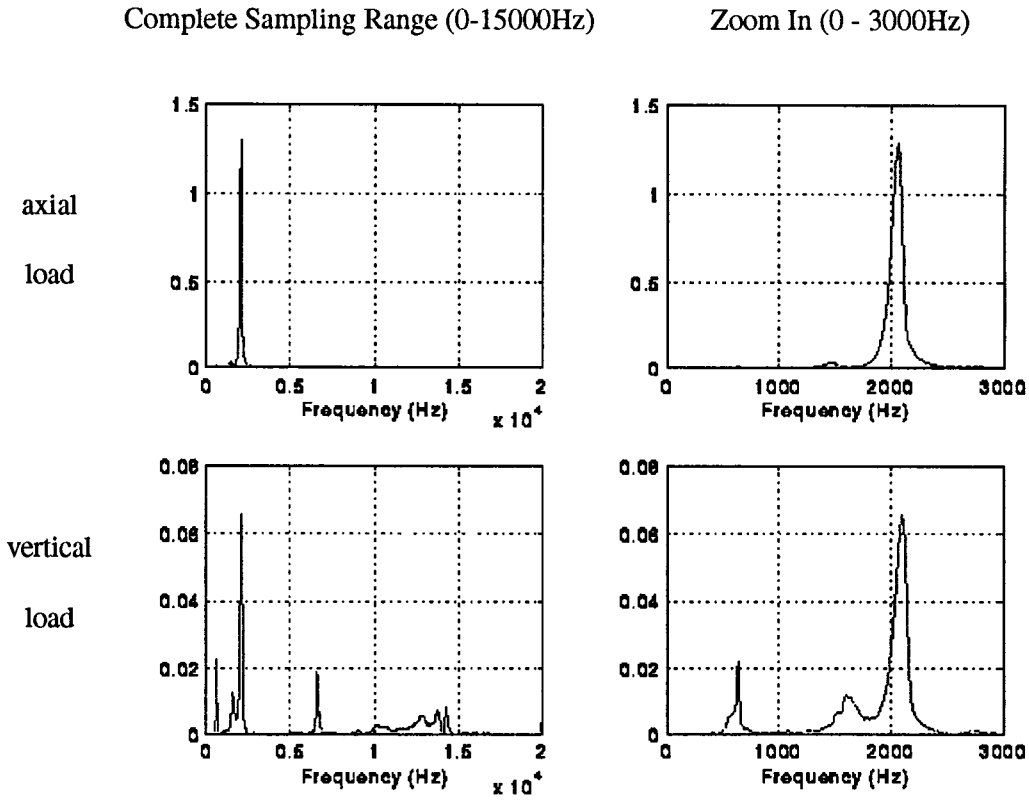

Figure 6-10 Power Spectral Density for Tool Post with Short-Circuit Actuators at 40kHz

Table 6-1 is a summary of the results obtained in this series of testing.

Table 6-1 Summary of the Natural Frequencies Under Various Settings

Thin Membrane	$f_{est.}$ (Hz)	f_{n1} (Hz)	f_{n2} (Hz)	f_{nx} (Hz)
Without Actuators (along axis)	1746.60	500	4600	N/A
Without Actuators (from top)	N/A	600	4800	13000
Open-Circuit Actuators (along axis)	6722.04	1500	2050	N/A
Open-Circuit Actuators (from top)	N/A	1600	2050	6500, 14000
Short-Circuit Actuators (along axis)	6722.04	1500	2050	
Short-Circuit Actuators (from top)	N/A	1600	2050	7000

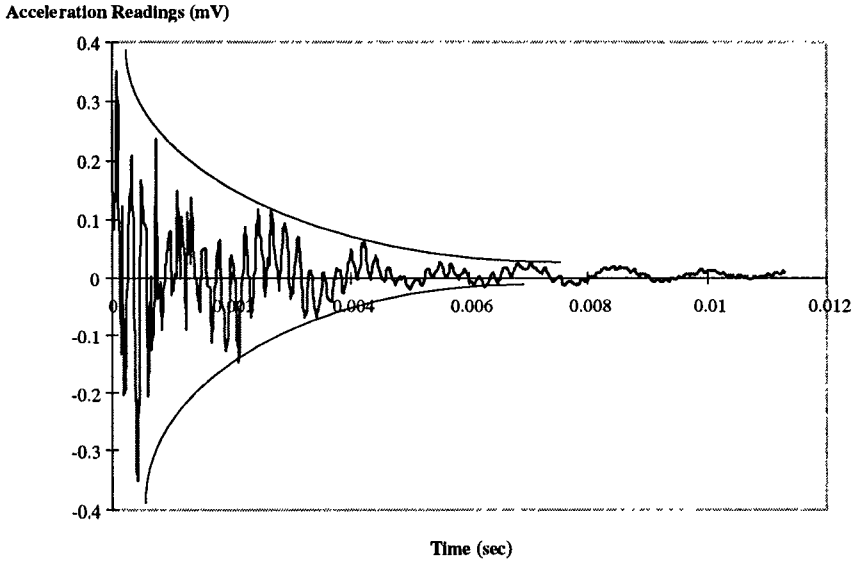

Figure 6-11 A Sample Impulse Response of the Tool Post with No Actuator (from top)

Based on the time response plot as shown in Figure 6-11, two local maximals are selected;

Table 6-2 Time Response Data for the Tool Post under Different Loading Conditions

Along the vertical direction		Along the axial direction	
Time	Accelerometer Reading	Time	Accelerometer Reading
0.002667 s	0.11349 mV	0.001600 s	0.29178 mV
0.007033 s	0.02576 mV	0.009667 s	0.03125 mV

Given that the lowest natural frequency obtained earlier for the smart tool post without actuator under vertical loading is 600Hz, and substituting the data for vertical loading condition in Table 6-2 into equation (6-7)

$$\zeta_{vertical} = 0.090$$

Similarly, for the axial direction, the lowest natural frequency is 500Hz. Thus,

$$\zeta_{axial} = 0.088$$

The rest of the damping factors for other settings are computed and summaried in the table below.

Table 6-3 Summary of the Damping Factors for Various Settings

Condition	No Actuator	Open-Circuit Actuators	Short-Circuit Actuators
ζ_{axial}	0.088 (f_n=500Hz)	0.029 (1500)	0.032 (1500)
$\zeta_{vertical}$	0.090 (600)	0.036 (1600)	0.038 (1600)

6.3.4. Discussion

The estimated natural frequency does not show up in the smart tool post structure. The actual natural frequencies possesed by the smart tool post fall at both lower and higher frequencies than the expected value. This discrepancy shows the smart tool post structure is not a simple one-degree of freedom dynamic system. On the contrary, the smart tool post structure is a two degree-of-freedom system since there are two observed natural frequencies in the system. This verifies the accurate mechanical realization of the design concept.

About the experimentation technique, in the early impulse tests, the results are not acceptable which do not show an observable peak in the power spectrum density. The final satisfactory results are obtained at a higher sampling rate (30kHz) comparing with the initial

2kHz sampling rate. A possible cause of the wide spread of power over a wide frequency range is the alias effect of low sampling frequency.

6.4. Experiment #2 -- Frequency Response of the Structure

6.4.1. Objective

The objective is to identify the number of degree of freedom of the structure by plotting the amplitude gains and phase angles of the smart tool post structure against a load at various frequencies.

6.4.2. Introduction

Although the structure is developed based on a two degree-of-freedom structure, the real dynamic characteristics of the structure are heavily influenced by the production and assembly methods. Since a large part of the mathematical analysis of the overall system is based upon the dynamics of the structure, there is a need to identify the validity of the dynamic model.

6.4.3. Methodology

Since only the gain in amplitude and the change in phase angle of the smart tool post under different frequency are the concerns, a time-domain measurement of the structure is used. The unit of measurement is the acceleration at the cutting tool holder. The response in acceleration is recorded and conditioned.

The gain is defined as the ratio of the force transmitted to the force applied to the smart tool post. Since the force transmitted is difficult to be measured, an indirect unit of

measure is used. In the experiment, the acceleration of the smart tool post is used to reflect the transmitted force because they are directly proportional to each other. The effective mass of the tool post can be approximated as the actual mass of the tool holder and its membranes because of the insignificance of the mass of membranes.

The phase change is defined as the phase difference between the input force and the resultant acceleration. Since the phase lead and phase lag basically describe the same measure, an arbitary starting point on the input force waveform is picked as reference and the phase lead is measured. However, special attention is paid on using the same method. For instance, if phase lead is used in the first experiment of a series, the rest of the experiments in that series will use phase lead too.

Theoretically, the steady-state motion of a structure subjected to a harmonic excitation will assume the harmonic frequency possessed by the excitation independent of the number of degree-of-freedom of the structure. Therefore, in addition to the jumps in amplitude gain at the natural frequencies identified by the impulsive load tests, the following observations are expected:

1. the acceleration signal is a sinusodial signal at a frequency same as the excitation frequency.

2. the amplitude of the acceleration is going to be peaked at least twice as the exciting frequency increases. The frequencies that the acceleration reaches its local maximal should be close to the natural frequencies identified by the impulse test.

3. the phase change between the excitation and the resultant acceleration is going to be 180° at a low exciting frequency because the excitation is almost a static one at low frequency. The displacement of a structure is always in phase with the applied force under static situations. Note that the acceleration is always 180° out of phase to the displacement, the acceleration is, therefore, expected to be 180° out of phase to the exciting load.

6.4.4. Experiment Seup

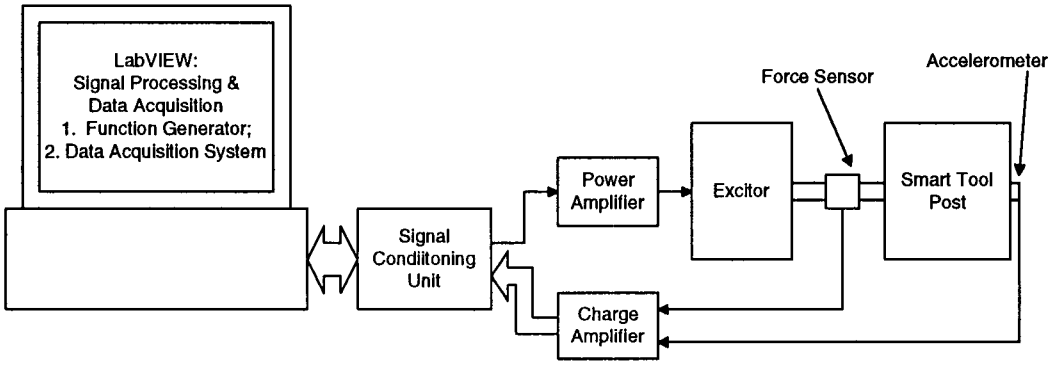

Figure 6-12 Frequency Response Test Setup

6.4.5. Results

Table 6-4 Frequency Response of the Tool Post without Actuators

Frequency (Hz)	Transmissitivity (Fout/Fin)	Acceleration/Force (kg^{-1})	Phase (degree)
100.00	0.06	0.07	183.38
200.00	0.17	0.19	198.51
307.69	0.39	0.44	180.69
400.00	0.77	0.85	189.18
444.44	1.24	1.37	182.20
500.00	3.59	3.97	198.27
571.43	3.29	3.63	317.71
666.67	1.18	1.30	280.00
1000.00	1.59	1.75	0.00

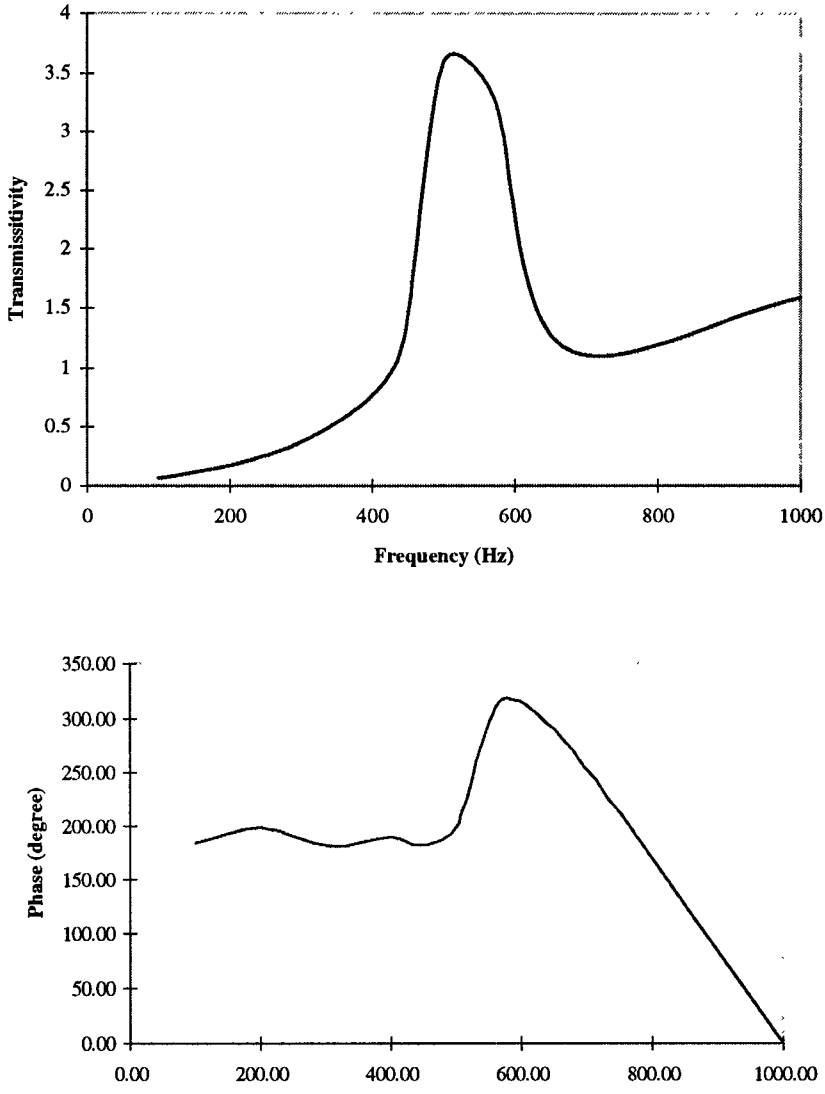

Figure 6-13 Bode Plot for the Smart Tool Post without Actuator

The results for the smart tool post with actuators in place are shown in Table 6-5.

Table 6-5 Frequency Response of the Tool Post with Actuators at Different Conditions

Frequency (Hz)	Open Circuit Transmissibvity (F_{out}/F_{in})	Open Circuit Phase Angle (degree)	Close Circuit Transmissitivity (F_{out}/F_{in})	Close Circuit Phase Angle (degree)
100.00	0.20	N/A	0.22	145.62
200.00	0.21	186.08	0.29	218.85
300.00	0.30	192.43	0.28	164.51
400.00	0.32	196.23	0.36	185.81
500.00	0.51	193.02	0.56	201.62
526.32	0.47	214.99	0.46	232.55
555.56	0.71	211.41	0.60	216.12
588.24	1.24	246.07	1.19	251.10
599.16	1.07	279.37	1.07	276.23
666.67	0.55	317.62	0.55	340.53
699.35	0.47	302.43	0.46	319.97
800.35	0.35	360.00	0.24	360.00
900.90	0.20	208.44	0.23	342.13
1000.00	0.41	205.61	0.43	214.43
1098.90	0.41	218.31	0.43	200.87
1204.82	0.67	196.67	0.62	177.61
1298.70	0.94	192.77	0.87	209.57
1398.60	1.26	185.42	1.24	188.26
1499.70	1.82	204.72	1.75	216.00
1600.00	1.67	360.00	1.57	360.00
1700.68	1.02	98.30	1.21	114.00
1801.80	1.11	237.23	1.22	246.52
1901.14	1.85	228.92	1.87	226.55
1831.50	1.28	219.43	1.20	205.71
1960.78	3.34	212.40	3.68	213.86
2000.00	2.98	221.76	3.25	225.27
2040.82	3.83	252.91	3.50	239.75
2083.33	4.32	253.45	3.95	300.00
2127.66	4.93	360.00	4.79	320.99
2173.91	4.29	360.00	4.36	360.00
2222.22	4.52	360.00	4.07	360.00
2325.58	3.69	360.00	3.72	360.00
2380.95	3.91	360.00	3.96	360.00
2439.02	3.30	360.00	3.46	360.00
2500.00	2.75	360.00	2.92	360.00
2631.58	2.17	360.00	2.28	360.00

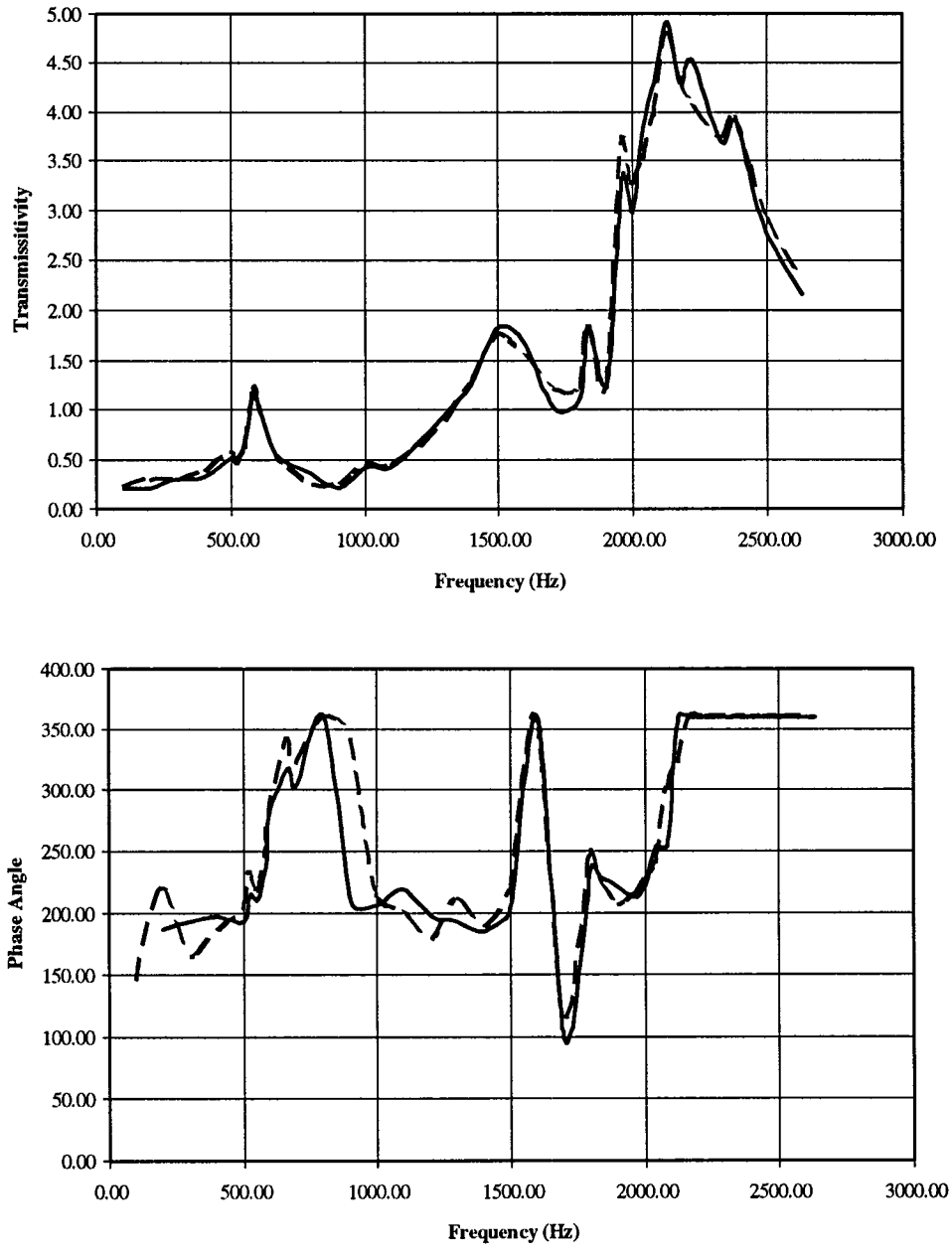

Figure 6-14 Bode Plot for Tool Post with Actuators (—:open circuit, ----:short circuit)

6.4.6. Discussion

The dynamic behavior of the smart tool post is verified to be a two degree-of-freedom system. The two natural frequencies have been identified at around 1600Hz and around 2050Hz respectively when the 1.5mm thick membrane is used. The two frequencies are consistent with the frequencies identified by the impulse test.

During the experiment, there was a consistent electric noise in a low frequency range presented in the sensing system. Different techniques such as the use of coaxial cable, shielding all electrical components were used to eliminate the noise to improve the data accuracy.

Although the general characteristics of a Butterworth band-pass filter depend heavily on the order of power, the actual behavior of the filter also depends on the nature of the noise. Thus, an investigation of the Butterworth filter on the noise in this experiment was carried out using 2^3 factorial experimentation technique and details about the investigation is presented in the Appendix section. Briefly, the results agree with the basic concept that a higher order filter provides a sharper cutoff frequency, but distorts the phase of a signal more. On the other hand, a lower order filter provides a wider cutoff frequency, but preserves the phase of a signal better. Therefore, the signals were passed through two different order filters to obtain the desire information. Specifically, a second order Butterworth filter was used to obtain the phase shift information while a 5^{th} order Butterworth filter was used to obtain the amplitude information.

6.5. Summary

The smart tool post operates satisfactory. Its dynamic behavior matches the design expectation: a two degree-of-freedom dynamic system. The two natural frequencies possessed by the smart tool post structure with the 1.5mm thick membrane installed are 1600Hz and 2050Hz respectively.

7. Conclusions and Recommendations

The work accomplished in this thesis investigation represents a two-year effort. During the past two years, the university has been working with its industrial partners, starting from the formulation of a simple design concept to the development of a sophisticated electro-mechanical device called "smart tool post'. The accomplished work indicates the importance of applying the systems engineering approach which brings the knowledge and intelligence from the mechanical, electrical and material engineering disciplines together. In this chapter, several conclusions will be drawn from the work completed to this date, and suggestions for the future work in this investigation will be presented.

7.1. Conclusions

1. A successful mathematical modeling of a complicated turning machining system has been completed. The built model has successfully served as a test bed in a virtual format for the design of the smart tool post structure. By providing a mechanism to simulate the system response without the presence of a physical entity, this virtual machining system is valuable to machine tool designers, production engineers on the shop floor and machining shop operators.

2. A tool post is fabricated based on the design presented in this thesis work. The fabricated tool post has been successfully tested. Results from the initial tests have confirmed that the mechanical structural design is a great success in terms of

a. the elegant balance between the structural rigidity and the actuator compensation capability, allowing the maximization of the actuator's authority to respond to the instant call for the vibration cancellation during machining.

b. the flexibility offered by the exchangeable membrane components to accommodate a wide range of machining conditions in which effective vibration compensation is needed.

3. An important contribution of the tool post design is that membranes are selected to be the energy conservation components in the tool post structure. Such a selection provides the designed vibration control system with the following unique characteristics:

   a. making the smart tool post structure compact in size while achieving the needed rigidity in both horizontal and vertical directions.

   b. eliminating the contact friction and backlash effects on the motion of the designed tool post structure, thus keeping the simplicity of the controller design

4. PMN (lead-magnesium-niobate) type smart material made actuators are used in the design of a tool post structure for vibration control during machining. Results from the experiments on characterizing the PMN actuator performance and machining tests indicate that PMN are capable of providing a compact and high powered actuator for machine tool vibration control applications.

7.2. Suggestions for the Future Work

1. In the mechanical structural design, a solid basis to house sensors for signal detection is needed. This addition will reduce, if not eliminate, the noise in the signal to be fed to the controller. In the initial tests, the noise coming from the vibration of the base on which the sensors are attached had a sizable effect on the effectiveness of vibration compensation.

2. The outfit of the PMN actuators should be modified in such a way that the alignment accuracy can be assured. The present outfit form has created difficulties in housing the actuators in a designed position, leading to the tensile stress within the actuator and cracks formed on the actuator, which is totally undesirable.

3. The controller design represents the major challenge to the completion of this investigation. This design calls for an integration of an adaptive mechanical structure and an intelligent controller. Optimization principles should be applied. CONSOL-OPCAD, a computer-aided design software tool has been used in this kind of investigations with success. It is suggested that CONSOL-OPCAD be used in the future work to complete this investigation.

Appendix A Matlab Script File for Machining System Model

The following is the program listing of the Matlab script file for simulating a machining system based on a one degree-of-freedom structural dynamics model.

```
%
%     This is a matlab script file used to store all the
%     parameter values and transfer functions for a
%     cutting processing and machine tool dynamics
%
%     The model is based on the following setup
%
%        |           <--| x_1
%        |          ___________________
%       /|         |                   |
%       /|-^v^v--  |                   |
%       /|  k_1    |                   |
%       /|  ___    |        m_1        |<-- Ft
%       /|---| |-  |                   |
%       /|   _|_|  |                   |
%       /|  c_1    |___________________|
%
  clear;
  format long e;
%
%     INPUT VALUES
%     ============
%
  chip_load  =input('chip_load [0.0001 m]: ');
              if isempty(chip_load) chip_load=0.0001; end;
  m_1        =input('m_1 [0.9053 kg]: ');
              if isempty(m_1) m_1=0.9053; end;
  k_1        =input('k_1 [1.0xe8 N/m]: ');
              if isempty(k_1) k_1=1e8; end;
  damp_factr =input('damping factor [0.09]: ');
              if isempty(damp_factr) damp_factr=0.09; end;
              c_1=sqrt(4*m_1*damp_factr^2*k_1);
  td        =input('regenerative time delay [0.001 sec]: ');
              if isempty(td) td=0.001; end;
  k_c      =input('cutting stiffness, k_c [1.0e6.0 N/m]: ');
              if isempty(k_c) k_c=1e6; end;
  overlap    =0.8;
%
%     STRUCTURAL DYNAMICS
%     ===================
%     d/dt[X] = tp_A[X] + tp_B[u]
%     [Y] = x_1 = tp_C[X] + tp_D[u]
%
```

```
%      [X] = [ d/dt(x_1);    x_1 ]
%      [u] = Ft
%
  tp_A = [ -c_1/m_1    -k_1/m_1;
                1            0   ];
  tp_B = [ 1/m_1;
             0  ];
  tp_C = [ 0   1 ];
  tp_D = 0;
%
%      CUTTING KINEMATICS
%      ==================
%      Ft = k_c * u
%
%  REGENERATIVE TIME DELAY
%      ======================
%      A 3rd order Pade approximation to a time delay is used
%
  [ A_td, B_td, C_td, D_td ] = pade(td,3);
```

Appendix B Matlab Script File for Complete Control System

The following is the program listing of the Matlab script file for simulating a machining system based on a two degree-of-freedom structural dynamics model and an add-on vibration control system.

```
%     This is a matlab script file used to store all the
%     parameter values and transfer functions for a
%     cutting processing and machine tool dynamics
%
%     The model is based on the following setup
%
%       |           <--| x_1                <--| x_2
%       |         _____________________    k_2   ______
%      /|        |                     |--^v^v--|      |
%      /|-^v^v--|                     |  ___   | m_2  |
%      /|  k_1  |                     |___| |__|      |
%      /|  ___  |        m_1          |  _|_|  |______|
%      /|___| |_|                     |
%      /|  _|_| |                     |<-- Ft
%      /|  c_1  |                     |
%      /|       |                     |
%      /|  Fa-->|_____________________|
%
  clear;
  format long e;
%
%     INPUT VALUES
%     ============
%
  chip_load  =input('chip_load [0.0001 m]: ');
              if isempty(chip_load) chip_load=0.0001; end
  m_1        =input('m_1 [0.1kg]: ');
              if isempty(m_1) m_1=0.1; end
  m_2        =input('m_2 [0.02kg]: ');
              if isempty(m_2) m_2=0.02; end
  k_1        =input('k_1 [1.0xe8 N/m]: ');
              if isempty(k_1) k_1=1e8; end
  k_2        =input('k_2 [1.0xe6 N/m]: ');
              if isempty(k_2) k_2=1e6; end
  damp_coeff =input('damping coeff. [0.03]: ');
              if isempty(damp_coeff) damp_coeff=0.03; end
              c_1=sqrt(4*m_1*damp_coeff^2*k_1);
              c_2=sqrt(4*m_2*damp_coeff^2*k_2);
  td        =input('regenerative time delay [0.001 sec]: ');
              if isempty(td) td=0.001; end
```

```
  k_c        =input('cutting stiffness, kc [1.0e6.0 N/m]: ');
               if isempty(k_c) k_c=1e6; end
  overlap     =0.8;
  kd          =input('kd [.01]: ');
               if isempty(kd) kd=0.01; end
  kp          =input('kp [1]: ');
               if isempty(kp) kp=1; end
  ki          =input('ki [1]: ');
               if isempty(ki) ki=1; end
 actu_volt2force=input('actuator force per volt [1 N/m]: ');
          if isempty(actu_volt2force) actu_volt2force=1; end
%
%     STRUCTURAL DYNAMICS
%     ===================
%     d/dt[X] = tp_A[X] + tp_B[u]
%   [Y]=[d/dt(d/dt(x_1));d/dt(x_1); x_1] = tp_C[X] + tp_D[u]
%
%     [X] = [ d/dt(x_1); d/dt(x_2); x_1; x_2 ]
%     [u] = Fr = Ft - Fa
%
  tp_A=[-(c_1+c_2)/m_1   c_2/m_1    -(k_1+k_2)/m_1    k_2/m_1;
         c_2/m_2       -c_2/m_2        k_2/m_2     -k_2/m_2;
             1              0               0             0   ;
             0              1               0             0  ];
  tp_B = [ 1/m_1 ; 0 ; 0 ; 0 ];
  tp_C=[-(c_1+c_2)/m_1   c_2/m_1    -(k_1+k_2)/m_1    k_2/m_1;
               0              0               1             0  ];
  tp_D = [ 1/m_1 ; 0 ];
%
%     CUTTING KINEMATICS
%     ==================
%     Ft = k_c * u
%
% REGENERATIVE TIME DELAY
%     ========================
%     A 3rd order Pade approximation to a time delay is used
%
  [ A_td, B_td, C_td, D_td ] = pade(td,3);
%
%     CONTROLLER
%     ==========
% Control law bases on output,
%      Y=[d/dt(d/dt(x_1));d/dt(x_1); x_1]
%
%     [X]=[ d/dt(x_1) ; x_1 ; integral(x_1) ];
%
  cl_a = [ 0  0  0  ;
           1  0  0  ;
           0  1  0 ];
  cl_b = [ 1 ; 0 ; 0 ];
  cl_c = [ kd kp ki ];
  cl_d = 0;
```

Appendix C Calibration of Fotonic Measurement System

Since the Fotonic measurement system operates by emitting a condensed light beam on the object to be measured and receiving the reflected light. Based upon the intensity of the reflected light, the distance between the object and the receiver of the system is estimated. However, different material and different incident angle of the light results different level of intensity, thus, the Fotonic system has to be calibrated for each experiment settings.

Using the same experiment setup with minor modifications, the system is used to measure a series of known distances. The results are presented in Figure C-1.

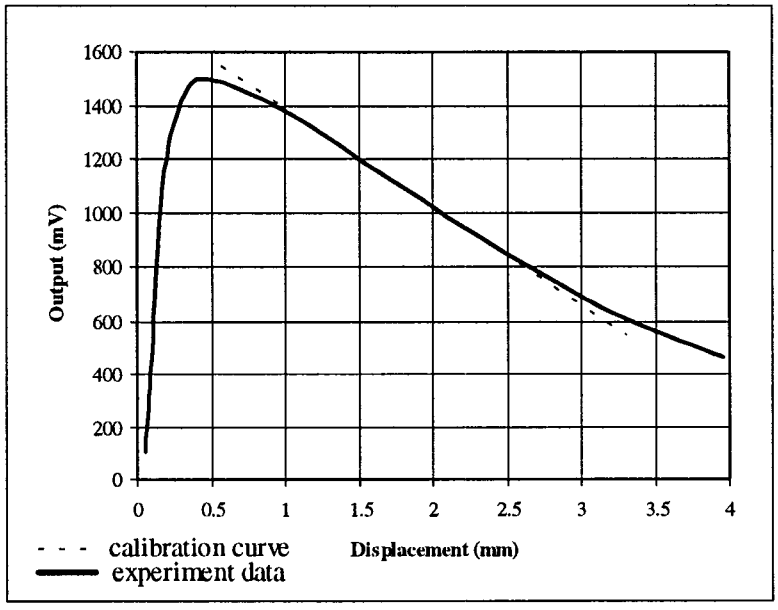

Figure C-1 Calibration Curve for the Fotonic System

References

1 Machine Tool Panel, Committee on Technology and International Economic and Trade Issues of the Office of the Foreign Secretary, National Academy of Engineering and the Combustion on Engineering and Technical Systems, National Research Council, "The Competitive Status of the U.S. Machine Tool Industry," National Academy Press, 1983.

2 DiFilippo, A., "Military Spending and Industrial Decline: A Study of the American Machine Tool Industry," Greenwood Press, 1986.

3 Kalpakjian, S., Manufacturing Processes for Engineering Materials, 2nd Ed., Addison-Wesley Publishing Company., 1992.

4 Merritt, H.E., "Theory of Self-Excited Machine-Tool Chatter," Journal of Engineering for Industry, November 1965, P.447-454.

5 Merchant, M.E., "Basic Mechanics of the Metal-Cutting Process," Journal of Applied Mechanics, Vol. 11, Transactions of the ASME, Vol. 66, 1944, P.A-168.

6 Zhang, G.M., Yerramareddy, S., Lee, S.M., Lu, S. C-Y., "Simulation of Intermittent Turning Processes," Journal of Dynamic Systems, Measurement, and Control, September 1991, P.458-466.

7 Tlusty, J., Polacek, M., "Beispiele der Behandling der selbsterregten Schwingung der Werkzeugmaschinen," 3. FokoMa, Vogel-Verlag Wuerzburg, October, 1957.

8 Tobias, S.A., Fishwick, W., "The Chatter of Lathe Tools Under Orthogonal Cutting Conditions," Transactions of ASME, Vol. 80, 1958, P.1079-1088.

9 Kuo, B.C., "Automatic Control Systems," Third Edition, Prentice-Hall, Inc., 1975.

10 Nise, N.S., "Control Systems Engineering," The Benjamin/ Cummings Publishing Company, Inc., 1992.

11 Rao, S.S., "Mechanical Vibrations," Addison-Wesley Publishing Company, Inc., 1995.

12 Kingery, W.D., Bowen, H.K., Uhlmann, D.R., "Introduction to Ceramics," Second Edition, John Wiley & Sons, 1975.

13 Askeland, D.R., "The Science and Engineering of Materials," Second Edition, PWS-KENT Publishing Company, 1989.

14 "Introduction to Piezoelectric Ceramics," Technical Report, Vernitron Piezoelectric Division, 1986.

15 "Quarter Report to the SMS Team," University of Maryland, November, 1993.

16 "SMS News," The SMS Partnership for Synthesis and Processing of Smart Materials, July, 1993.

17 "Final Program Review," The SMS Partnership for Synthesis and Processing of Smart Materials, April, 1995.

18 "Machinery Handbook, 24th Ed.", Edited by R.E. Green, Industrial Press Inc., 1991.

19 Douglas, J.M., "Process Dynamics and Control, Volume 2 Control System Synthesis," Prentice-Hall, Inc., 1972.

20 Benham, P.P., Crawford, R.J., "Mechanics of Engineering Materials," Longman Scientific & Technical, 1987.

21 Fan, M.K.H., Tits, A.L., Zhou, J.L., Wang, L.-S., Koninckx, J., "CONSOL-OPTCAD User's Manual," Systems Research Center, 1992

22 Zhang, G., Ko, W., Luu, H., Wang, X.J., "Design of a Smart Tool Post for Precision Machining," Proceedings of the 27th CIRP International Seminar on Manufacturig Systems, May 1995, P.157-164.